TARGETING MDR1 AND ENDOCRINE THERAPY-RESISTANT CANCERS THROUGH ESTROGEN RECEPTOR

BY

XIAOBIN ZHENG

DISSERTATION

Submitted in partial fulfillment of the requirements
for the degree of Doctor of Philosophy in Biochemistry
in the Graduate College of the
University of Illinois at Urbana-Champaign, 2016

Urbana, Illinois

Doctoral Committee:

Professor David J. Shapiro, Chair
Associate Professor Rutilio A. Fratti
Assistant Professor Erik R. Nelson
Assistant Professor Kai Zhang

ABSTRACT

Estrogens, acting via estrogen receptor α (ERα), stimulate cell proliferation and are associated with the development of aggressive breast and ovarian cancers. Endoplasmic reticulum (EnR) stress signaling cascade, the unfolded protein response (UPR), has documented in various human cancers and diseases. However, the precise roles of UPR signaling in development of hormone-dependent gynecological cancers were unknown. Here we show that the activation of UPR prior to EnR stress, also known as the anticipatory UPR activation, is a new paradigm for estrogen-ERα action. We found that 17β-estradiol (E_2), acting through ERα, rapidly activates Phospholipase C γ (PLCγ) leading to the production of inositol triphosphate (IP_3). The IP_3 binds to and opens endoplasmic reticulum (EnR) IP_3 receptors (IP_3R) leading to extremely rapid (<1 min.) efflux of calcium (Ca^{2+}) from the lumen of the EnR into the cell body. Elevated intracellular Ca^{2+} primes cells for subsequent actions of E_2-ERα; depletion of EnR Ca^{2+} activates the unfolded protein response (UPR), inducing the important chaperone BiP/GRP78 (glucose-regulated protein 78 kDa). Activation of this pathway is required for E_2-ERα-regulated gene expression, cell proliferation and protects cells against stress. We target this pathway with our medically promising ERα biomodulator, BHPI, which uses the same pathway as E_2, but induces toxic hyperactivation of the anticipatory UPR, shifting it from protective to cytotoxic. As a result, at nanomolar concentration, BHPI blocked growth and often killed diverse therapy-resistant and ERα-positive breast, ovarian, and endometrial cancer cells. Moreover, in a mouse xenograft, BHPI treatment resulted in rapid and substantial regression of pre-existing tumors. Extending the novel action of BHPI by hyperactivating anticipatory UPR, a new approach to inactivating multidrug resistance protein 1 (MDR1) in therapy resistant breast

and ovarian cancer cells was developed. To evaluate the effectiveness of BHPI in reversing multidrug resistance *in vivo*, multidrug resistant OVCAR-3 ovarian cells, that are resistant to all known anticancer agents, were used in an orthotopic mouse tumor model. This study demonstrated that BHPI in combination with the taxane, paclitaxel, reduced ovarian tumor burden and the circulating tumor antigen, CA125, to undetectable levels.

Taken together, these studies demonstrate the importance of cross-talk between steroid hormone action and the anticipatory UPR pathway in the development of hormone-dependent cancer. We show that targeting anticipatory UPR signaling is a promising new way to attack therapy-resistant cancers. Moreover, estrogens are known to have significant effects in neurodegenerative diseases, metabolic syndrome, and diabetes. Our studies of the anticipatory UPR pathway stimulated by steroid hormones in cancer cells open the way for further studies of the role of the estrogen-activated anticipatory UPR pathway in the pathology of these diverse disease states.

ACKNOWLEDGEMENTS

I would like to thank all the scientists and colleagues, who have played an instrumental role in my career development as a scientist. First, I would like to thank my advisor, Dr. David Shapiro, for enduring my seemingly endless drafts, his tremendous support, and investment in my growth. I would like to thank former and current members of the Shapiro lab for their ideas and assistances: Dr. Chenjian Mao, Dr. Neal Andruska, Dr. Lily Mahapatra, Matthew Cherian, Liqun Yu, Mara Livezey, and Ji Eun Kim. The research would not have been possible without the support from the collaborators, I would like to thank Dr. Sandra McMasters for providing media, Dr. Mayandi Sivaguru at the IGB core facilities for assistance in Real-time Calcium Imaging; Sisi He for assistance in carrying out mouse xenografts; Dr. Christopher Mayne for computational BHPI docking studies; Dr. Michael Lambrecht for synthesis of BHPI.

I would like to express my appreciation to the members of my committee, Dr. Rutilio Fratti, Dr. Erik Nelson, and Dr. Kai Zhang for attending my seminars and providing insightful advice on my research.

Above all else, I would like to thank my family for their tremendous love, support, and faith. They have been with me every step of this journey and nothing would be possible without them. Thanks for always believing in me and supporting my dreams – it means a lot to me!

TABLE OF CONTENTS

CHAPTER 1

INTRODUCTION

THE ESTROGEN RECEPTOR AND ITS ACTIONS

Estrogens play a crucial role in the development of the female reproductive system including the breast, uterus, and ovaries. The potent circulating estrogen, 17β-estradiol (E_2), can promote abnormal cell growth, and cause the development of cancer [1]. This effect of estrogens is primarily mediated through binding to estrogen receptor α (ERα). ERα consists of six functional domains that elicit its biological activities [2, 3]. The N-terminal (A/B) domain contains a ligand-independent activating function (AF)-1 domain. The DNA binding domain contains the zinc finger motif that interact with E_2-ERα specific DNA response elements. The carboxyl-terminal end of the DNA binding domain and hinge domain contains the nuclear localization signal. The hinge domain interacts with heat shock proteins. The ligand binding domain interacts with E_2, inducing activation of the ligand-dependent transcriptional activation function (AF)-2 domain. Last, the C-terminal region prevents protein self-dimerization in the absence of ligand.

There has been extensive research on how binding of E_2 to ERα triggers activation of its nuclear transcription program. Before ligand activation, ERα is largely localized in the nucleus and is in a monomeric complex with heat shock proteins. When estrogens enter the cell and bind to the ligand binding domain of ERα, this induces conformational changes in ERα protein, allowing ERα to dissociate from heat shock proteins [4]. Subsequently, the ligand-activated ERα forms a homodimer with another ERα monomer and binds to E_2-ERα specific DNA response elements; this allows the recruitment and docking of a series of

coactivators including members of the p160 superfamily [5]. The p160 coactivators then recruit additional coactivators including p300/CBP histone acetyltransferase, CARM1 methyltransferase, and ubiquitin ligases [6, 7]. This series of events leads to chromatin remodeling and RNA polymerase recruitment to the promoter regions of ERα-regulated genes to execute transcriptional activities of ERα.

While ERα often interacts directly with specific DNA response elements, ERα can also indirectly regulate gene transcription through a tethering mechanism. E2-ERα can occupy half sites of specific DNA response elements and be brought to DNA through interaction with transcriptional factors, including activator protein 1 (AP1), Sp1, and NFκB, at SP1 and AP-1 sites [8-11]. Numerous E_2-ERα targeted genes are regulated through tethering mechanisms.

Estrogen-regulated transcriptional activities of ERα usually play out over many hours, but estrogens can also trigger rapid cellular responses that occur outside of nucleus, commonly known as non-genomic or extranuclear actions of ERα [12]. A disparate set of rapid extranuclear actions of ERα, often initiated at or near the plasma membrane, influences diverse cell functions and also play pivotal roles in modulating its genomic program [12, 13]. These events occur within seconds to minutes and can be activated by ERα lacking a nuclear localization signal, or by directly targeting ERα to the plasma membrane [12]. These data indicate these extranuclear effects of estrogen are mediated through ERα that is outside of the nucleus.

Rapid estrogen signaling from the plasma membrane was described many years ago. It appears 5-10% of cellular ERα is usually localized to the plasma membrane [14, 15]. Moreover, numerous studies demonstrate that ERα associates with the plasma membrane

through a post-translational palmitoylation at the amino acid cysteine 447 [16, 17]. This allows ERα to interact with caveolin-1 [16, 18]. Membrane-bound ERα also interacts with several G proteins, including G_{α} and $G_{\beta\gamma}$ proteins, leading to activation of various kinases, such as PI3K, ERK, Src, and AKT [19]. While the exact mechanism underlying the plasma membrane localized ERα activation remains elusive, these extranuclear actions of ERα exhibit cross-talk with transcriptional activities of nuclear ERα.

ESTROGEN RECEPTOR IN BREAST AND OVARIAN CANCER

Prolonged exposure to estrogens is an established risk factor in breast cancer. Estrogens, acting via ERα, stimulate cell proliferation and tumor growth [1]. At diagnosis, about 70% breast cancers are ERα positive [1]. Thus, endocrine therapies that interferes with ERα activities have remained a mainstay in breast cancer treatment. The mode of action of endocrine therapies can be divided into two types: (1) Tamoxifen, Fulvestrant/Faslodex/ICI 182,780 and other antiestrogens work by competing estrogens from binding to ERα, and (2) aromatase inhibitors prevent synthesis of estrogen [20, 21]. In clinical trials, endocrine therapy for 5-years immediately following surgery in patients diagnosed with early-stage ERα-positive breast cancer reduced breast cancer mortality by 25% - 30%.

Despite initial success, endocrine therapy for ERα-positive breast cancers often leads to resistance and progressive development of resistance to therapy presents a major problem in breast cancer treatment [22]. Many resistance mechanisms have been characterized in response to endocrine therapy [22]. Since aromatase inhibitors and antiestrogens target estrogen synthesis or estrogen binding to ERα, changes that result in

estrogen-independent proliferation makes breast cancer cells resistant to endocrine therapy. (i) Alterations in expression of ERα and in the level of ERα protein can play a significant role in resistance to endocrine therapy. Furthermore, estrogenic activity depend on the presence of ERα protein, loss of ERα expression with retention of cell proliferation remains a primary mechanism for acquisition of resistance to endocrine therapy. In contrast, ERα overexpression commonly occurs in the majority of breast cancers in postmenopausal women, and it is tightly associated with increased recurrence and reduced sensitivity to endocrine therapy. (ii) Due to the diverse transcriptional effects of ERα, altered regulation of ERα co-regulators is linked to resistance to endocrine therapy. These include overexpression of ERα co-activator molecules, such as SRC3/AIB1/nCOA3, which can lead to constitutive ERα-mediated transcriptional activation. (iii) Increasing evidence suggests that tumors resistant to endocrine therapy display altered signal transduction pathways that can activate ERα activities independent of binding to estrogen. Cross-activation between ERα and growth factor signaling pathways can post-translationally modify ERα protein and activate ERα activities in the absence of estrogen [23]. Gene amplification of EGFR and ERBB2 (HER2/neu) and insulin-like growth factor receptor (IGFR) family are commonly present in therapy-resistant ERα-positive breast cancers. Activation of the MAPK/ERK pathway by the EGFR and ERBB2 growth factors, the AKT/PI3K pathway by IGF growth factors, and activation of the p38 MAPK pathway by stress and/or cytokines can all phosphorylate critical residues in the AF-1 domain of ERα and lead to ligand-independent activation of ERα [24, 25]. Thus, ERα exhibits complex cellular functions making it challenging to overcome therapy resistance in breast cancer. Despite the fact that recurrent tumors develop diverse therapy resistance mechanisms and

acquire multiple growth signaling pathways, many resistant tumors contain ERα, suggesting additional unexplored modes of ERα action potentially targetable with small molecules.

Most epithelial ovarian cancer (EOC) presents at an advanced stage [26]. Although 30-70% of these tumors contain ERα, most ERα-positive EOC do not depend on estrogens or ERα for growth and, therefore, endocrine therapies are largely ineffective in ovarian cancer. However, ERα expression is strongly correlated with increased risk of lymphovascular space invasion (LVSI) and LVSI is correlated with poor clinical outcome [27-29]. Thus, ovarian cancer patients following surgery are treated with combination chemotherapy using taxanes and platinum [30]. After several cycles of treatment, selection and outgrowth of therapy resistant tumors are common. Therapeutic options for these resistant tumors are poor, and most ovarian cancer patient die within 5 years. Paclitaxel resistance in recurrent ovarian cancer is mostly driven by overexpression of the ATP-dependent membrane efflux pump, multidrug resistance protein 1 (MDR1)/P-glycoprotein/ABCB1 [31]. Although inhibition of MDR1 presents an intriguing molecular target, development of nontoxic small molecule inhibitors targeting MDR1 has remained a difficult therapeutic challenge [32].

THE UNFOLDED PROTEIN RESPONSE

Protein folding homeostasis and quality control are maintained by the endoplasmic reticulum (EnR) stress sensor system, the unfolded protein response (UPR) [33, 34]. The UPR composes of three main branches that together balance the synthesis of new proteins, with the availability of chaperones and other proteins to help fold and transport proteins within cells. EnR stress activates the three main arms of the UPR. Autophosphorylation

activates the transmembrane protein kinase RNA-like endoplasmic reticulum kinase (PERK). P-PERK phosphorylates downstream eukaryotic initiation factor 2α (eIF2α), resulting in transient inhibition of most protein synthesis. In parallel, UPR activation induces proteolytic cleavage and activation of activating transcription factor 6 α (ATF6α). Activated ATF6α (p50-ATF6α), acts as a transcriptional factor, enters the nucleus and regulates expression of UPR targeted genes. Also, upon activation by oligomerization and autophosphorylation, the third UPR sensor, inositol-requiring enzyme 1 α (IRE1α), alternatively splices inactive XBP1 mRNA, producing active spliced XBP1 (sp-XBP1). IRE1α and ATF6α activation leads to induction of the chaperone BiP/GRP78/HSPA5 (binding immunoglobulin protein/glucose regulated protein 78 kDa/heat shock protein A5) and other chaperones that increase protein-folding capacity, and to altered mRNA decay and translation. Simultaneously, degradation of misfolded protein is increased.

In this “reactive” mode, EnR stress resulting from the accumulation of unfolded or misfolded protein, or other stresses, triggers UPR activation. While the exact mechanism of the UPR sensors activation is unclear, there is a general agreement that IRE1α directly binds unfolded proteins, leading to structural alterations that might result in oligomerization and autophosphorylation [35]. The EnR membrane contains ATP-dependent SERCA (sarcoplasmic/endoplasmic reticulum calcium ATPase) pumps that maintain a high concentration of calcium in the lumen of the EnR. The SERCA pump inhibitor, thapsigargin, and the ionophore, ionomycin, activate the UPR by depleting EnR calcium [35]. The calcium-dependent chaperone BiP is thought to bind to the 3 UPR sensors, inhibiting their activation. Unfolded protein or loss of calcium from the lumen of the EnR may disassociate BiP from UPR sensors, allowing sensor oligomerization and UPR activation [36].

Diverse mitogenic hormones, acting through their respective receptors, stimulate cell proliferation and tumor growth [37, 38]. Enhanced cell proliferation requires increased protein production, potentially leading to insufficient protein folding capacity and EnR stress. In addition, UPR activation has been described across multiple cancers as a survival mechanism in response to nutrient deprivation in the tumor microenvironment and resistance to cancer therapies [34, 39]. However, the biological importance of the UPR in hormone-dependent gynecological cancers was largely unexplored.

OVERVIEW OF THESIS

An evolutionally conserved mechanism that links the action of several mitogenic hormone actions to the UPR stress response pathway was characterized. This anticipatory UPR activation provides an authorizing signal for subsequent mitogenic gene expression and cell proliferation. Furthermore, expression levels of mRNAs encoding UPR sensors and UPR induced genes offers a powerful prognostic marker in ERα containing breast cancer, tightly associated with reduced time to recurrence, tamoxifen resistance, and poor clinical outcome. In addition, I identified the binding site of our preclinical non-competitive ERα inhibitor in the receptor, and showed it binds with nanomolar affinity with a high structural specificity. BHPI exhibits promising anti-cancer activity against a broad spectrum of ERα breast cell lines and in a mouse tumor model. I also characterized the mode of BHPI action and showed it distorts a normal action of ERα by selectively hyperactivating the anticipatory UPR pathway, converting it from protective to cytotoxic. Its unique mechanism of action suggested that I might be able to use BHPI to inactive MDR1. I showed that BHPI action depletes intracellular ATP, inactivating the ATP-dependent MDR1 drug efflux pump. This restores sensitivity to paclitaxel and doxorubicin in multidrug resistant ovarian cancer cells

and paclitaxel sensitivity in paclitaxel-resistant breast cancer cells. Moreover, I extended the promise of combination therapy successfully using BHPI together with paclitaxel in an orthotopic mouse model that we developed using multidrug resistant OVCAR-3 ovarian cancer cells. Together, my research thesis not only integrated the EnR stress pathway with mitogenic hormone actions but also offered a new avenue to understand hormone-dependent cancer development and provided a novel strategy to target therapy-resistant cancers.

REFERENCES

1. Deroo, B.J. and K.S. Korach, *Estrogen receptors and human disease.* J Clin Invest, 2006. **116**(3): p. 561-70.
2. Metzger, D., et al., *Characterization of the amino-terminal transcriptional activation function of the human estrogen receptor in animal and yeast cells.* J Biol Chem, 1995. **270**(16): p. 9535-42.
3. Tora, L., et al., *The human estrogen receptor has two independent nonacidic transcriptional activation functions.* Cell, 1989. **59**(3): p. 477-87.
4. Onate, S.A., et al., *Sequence and characterization of a coactivator for the steroid hormone receptor superfamily.* Science, 1995. **270**(5240): p. 1354-7.
5. Anzick, S.L., et al., *AIB1, a steroid receptor coactivator amplified in breast and ovarian cancer.* Science, 1997. **277**(5328): p. 965-8.
6. McKenna, N.J., R.B. Lanz, and B.W. O'Malley, *Nuclear receptor coregulators: cellular and molecular biology.* Endocr Rev, 1999. **20**(3): p. 321-44.
7. McKenna, N.J. and B.W. O'Malley, *Nuclear receptors, coregulators, ligands, and selective receptor modulators: making sense of the patchwork quilt.* Ann N Y Acad Sci, 2001. **949**: p. 3-5.
8. Johnston, S.R., et al., *Increased activator protein-1 DNA binding and c-Jun NH2-terminal kinase activity in human breast tumors with acquired tamoxifen resistance.* Clin Cancer Res, 1999. **5**(2): p. 251-6.
9. Porter, W., et al., *Role of estrogen receptor/Sp1 complexes in estrogen-induced heat shock protein 27 gene expression.* Mol Endocrinol, 1996. **10**(11): p. 1371-8.
10. Schiff, R., et al., *Oxidative stress and AP-1 activity in tamoxifen-resistant breast tumors in vivo.* J Natl Cancer Inst, 2000. **92**(23): p. 1926-34.

11. Zhou, Y., et al., *Enhanced NF kappa B and AP-1 transcriptional activity associated with antiestrogen resistant breast cancer.* BMC Cancer, 2007. **7**: p. 59.

12. Levin, E.R., *Plasma membrane estrogen receptors.* Trends Endocrinol Metab, 2009. **20**(10): p. 477-82.

13. Song, R.X. and R.J. Santen, *Membrane initiated estrogen signaling in breast cancer.* Biol Reprod, 2006. **75**(1): p. 9-16.

14. Pietras, R.J. and C.M. Szego, *Specific binding sites for oestrogen at the outer surfaces of isolated endometrial cells.* Nature, 1977. **265**(5589): p. 69-72.

15. Szego, C.M. and J.S. Davis, *Adenosine 3',5'-monophosphate in rat uterus: acute elevation by estrogen.* Proc Natl Acad Sci U S A, 1967. **58**(4): p. 1711-8.

16. Acconcia, F., et al., *Palmitoylation-dependent estrogen receptor alpha membrane localization: regulation by 17beta-estradiol.* Mol Biol Cell, 2005. **16**(1): p. 231-7.

17. Marino, M., P. Ascenzi, and F. Acconcia, *S-palmitoylation modulates estrogen receptor alpha localization and functions.* Steroids, 2006. **71**(4): p. 298-303.

18. Razandi, M., et al., *Identification of a structural determinant necessary for the localization and function of estrogen receptor alpha at the plasma membrane.* Mol Cell Biol, 2003. **23**(5): p. 1633-46.

19. Kumar, P., et al., *Direct interactions with G alpha i and G betagamma mediate nongenomic signaling by estrogen receptor alpha.* Mol Endocrinol, 2007. **21**(6): p. 1370-80.

20. Howell, A., *The endocrine prevention of breast cancer.* Best Pract Res Clin Endocrinol Metab, 2008. **22**(4): p. 615-23.

21. Jordan, V.C., *Chemoprevention of breast cancer with selective oestrogen-receptor modulators.* Nat Rev Cancer, 2007. **7**(1): p. 46-53.

22. Musgrove, E.A. and R.L. Sutherland, *Biological determinants of endocrine resistance in breast cancer.* Nat Rev Cancer, 2009. **9**(9): p. 631-43.

23. Osborne, C.K. and R. Schiff, *Mechanisms of endocrine resistance in breast cancer.* Annu Rev Med, 2011. **62**: p. 233-47.

24. Prat, A. and J. Baselga, *The role of hormonal therapy in the management of hormonal-receptor-positive breast cancer with co-expression of HER2.* Nat Clin Pract Oncol, 2008. **5**(9): p. 531-42.

25. McClelland, R.A., et al., *Enhanced epidermal growth factor receptor signaling in MCF7 breast cancer cells after long-term culture in the presence of the pure antiestrogen ICI 182,780 (Faslodex).* Endocrinology, 2001. **142**(7): p. 2776-88.

26. Bast, R.C., Jr., B. Hennessy, and G.B. Mills, *The biology of ovarian cancer: new opportunities for translation.* Nat Rev Cancer, 2009. **9**(6): p. 415-28.

27. van Kruchten, M., et al., *Hormone receptors as a marker of poor survival in epithelial ovarian cancer.* Gynecol Oncol, 2015. **138**(3): p. 634-9.

28. Matsuo, K., et al., *Estrogen receptor expression and increased risk of lymphovascular space invasion in high-grade serous ovarian carcinoma.* Gynecol Oncol, 2014. **133**(3): p. 473-9.

29. Spillman, M.A., et al., *Tissue-specific pathways for estrogen regulation of ovarian cancer growth and metastasis.* Cancer Res, 2010. **70**(21): p. 8927-36.

30. Yap, T.A., C.P. Carden, and S.B. Kaye, *Beyond chemotherapy: targeted therapies in ovarian cancer.* Nat Rev Cancer, 2009. **9**(3): p. 167-81.

31. Silva, R., et al., *Modulation of P-glycoprotein efflux pump: induction and activation as a therapeutic strategy.* Pharmacol Ther, 2015. **149**: p. 1-123.

32. Santos, S.A. and A. Paulo, *Small molecule inhibitors of multidrug resistance gene (MDR1) expression: preclinical evaluation and mechanisms of action.* Curr Cancer Drug Targets, 2013. **13**(8): p. 814-28.

33. Ron, D. and P. Walter, *Signal integration in the endoplasmic reticulum unfolded protein response.* Nat Rev Mol Cell Biol, 2007. **8**(7): p. 519-29.

34. Wang, M. and R.J. Kaufman, *The impact of the endoplasmic reticulum protein-folding environment on cancer development.* Nat Rev Cancer, 2014. **14**(9): p. 581-97.

35. Korennykh, A. and P. Walter, *Structural basis of the unfolded protein response.* Annu Rev Cell Dev Biol, 2012. **28**: p. 251-77.

36. Preissler, S., et al., *Physiological modulation of BiP activity by trans-protomer engagement of the interdomain linker.* Elife, 2015. **4**: p. e08961.

37. Zheng, X., et al., *Interplay between steroid hormone activation of the unfolded protein response and nuclear receptor action.* Steroids, 2016.

38. Shapiro, D.J., et al., *Anticipatory UPR Activation: A Protective Pathway and Target in Cancer.* Trends Endocrinol Metab, 2016.

39. Chen, Y. and F. Brandizzi, *IRE1: ER stress sensor and cell fate executor.* Trends Cell Biol, 2013. **23**(11): p. 547-55.

CHAPTER 2

ANTICIPATORY ESTROGEN ACTIVATION OF THE UNFOLDED PROTEIN RESPONSE IS LINKED TO CELL PROLIFERATION AND POOR SURVIVAL IN ESTROGEN RECEPTOR α POSITIVE BREAST CANCER CELLS [1]

ABSTRACT

In response to cell stress, cancer cells often activate the endoplasmic reticulum (EnR) stress sensor, the unfolded protein response (UPR). Little was known about the potential role in cancer of a different mode of UPR activation; anticipatory activation of the UPR prior to accumulation of unfolded protein or cell stress. We show that estrogen, acting via estrogen receptor α (ERα), induces rapid anticipatory activation of the UPR, resulting in increased production of the antiapoptotic chaperone BiP/GRP78, preparing cancer cells for the increased protein production required for subsequent estrogen-ERα induced cell proliferation. In ERα containing cancer cells, the estrogen, 17β-estradiol (E_2) activates the UPR through a phospholipase C γ (PLCγ)-mediated opening of EnR IP_3R calcium channels, enabling passage of calcium from the lumen of the EnR into the cytosol. siRNA knockdown of ERα blocked the estrogen-mediated increase in cytosol calcium and UPR activation. Knockdown or inhibition of PLCγ, or of IP_3R, strongly inhibited the estrogen-mediated increases in cytosol calcium, UPR activation and cell proliferation. E_2-ERα activates all three arms of the UPR in breast and ovarian cancer cells in culture and in a mouse

[1] This chapter appeared in its entirety in *Oncogene*. Andruska N, **Zheng X**, Yang X, Helferich WG, Shapiro DJ. (2014) Anticipatory estrogen activation of the unfolded protein response is linked to cell proliferation and poor survival in estrogen receptor α-positive breast cancer. Oncogene. DOI: 10.1038/onc.2014.292. **My contributions to the research are denoted under the figure legends**.

xenograft. Knockdown of ATF6α, which regulates UPR chaperones, blocked estrogen induction of BiP and strongly inhibited E_2-ERα stimulated cell proliferation. Mild and transient UPR activation by estrogen promotes an adaptive UPR response that protects cells against subsequent UPR-mediated apoptosis. Analysis of data from ERα positive breast cancers demonstrates elevated expression of a UPR gene signature that is a powerful new prognostic marker tightly correlated with subsequent resistance to tamoxifen therapy, reduced time to recurrence and poor survival. Thus, as an early component of the E_2-ERα proliferation program, the mitogen estrogen, drives rapid anticipatory activation of the UPR. Anticipatory activation of the UPR is a new role for estrogens in cancer cell proliferation and resistance to therapy.

INTRODUCTION

Estrogens, acting via estrogen receptor α (ERα), stimulate cell proliferation and tumor growth (1-3). The importance of estrogens and ERα in breast cancer is illustrated by the central role of endocrine therapy targeting estrogens and ERα in treatment of $ER\alpha^+$ breast cancer (1-5). To help fold and sort the increased protein required for estrogen-ERα induced cell proliferation, cells must increase chaperone levels. The endoplasmic reticulum (EnR) stress sensor, the unfolded protein response (UPR) monitors and maintains protein-folding homeostasis (6, 7). The UPR responds to misfolded proteins, or other forms of stress, by activating three signal transduction pathways, which reduce protein production and increase EnR protein-folding capacity. Protein production is regulated by autophosphorylation of the stress-activated transmembrane kinase, PERK (6, 7). P-PERK phosphorylates eukaryotic initiation factor 2α (eIF2α), resulting in transient

inhibition of protein synthesis. The other UPR arms initiate with proteolytic activation of the transcription factor ATF6α, leading to increased chaperone production and activation of the EnR splicing factor IRE1α, which alternatively splices the transcription factor XBP1, leading to production of active spliced-XBP1, increased protein folding capacity and altered mRNA decay and translation (6, 7).

The UPR is usually inactive in normal cells, but is overexpressed in several cancers (8). Chronic UPR activation leads to increased expression of EnR chaperones, such as BiP (GRP78/HSAP5), $p58^{IPK}$ and calreticulin that facilitate protein folding and promote survival, proliferation, angiogenesis, and resistance to chemotherapy and endocrine therapy (9-12). In the widely studied "reactive mode", the UPR in tumor cells is activated in response to accumulation of stress from rapid cell division, hypoxia and therapy. A few studies in immune cells describe a different type of UPR activation; in this "anticipatory mode", the UPR is activated in the absence of EnR stress and prior to the accumulation of unfolded proteins (13, 14). We explored whether estrogen induces anticipatory activation of the UPR in the absence of EnR stress, increasing protein folding capacity prior to the increased protein production and protein folding load that accompanies activation of the genomic estrogen-ERα cell proliferation program. Previous studies of the UPR and of estrogen-ERα action focused on the estrogen-inducible UPR gene, XBP1. XBP1 binds to and activates ERα; XBP1 expression is associated with tamoxifen resistance in $ER\alpha^+$ breast cancer (15-18).

The plasma membrane enzyme phospholipase C γ (PLCγ) hydrolyzes PIP2 to diacyglycerol (DAG) and inositol 1,4,5-triphosphate (IP_3). We show that the mitogen estrogen, 17β-estradiol (E_2), acting through a rapid extranuclear action of ERα, elicits a

PLCγ-mediated opening of EnR IP_3R calcium channels, increasing cytosol calcium and triggering anticipatory activation of each arm of the UPR. Opening the IP_3R calcium channel and activating the ATF6α arm of the UPR, resulting in BiP induction, are important for subsequent E_2-ERα induced cell proliferation. Consistent with an important role in cancer for anticipatory activation of the UPR, analysis of data from ~1,000 $ER\alpha^+$ breast cancer patients demonstrates that elevated expression of a UPR gene signature is tightly correlated with subsequent resistance to tamoxifen therapy, time to tumor recurrence and poor survival.

MATERIALS AND METHODS

Cell Culture and Reagents

Cell culture medium and conditions were previously described (19-21). MCF-7, T47D, and T47D-kBluc cells were obtained from the ATCC. Drs. S. Kaufmann and K. Korach provided PEO4 cells and BG-1 cells, respectively. E2, 4-OHT, U73122, 2-APB, and tunicamycin were from Sigma Aldrich. ICI 182,780 was from Tocris Biosciences and ryanodine was from Santa Cruz Biotechnology. Phospho-eIF2α (#3398), eIF2α (#5324), Phospho-PERK (#3179), PERK (#5683), and BiP (#3177) antibodies were from Cell Signaling. Pan-IP3R (sc-28613), XBP1 (sc-7160), and ERα (sc-56836) antibodies were from Santa Cruz Biotechnology. Other antibodies used were ATF6α (Imgenex) and β-Actin (Sigma).

Cell Proliferation Assays

Cells proliferation assays were carried out as described (19-21).

Protein Synthesis

Protein synthesis was evaluated by measuring incorporation of 35S-Methionine into newly synthesized protein. Cells were incubated in 96 well plates for 20 minutes with 3 μCi of 35S-methionine per well (PerkinElmer), lysed, and clarified by centrifugation. The appropriate volume, normalized to total protein, was spotted onto Whatman 540 filter paper discs and immersed in cold 10% TCA and washed in 5% TCA. Trapped protein was solubilized and filters counted.

Calcium Imaging

Cytoplasmic Ca^{2+} concentrations were measured using the calcium-sensitive dye, Fluo-4 AM (22, 23). Cells were grown on 35 mm-fluorodish plates (World Precision Instruments) for two days prior to experiments. Cells were loaded with 5 μM Fluo-4 AM (Life Technologies) in buffer (140 mM NaCl, 4.7 mM KCl, 1.13 mM MgCl2, 10 mM HEPES, 10 mM Glucose, pH = 7.4) for 30 minutes at 37 ^{o}C. The cells were washed three times with this buffer and incubated with either 2 mM or 0 mM CaCl2 for 10 minutes. Images were captured for one minute to determine basal fluorescence intensity, and then the appropriate treatment was added. Measurements used a Zeiss LSM 700 confocal microscope with a Plan-Four 20X objective (N.A. = 0.8) and 488-nM laser excitation (7% power). Images were obtained through monitoring fluorescence emission at 525 nM, and analyzed with AxioVision and Zen software (Zeiss).

Luciferase Assays, qRT-PCR, and siRNA Transfections

Reporter gene assays and qRT-PCR were previously described (19, 20). siRNA knockdowns were performed using DharmaFECT1 Transfection Reagent and 100 nM ON-TARGETplus non-targeting pool or SMARTpools for ERα (ESR1), PLCγ (PLCG1), PERK (EIF2AK3), ATF6α (ATF6α), XBP1, or pan-IP3R (Dharmacon). The pan-IP3R SmartPool consisted of three individual SmartPools, each at 33 nM, directed against each isoform of the IP3R (ITPR1, ITPR2, and ITPR3).

MCF-7 Xenograft

Experiment were approved by the Institutional Animal Care Committee (IACUC) of the University of Illinois at Urbana-Champaign. The MCF-7 cell mouse xenograft model has been described previously (24). Estrogen pellets (1 mg:19 mg estrogen:cholesterol) were implanted into 30 athymic female OVX mice at 7 weeks of age. Three days later, 1 million MCF-7 human breast cancer cells suspended in matrigel were subcutaneously injected into two sites on each flank, for a total of 4 tumors per mouse. When average tumor size reached 17.6 mm^2, E2 pellets were removed and a lower dose of E2 in sealed silastic tubing (1:31 estrogen:cholesterol, 3 mg total weight) was implanted. When average tumor size reached 23.5 mm2, 15 mice retained E2 silastic tubes (+E2 group) and 15 mice received silastic tubes containing only cholesterol (-E2 group). Tumors were measured every 4 days with a caliper. Tumor cross sectional area was calculated as (a/2)*(b/2)*3.14, where a and b were the measured diameters of each tumor. On termination of the experiments mice were euthanized and tumors were excised.

Tumor Microarray Data Analysis

Analysis was performed using several publically available tumors cohorts. ERα and UPR gene expression profiles of histologically normal breast epithelium (GSE20437) (25) were compared to IDC tumors from ERα$^+$ breast cancer patients (GSE20194). ERα and UPR correlation analysis was performed on 278 invasive ductal carcinoma samples (GSE20194) (26). A "UPR Gene Signature" was constructed to carry out risk prediction analysis. The UPR gene signature was evaluated for its ability to predict: (i) tumor relapse in 261 early-stage ERα+ breast cancers (GSE6532), (ii) tumor relapse in 474 ER + patients receiving solely tamoxifen therapy for 5 years (GSE6532, GSE17705) (27, 28), and (iii) overall survival in a mixed-cohort of 236 breast cancer patients (GSE3494) (29). Microarray data analysis was performed using BRB ArrayTools (version 4.2.1) and R software version 2.13.2. Gene expression values from CEL files were normalized by use of the standard quantile normalization method (30). Pearson correlation tests and Spearman log rank tests were used to determine gene expression correlation coefficients. Wald tests were used to test whether UPR genes were predictive of tumor recurrence and overall survival. Univariate and multivariate hazard ratios were estimated using Cox regression analysis. Covariates statistically significant in univariate analysis were further assessed in multivariate analysis. A patient was excluded from multivariate analysis, if data for one or more variables were missing. Risk prediction using the UPR gene signature was carried out using the supervised principle components method (31), and visualized using Kaplan-Meier plots and compared using log-rank tests.

Statistical Analysis

Calcium measurements are reported as mean ± SE. All other data is reported as mean ±

S.E.M. Two-tailed student's t-test used for comparisons between groups. One- way ANOVA followed by Fisher's LSD or Tukey's post hoc test used for multiple comparisons. $P < 0.05$ was considered significant.

RESULTS

Estrogen Activates all 3 Arms of the UPR

To evaluate the ability of E_2-ERα to activate the UPR, we focused on production of spliced and modified proteins that result from activating the three arms of the UPR (Figure 2.1). E_2 rapidly activated the IRE1α arm of the UPR, as shown by increases in spliced-XBP1 (sp-XBP1) mRNA in T47D and MCF-7 breast and PEO4 ovarian cancer cells (Figure 2.2A and B), and by induction of downstream sp-XBP1 targets, SERP1 and ERDJ (Figure 2.3A) (32). The antiestrogens ICI 182,780/Faslodex/fulvestrant (ICI) and 4-hydroxytamoxifen, (4-OHT), which compete with E_2 for binding to ERα, blocked the E_2-mediated increase in sp-XBP1 (Figure 2A). Consistent with E_2-ERα activating the IRE1α arm of the UPR, RNAi knockdown of ERα blocked E_2-induction of sp-XBP1 mRNA (Figure 2.2C), and induction of GREB1 by nuclear E_2-ERα (Figure 2.3B).

We next assessed whether estrogen activates the ATF6α arm of the UPR. ATF6α is a 90 kDa protein (p90-ATF6α) that translocates from the EnR to the Golgi in response to stress, where it undergoes proteolytic cleavage to its active 50 kDa form (p50-ATF6α) (Figure 2.1B) (6, 7, 33). Increased ATF6α proteolysis in T47D cells and PEO4 cells demonstrates that E_2-ERα transiently activates the ATF6α arm of the UPR (Figure 2.2D and Figure 2.3C). Since pretreatment with ICI, abolished the E_2-mediated increase in

p50-ATF6α, this effect is mediated through ERα (Figure 2.2D). Active cleaved ATF6α regulates induction of BiP and other EnR chaperones (33, 34). Consistent with this, ATF6α knockdown in T47D cells blocked BiP induction (Figure 2.2E). BiP increases EnR protein folding capacity, contributing to resolution of the stress, and helps reverse UPR activation; likely preventing the cytotoxicity that would result if UPR activation was sustained. Consistent with its antiapoptotic role, in several cancers, elevated levels of BiP are associated with a poor prognosis (9). Estrogen rapidly induced BiP mRNA in breast and ovarian cancer cells (Figure 2.2F), leading to a 2.3-fold increase in BiP protein (Figure 2.2G). RNAi knockdown of ERα prevented E_2-induction of BiP mRNA (Figure 2.2H).

PERK activation leads to inhibition of protein synthesis (Figure 2.1C). Surprisingly, E_2 induces a rapid and transient increase in PERK phosphorylation (Figure 2.4A), resulting in increased phosphorylation of eIF2α (Figure 2.4B) and a modest transient decline in overall protein synthesis (Figure 2.4C). Consistent with p-PERK catalyzing formation of p-eIF2α, PERK knockdown inhibited formation of p-eIF2α (Figure 2.4D). Consistent with E_2 acting through ERα, ICI inhibited E_2-stimulated phosphorylation of PERK and eIF2α and largely reversed the E_2-mediated inhibition of protein synthesis (Figure 2.4A, B, and C). PERK activation leads to ATF4 expression, and we observed a transient increase in ATF4 expression (Figure 2.4E). However, the proapoptotic protein CHOP was not induced because mild and transient activation of PERK does not induce CHOP (Figure 2.3D, Figure 2.4F) (35). Together, this data demonstrates that E_2, acting through ERα, activates all three UPR arms.

E_2-ERα Rapidly Increases Cytosol Ca^{2+} by a PLCγ-mediated Opening of the EnR IP_3R Ca^{2+} Channel, Activating the UPR

Rapid UPR activation by E_2-ERα suggested accumulation of unfolded protein was not triggering UPR activation. Some UPR activators, such as thapsigargin, rapidly activate the UPR by depleting Ca^{2+} stores in the lumen of the EnR, increasing intracellular Ca^{2+}. To test whether E_2 rapidly alters cytosol Ca^{2+}, we monitored cytosol calcium using the sensor dye Fluo-4 AM. In the presence or absence of extracellular Ca^{2+}, estrogen produced a rapid and transient increase in fluorescence in T47D breast cancer cells (Figure 2.5A and B). Since E_2 increases cytosol Ca^{2+} when there is no extracellular Ca^{2+}, and the EnR lumen is the major Ca^{2+} store available to increase cytosol Ca^{2+}, E_2 is acting by depleting the EnR Ca^{2+} store. Estrogen also increased cytosol calcium in PEO4 ovarian cancer cells (Figure 2.6). Inhibition of the IP_3R channel with 2-APB, which locks the IP_3R Ca^{2+} channels closed, and RNAi knockdown of the three isoforms of the IP_3R channels (Figure 2.5C), abolished the rapid E_2-ERα-mediated increase in cytosol Ca^{2+} (Figure 2.5A, B, and D). In contrast, high concentration ryanodine (Ry), which closes the ryanodine receptor (RyR) Ca^{2+} channels, did not block the increase in cytosol Ca^{2+} (Figure 2.5A and B). We next assessed whether Ca^{2+}-release was necessary for UPR activation using 2-APB and ryanodine individually, or in combination. 2-APB, but not ryanodine, inhibited E_2-ERα activation of the PERK arm of the UPR, as shown by inhibition of formation of p-eIF2α (Figure 2.7A). RNAi knockdown of IP_3R (Figure 2.5C) blocked E_2-induced Ca^{2+} release (Figure 2.5D), activation of the IRE1α arm of the UPR (Figure 2.7B), and blocked E_2-induction of BiP (Figure 2.5C), which is a commonly used surrogate readout for UPR activation.

We next tested the possibility that activation of PLCγ, which hydrolyzes PIP_2 to DAG and IP_3, plays a role in E_2-mediated opening of the IP_3R Ca^{2+} channels. Treating T47D cells with the PLCγ inhibitor, U73122, or siRNA knockdown of PLCγ, abolished the rapid E_2-ERα-mediated increase in cytosol Ca^{2+} (Figure 2.5E and Figure 2.8). Since PLCγ mediates E_2-dependent opening of the IP_3R Ca^{2+} channels and calcium release (Figure 2.5F), we examined the effect of siRNA knockdown of PLCγ on E_2-ERα-dependent activation of the UPR. siRNA knockdown of PLCγ blocked E_2-ERα activation of the ATF6α arm of the UPR, as shown by a reduction in p50-ATF6α, and inhibition of BiP induction (Figure 2.5E).

To evaluate the role of ERα in the E_2-mediated increase in cytosol calcium, we performed siRNA knockdown. In T47D cells, RNAi knockdown of ERα, in the absence of extracellular Ca^{2+}, prevented E_2-stimulated calcium release (Figure 2.5G and H). PLCγ is on the inner leaflet of the plasma membrane and the E_2-ERα-mediated increase in cytosol Ca^{2+} occurs in <2 min. Thus, the E_2-ERα-mediated increase in intracellular Ca^{2+} that leads to UPR activation is a rapid, extranuclear action of ERα at the plasma membrane.

The UPR and E_2-ERα Action in E_2-ERα Stimulated Cell Proliferation

We explored the role of Ca^{2+}-release from the EnR in promoting E_2-ERα induced gene expression, UPR activation, and subsequent cell proliferation. Consistent with a possible role for intracellular Ca^{2+} in E_2-ERα action (36), chelating intracellular Ca^{2+} with BAPTA-AM blocked E_2-stimulated cell proliferation (Figure 2.9A). In T47D cells, PLCγ or

IP_3R knockdown, or locking IP_3R with 2-APB, strongly inhibited the increase in cytosol Ca^{2+} (Figure 2.5A, B, D and F), UPR activation (Figure 2.5C and E, Figure 2.7), and E_2-ERα stimulated cell proliferation (Figure 2.9A and B). However, IP_3R knockdown did not inhibit E_2-dependent down-regulation of ERα or E_2-induction of GREB1 or pS2 mRNA (Figure 2.9C; Figure 2.10B) (37, 38). Similarly, 2-APB did not abolish E_2-ERα induced expression of stably transfected ERE-luciferase in T47D cells, while 2-APB and Ry together, strongly inhibited reporter gene expression (Figure 2.9D). This suggests there are different intracellular Ca^{2+} requirements for E_2-ERα-mediated UPR activation and E_2-ERα-mediated gene expression. Importantly, the IP_3R knockdown data uncouples UPR activation from E_2-ERα-mediated gene expression, and demonstrates that blocking UPR activation is sufficient to inhibit estrogen-stimulated cell proliferation.

We next evaluated the role of E_2-induction of EnR chaperones in E_2-ERα stimulated cell proliferation. Knockdown of PLCγ or IP_3R strongly inhibited E_2-induction of BiP and E_2-ERα stimulated cell proliferation (Figure 2.5C and E, Figure 2.9A). Knockdown of the primary UPR regulator of EnR chaperones, ATF6α, also strongly inhibited E_2- induction of BiP and E_2-ERα stimulated cell proliferation (Figure 2E and 9A). Thus, UPR activation and subsequent induction of EnR chaperones plays an important role in E_2- ERα stimulated cell proliferation.

We further evaluated the effects of PLCγ, IP_3R, ATF6α, XBP1, and PERK knockdown on E_2-stimulated proliferation of MCF-7 cells (Figure 2.11). Knockdown of the ATF6α and XBP1 arms of the UPR produced 40% declines in E_2-stimulated in cell proliferation, while PERK knockdown had no effect (Figure 2.10E). IP_3R knockdown produced a 50% decline

in E_2-ERα stimulated MCF-7 cell proliferation (Figure 2.9E). This is consistent with the 40% decline in proliferation following 2-APB treatment (Figure 2.10C), which did not fully abolish E_2-induction of pS2 and GREB1 mRNA (Figure 2.9F; Figure 2.10D). Targeting IP_3R in MCF-7 cells produced less dramatic inhibition of E_2-ERα stimulated cell proliferation compared to T47D cells or BG-1 ovarian cancer cells (Figure 2.9A, B, E; Figure 2.10C and E). Knockdown of PLCγ in MCF-7 cells nearly abolished E_2-ERα stimulated cell proliferation (Figure 2.9E). Together, this data demonstrates that weak anticipatory activation of the UPR, resulting in induction of chaperones, plays an important role in E_2-ERα-stimulated cell proliferation. This novel E_2-ERα pathway leading to cancer cell proliferation is shown (Figure 2.9G).

E_2-ERα Action Increases Levels of UPR Sensors and Downstream Targets

We investigated whether E_2-ERα facilitates UPR activation by inducing the sensors that trigger activation of the three UPR arms. E_2 rapidly induced mRNAs encoding sensors for all 3 UPR arms and the chaperones BiP and GRP94 (Figure 2.12A). These were early responses, usually visible within 2 hours. Although some responses declined at later times, estrogen produced sustained increases in resident chaperones and some UPR components, such as eIF2α (Figure 2.12A).

E_2-ERα-regulated Gene Expression and UPR Activation are Correlated In Vivo

To assess *in vivo* relevance, we used growing MCF-7 tumors receiving estrogen and regressing MCF-7 tumors receiving only cholesterol vehicle (Figure 2.12B) and

compared expression of classical measures of E_2-ERα activity to markers of UPR activation (24). In the +E_2 tumors, the markers for E_2-ERα activity, pS2 and GREB1 mRNAs (37, 38), were induced 12-fold and 17-fold and all three UPR arms were moderately activated (Figure 2.12C and D). Consistent with activation of the IRE1α arm of the UPR, active sp-XBP1 increased 3-fold while inactive XBP1 declined (Figure 2.12D). Consistent with E_2-activation of the ATF6α arm of the UPR, +E_2 tumors displayed 2.0 and 1.8-fold increases in BiP and GRP94 mRNAs, respectively (Figure 2.12D). Levels of CHOP and GADD34 mRNA were 2.1-fold and 1.4-fold higher in the +E_2 group, respectively, indicating weak activation of the PERK arm (Figure 2.12D). While levels of primary UPR sensors IRE1α and PERK were reduced in these tamoxifen-sensitive tumors, their immediate targets eIF2α and sp-XBP1 were increased (Figure 2.12D).

To assess UPR activity early in ERα^+ breast cancer development, we compared E_2-ERα activity and UPR pathway activity in samples of histologically normal breast epithelium and invasive ductal carcinoma (IDC). Compared to normal epithelium from IDC patients, IDC samples displayed elevated levels of ERα mRNA and E_2-ERα induced pS2 and GREB1 mRNAs, and reduced levels of E_2-ERα downregulated IL1-R1 mRNA (Figure 2.12E). IDC samples displayed elevated SERP1 mRNA, a marker for IRE1 activation (32); CHOP and GADD34, which are markers of PERK activation; and BiP and GRP94 chaperones, which are markers of ATF6α activation (Figure 2.12F). These data suggest UPR activation occurs very early in tumor development.

Using data from an independent cohort of 278 ERα^+ breast cancers we explored whether expression of ERα mRNA and protein, or E_2-ERα-regulated genes, correlates with

expression of UPR genes. Expression of several UPR genes displayed highly significant correlation with expression of ERα and ERα-target genes (Table 2.1).

Prior Estrogen Activation of the UPR Protect Cells from Subsequent Exposure to Cell Stress

Weakly activating, non-toxic, concentrations of the UPR activator, tunicamcyin (TUN), elicit an adaptive stress response that increases EnR chaperones, and renders cells resistant to subsequent exposure to an otherwise lethal concentration of tunicamycin (35, 39). Consistent with weak E_2 activation of the UPR, E_2 induces a 2.3-fold increase in BiP protein compared to a 5.5-fold increase in BiP following maximal UPR activation by a lethal concentration of tunicamycin (Figure 2.2G and Figure 2.13). We tested whether prior exposure of T47D cells to E_2, or a low concentration of tunicamycin, altered the concentration of tunicamycin required to subsequently induce substantial cell death. Pre-treating cells with estrogen or TUN had nearly identical effects; each elicited an ~10 fold increase in the concentration of tunicamycin required to induce apoptosis (Figure 2.14A). Thus, the E_2-induced weak anticipatory activation of the UPR both facilitates tumor cell proliferation and is a potential mechanism by which estrogen might protect ERα$^+$ breast tumors against subsequent apoptosis due to hypoxia, nutritional deprivation and therapy.

A UPR Gene Signature Predicts Clinical Outcome in ERα Positive Breast Cancer

To explore UPR activation as a potential prognostic marker in ERα$^+$ breast cancer, we developed a UPR gene signature consisting of genes encoding components of the UPR pathway and downstream targets of UPR activation (Table 2.2). Using data from 261

ERα+ breast cancer patients, each assigned to a high- or low-genomic UPR grade, we observed reduced time to relapse for patients overexpressing the UPR signature (hazard ratio (HR) = 5.5, 95% CI: 3.1-9.8) (Figure 2.15A and B). To evaluate the UPR signature in patients undergoing tamoxifen therapy, samples collected from 474 ERα+ breast cancer patients, prior to starting 5-years of tamoxifen therapy, were assigned to low, medium, or high UPR risk groups. Increased prior expression of the UPR gene signature was tightly correlated with subsequent reduced time to recurrence (Figure 2.14B and D; Figure 2.15C). Hazard ratios increased from 2.2 to 3.7 for the medium and high-risk groups, respectively, suggesting that recurrence risk is sensitive to levels of the UPR gene signature (Figure 2.14B). The UPR index provides prognostic information beyond current clinical covariates. In a cohort of 236 ERα+ breast cancer patients, UPR overexpression was strongly predictive of reduced survival (HR 2.69, 95% CI: 1.3-5.6), over and above clinical covariates alone (tumor grade, node involvement, tumor size and ERα status) (Figure 2.14C and D; Figure 2.15D). Thus, the UPR index is a powerful prognostic gene signature in ERα+ breast cancer with predictive power to stratify patients into high and low risk groups.

DISCUSSION

In contrast to the well-studied “reactive mode” of UPR activation that occurs in response to endoplasmic reticulum stress, there are few studies of UPR activation that anticipates the future need for increased capacity to fold and sort proteins, and occurs in the absence of endoplasmic reticulum stress (7). Anticipatory UPR activation is observed in B-cell differentiation where UPR activation in plasma cells precedes the massive

production and secretion of immunoglobulins (13, 14). Because the signals responsible for anticipatory activation of the UPR are largely unknown, it is poorly understood.

In the absence of cell stress or misfolded proteins, the mitogen, estrogen, acting via ERα, triggers anticipatory activation of the UPR in breast and ovarian cancer cells. In less than 2 minutes, E_2-ERα triggers PLCγ-mediated opening of EnR IP_3R calcium channels and release of Ca^{2+} into the cytosol. This increase in cytosol Ca^{2+} stimulates activation of all three arms of the UPR and is required for E_2-ERα-stimulated cell proliferation.

Anticipatory activation of the UPR by E_2-ERα enhances EnR protein folding capacity, and thereby primes cells to meet the higher protein folding and sorting demands that characterize the later growth phases of the cell cycle. The major EnR chaperone BiP, plays a central role in EnR homeostasis, protein processing, and UPR signaling. Since BiP knockdown stimulates UPR activation and promotes EnR stress- induced apoptosis (10, 40), and cells undergoing E_2-mediated apoptosis have lower levels of chaperones (41), we assessed the consequences of abrogating the expansion of EnR protein-folding capacity by blocking anticipatory activation of the UPR. PLCγ, IP_3R or ATF6α knockdown blocked E_2-induction of BiP and inhibited E_2-ERα stimulated proliferation of T47D cells. While IP_3R knockdown nearly abolished E_2-ERα-stimulated Ca^{2+}-release from the EnR, and this blocked UPR activation, it did not inhibit E_2-ERα- mediated gene expression. Thus, inhibition of E_2-ERα-stimulated UPR activation and chaperone induction is sufficient to inhibit E_2-ERα stimulated cell proliferation. Using 2-APB and ryanodine together, or chelating intracellular calcium with BAPTA, completely abrogated the increase in intracellular calcium, and blocked E_2-ERα-regulated gene expression. Based on the

inhibitor and knockdown data, we hypothesize that very small increases in intracellular calcium are sufficient to enable E_2-ERα-regulated gene expression and that somewhat larger increases in intracellular calcium are likely required for E_2-ERα activation of the UPR. E_2-ERα induces a substantial increase in intracellular calcium, which may promote coordination between the nucleus and endoplasmic reticulum, and couple activation of the E_2-ERα genomic program with UPR activation and expansion of the EnR protein-folding capacity.

We further validated the importance of this novel extranuclear pathway of E_2- ERα action using MCF-7 cells to assess how knockdown of each pathway component affects E_2-ERα stimulated cell proliferation. PERK knockdown produced a 20% in E_2- ERα-stimulated cell proliferation, and may be required to fully activate the ATF6α arm of the UPR (42). Knockdown of the XBP1 or ATF6α produced a 40% decline in E_2-ERα stimulated cell proliferation. IP_3R knockdown produced an even larger reduction in E_2- ERα stimulated cell proliferation, while PLCγ knockdown had the largest effect. Thus, anticipatory activation of the UPR plays an important role in E_2-ERα dependent proliferation of cancer cells.

As expected (1, 3), IDC tumor samples exhibited increased ERα expression and activation compared to normal breast epithelial tissue. Consistent with a role for the UPR in this proliferative phase of early tumor development, increased UPR expression and activation was observed in IDC tumor samples. This suggests that increased UPR expression occurs early in tumor development, long before detection, diagnosis, and the initiation of treatment.

Activation of the UPR by E_2-ERα exerts a long-term impact on the pathology of ERα

positive breast cancer. Weak activation of the UPR by estrogen, or by tunicamcyin, elicits an adaptive response that protects cells from subsequent exposure to higher levels of cell stress. We explored whether the effects of E_2-ERα on the UPR correlated with clinical resistance to tamoxifen therapy. Increased UPR activation and elevated expression of UPR components were predictive of a poor response to tamoxifen-therapy, shorter time to recurrence, and decreased overall survival. If UPR expression promotes resistance to tamoxifen therapy, some UPR genes should exhibit differential regulation in our tamoxifen-sensitive MCF-7 tumors (24), compared to their expression in the tamoxifen-resistance gene signature. Supporting this view, several genes encoding UPR components were E_2-downregulated in tamoxifen-sensitive MCF-7 tumors, but elevated in the human tumors expressing the tamoxifen-resistance gene signature (PERK, $p58^{IPK}$).

For ERα^+ breast cancers resistant to endocrine therapies, an important objective is development of more specific biomarkers that predict therapeutic response and identification of new therapeutic targets. The UPR is a new biomarker and therapeutic target in ERα^+ breast cancer; validated through mechanistic studies in culture, a mouse xenograft, and bioinformatics analysis of patient tumor samples. Anticipatory estrogen activation of the UPR is a novel extranuclear action of ERα, a previously undescribed early component of the estrogen-ERα cell proliferation program and a new paradigm by which estrogens may influence tumor development and resistance to therapy.

FIGURES AND TABLES

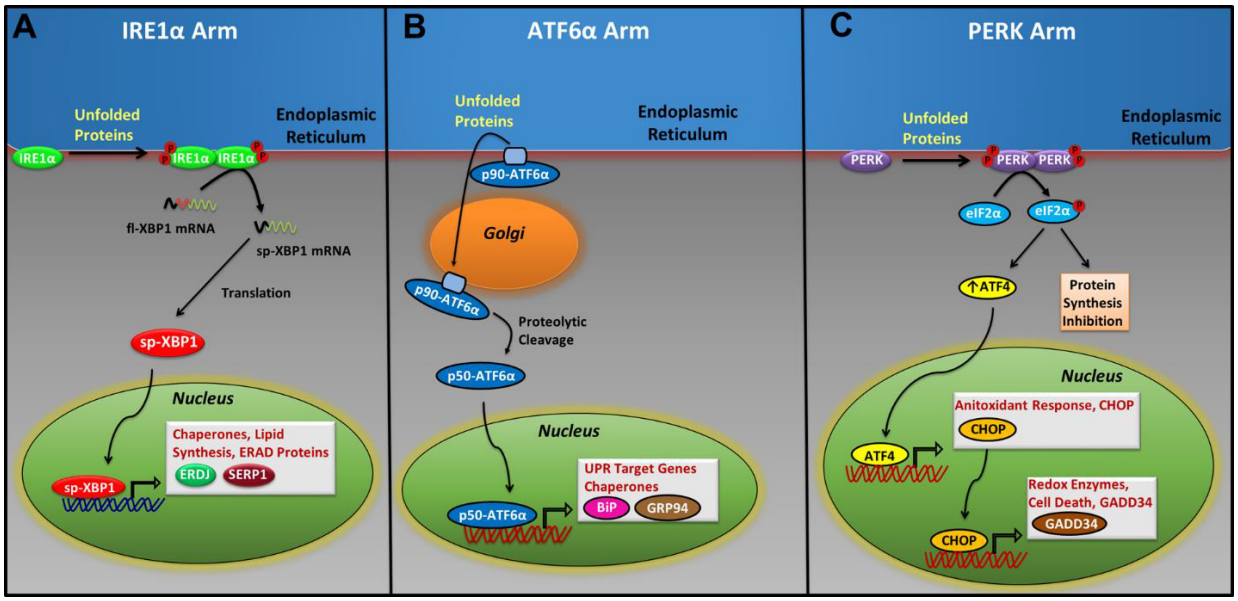

Figure 2.1. Endoplasmic reticulum (EnR) stress activates the three arms of the UPR. (**A**) EnR stress induces the oligomerization, autophosphorylation, and activation of the transmembrane endoribonuclease, IRE1α. Activated IRE1α removes an intron from full-length XBP1 (fl-XBP1) mRNA, producing spliced-XBP1 (sp-XBP1) mRNA, which is subsequently translated into active sp-XBP1 protein. sp-XBP1 enhances the protein-folding capacity of the EnR, increases turnover of misfolded proteins by inducing EnR-associated degradation (ERAD) genes, and alters mRNA decay and translation (6, 7). ERDJ and SERP1 are commonly used readouts of IRE1α activation (32, 43, 44). (**B**) EnR stress activates the transmembrane protein, activating transcription factor 6 α (ATF6α). Full-length ATF6α (p90-ATF6α) translocates from the EnR to the Golgi Apparatus, where it is cleaved by site-1 and site-2 proteases, resulting in the release of a 50-kDa ATF6α (p50-ATF6α) fragment into the cytosol. p50-ATF6α enters the nucleus and induces several UPR genes including BiP, GRP94, calreticulin, and other EnR chaperones (34). (**C**) EnR stress induces the oligomerization, autophosphorylation, and activation of the transmembrane kinase PERK (6, 7). P-PERK phosphorylates eukaryotic initiation factor 2α (eIF2α), leading to general inhibition of protein synthesis and a reduction in the endoplasmic reticulum protein folding load. However, increased eIF2α phosphorylation also leads to preferential translation of certain mRNA, including the transcription factor, ATF4 (6, 7). Increased translation of ATF4 induces the transcription factor CHOP, which induces GADD34 and several pro-apoptotic genes. Inhibition of protein synthesis is normally reversed by inactivating PERK and dephosphorylating eIF2α. $p58^{IPK}$ binds PERK, inhibiting PERK activation, and GADD34 forms a phosphatase complex with protein phosphatase 1 (PP1), which dephosphorylates eIF2α (45-47).

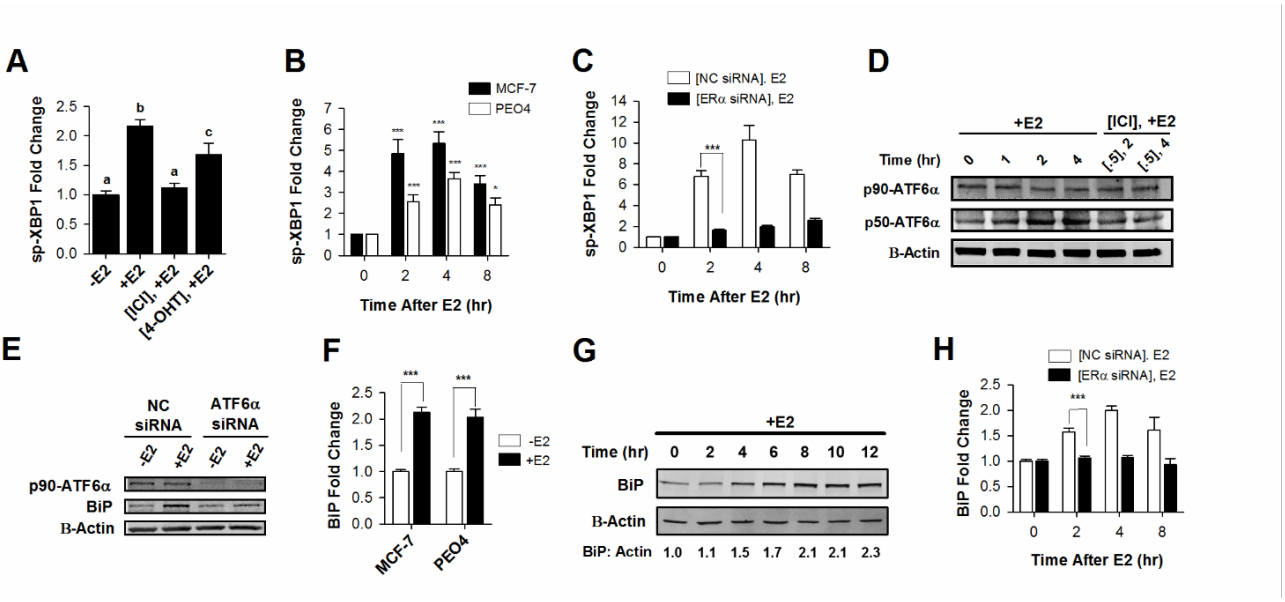

Figure 2.2. E_2-ERα activates the IRE1α and ATF6α arms of the UPR in breast and ovarian cancer cells, resulting in the induction of the major EnR chaperone, BiP. (**A**) qRT-PCR comparing the effect of estrogen (E2), ICI 182,780 (ICI) and 4- hydroxytamoxifen (4-OHT) on E_2-ERα induction of spliced-XBP1 (sp-XBP1) in T47D breast cancer cells (n = 3; -E_2 set to 1). Different letters indicate a significant difference among groups ($p < 0.05$) using one-way ANOVA followed by Tukey's post hoc test. (**B**) qRT-PCR showing the effect of E_2-ERα on sp-XBP1 mRNA in MCF-7 breast and PEO4 ovarian cancer cells (n = 3; -E_2 set to 1). P-values testing for significance between indicated group and -E2 group**.** (**C**) RNAi knockdown of ERα abolishes E_2-induction of sp-XBP1 in MCF-7 cells (n = 3). Cells treated with 100 nM non-coding control (NC) or ERα siRNA SmartPools for 3 days, followed by E_2 treatment for the indicated times (**D**) Western blot analysis showing full-length 90 kDa ATF6α (p90-ATF6α) and proteolytically cleaved 50 kDa ATF6α (p50-ATF6α) in E_2-treated T47D breast cancer cells. (**E**) RNAi knockdown of ATF6α blocks E_2-induction of BiP in T47D cells. Cells treated with 100 nM non-coding control (NC) or ATF6α siRNA SmartPool for 3 days, followed by E_2 treatment for 4 hours. (**F**) qRT-PCR showing the effect of E_2 on BiP mRNA in MCF-7 cells and in PEO4 ovarian cancer cells (n = 3; -E_2 set to 1). (**G**) Western blot analysis of BiP protein levels in MCF-7 cells treated with E_2. The fold- change in BiP protein levels is shown below each lane and was determined by quantifying BiP and β-Actin signals, and calculating the ratio of BiP/β-Actin (t=0, [-E_2], set to 1). (**H**) RNAi knockdown of ERα abolishes E_2-induction of BiP in MCF-7 cells (n = 3). Cells treated with 100 nM non-coding control (NC) or ERα siRNA SmartPools for 3 days, followed by E_2 treatment for the indicated times. Concentrations: E_2, 1 nM (A, D), 10 nM (B, C, E-H); ICI, 1 μM (A, D); 4-OHT, 1 μM (A). Data is mean ± S.E.M. * $p < 0.05$; ** $p < 0.01$; *** $p < 0.001$.

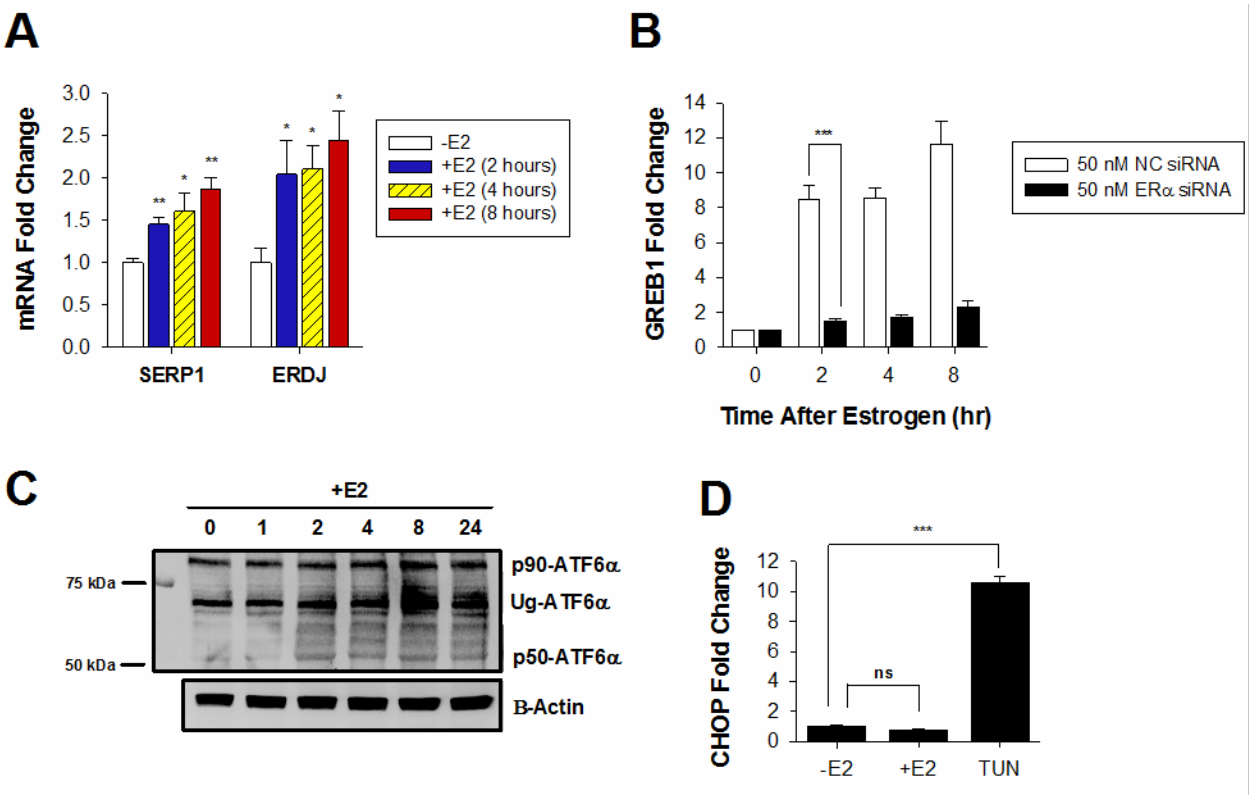

Figure 2.3. E_2-ERα induces the UPR. (**A**) E_2-ERα stimulates induction of downstream transcriptional targets of spliced-XBP1, SERP1 and ERDJ.(32, 43, 44) The increase in SERP1 and ERDJ mRNA coincides with increased splicing of XBP1 mRNA, which together indicate that E_2-ERα stimulates activation of the IRE1α-arm of the UPR. -E_2 treatment set to 1. P-values testing for significance between indicated group and -E2 group**.** (**B**) ERα knockdown abolishes E_2-induction of GREB1 (growth regulated by estrogen in breast cancer 1) mRNA, which is a well-established transcriptional target of E_2-ER (38, 48). (**C**) E_2-ERα activates the ATF6α arm of the UPR in PEO4 ovarian cancer cells. The increase in the level of p50-ATF6α (p50-ATF6α) demonstrates activation of the ATF6α arm of the UPR. Ug-ATF6α band represents the unglycosylated or underglyosylated precursor of p90-ATF6α, which has been described previously (49). (**D**) qRT-pCR analysis of CHOP mRNA following treatment of MCF-7 cells with E_2, or the UPR activator tunicamycin (TUN). Concentrations: E_2, 10 nM; TUN, 10 µg/mL. Data is mean ± SEM. * $P < 0.05$; ** $P < 0.01$; *** $P < 0.001$; ns, not significant.

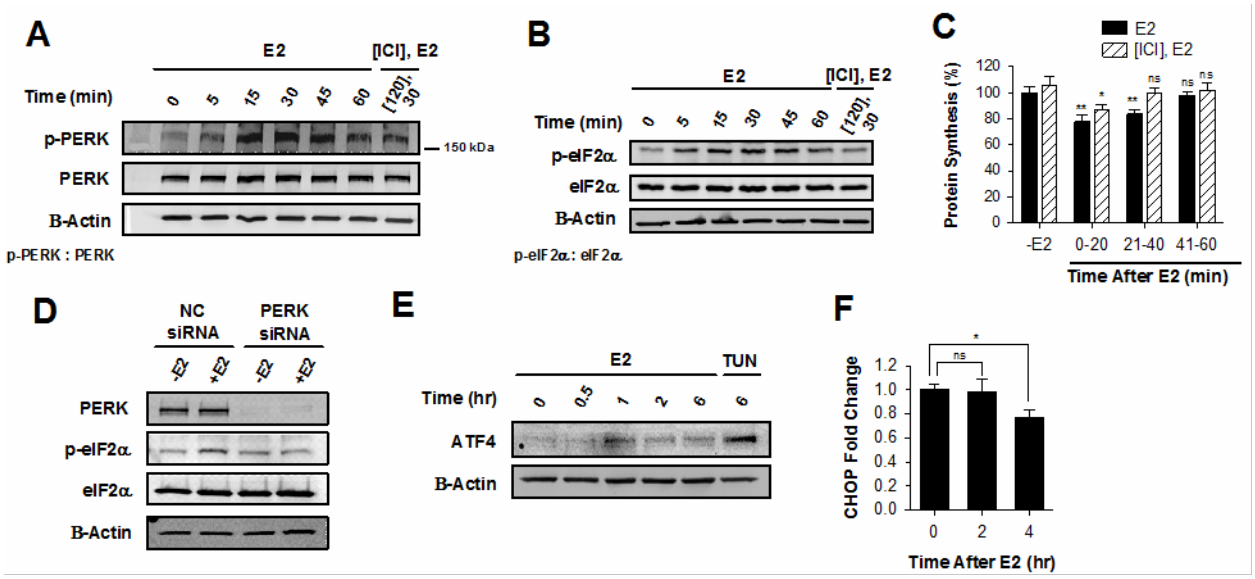

Figure 2.4. E_2-ERα activates the PERK arm of the UPR. Western blot analysis showing (**A**) p-PERK and total PERK levels and (**B**) p-eIF2α levels and total eIF2α levels in T47D cells treated with ICI 182,780 (ICI) or a vehicle control for 2 hours, followed by treatment with 10 nM 17β-estradiol (E2) (n = 3). Numbers below each lane are the ratio of p-PERK/PERK or p-eIF2α/eIF2α normalized to the vehicle-treated control. (**C**) Protein synthesis in ERα$^+$ T47D breast cancer cells treated with ICI 182,780 (ICI) or a vehicle control for 2 hours, followed by treatment with 10 nM 17β-estradiol (E2) (n = 3). P-values testing for significance between indicated groups and -E2 samples. (**D**) PERK knockdown inhibits downstream phosphorylation of eIF2α in T47D cells. (**E**) Western blot analysis of ATF4 following treatment of T47D cells with E_2, or the UPR activator tunicamycin (TUN). (**F**) qRT-pCR analysis of CHOP mRNA following treatment of T47D cells with E_2. Brackets denote pre-treatment with ICI for 2 hours. Concentrations: E_2, 1 nM (A-F); ICI, 1 μM (A, B, C); TUN, 10 μg/mL (E). Data is mean ± SEM. * $p < 0.05$; ** $p < 0.01$; *** $p < 0.001$; ns, not significant.

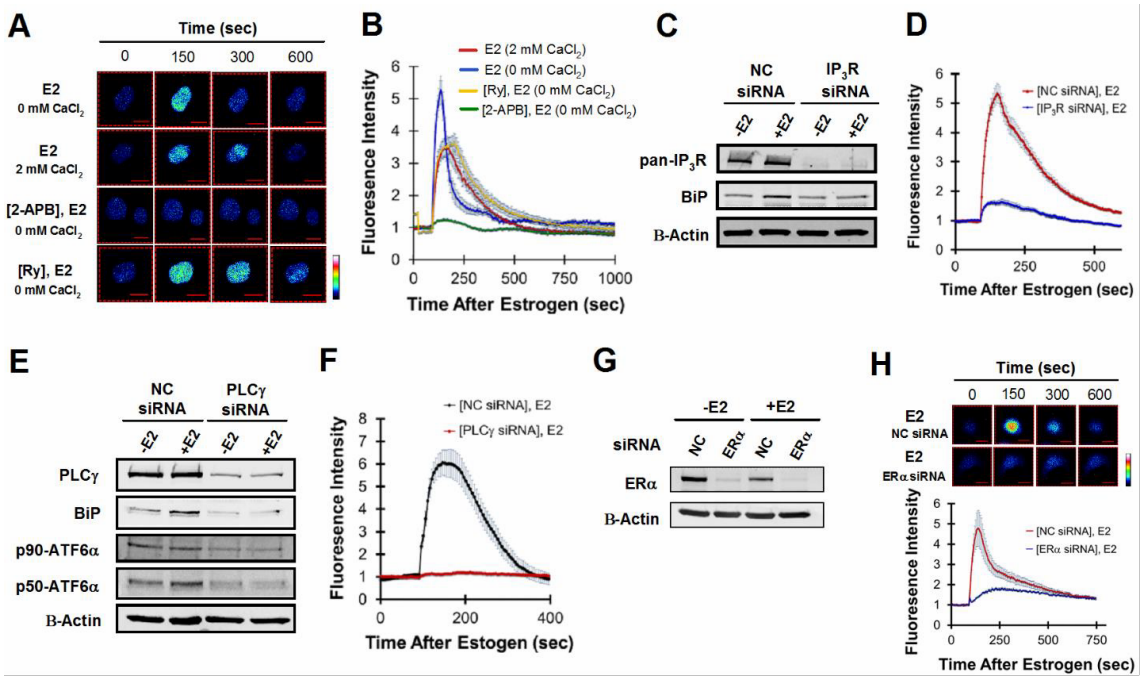

Figure 2.5. Estrogen stimulates the release of calcium from the endoplasmic reticulum, and this calcium release is necessary for UPR activation. (**A**) Effects of 300 nM estrogen (E2) on cytosolic calcium levels in T47D breast cancer cells conditioned in the presence (2 mM $CaCl_2$) or absence (0 mM $CaCl_2$) of extracellular calcium, or cells pre-treated with 2-APB or ryanodine (Ry) for 30 minutes in the absence of extracellular calcium (0 mM $CaCl_2$). Visualization of intracellular Ca^{2+} using Fluo-4 AM. Colors from basal Ca^{2+} to highest Ca^{2+}: Blue, green, red, white. (**B**) Graph depicts quantitation of cytosolic calcium levels in ERα^+ T47D breast cancer cells treated with E_2 in the presence or absence of extracellular calcium, and in cells pre-treated with 2-APB or ryanodine (Ry) in the absence of extracellular calcium (n = 10 cells). E_2 was added at 60 sec, and fluorescence intensity prior to 60 sec was set to 1. (**C**) Western blot analysis of IP_3R and BiP protein levels following treatment of T47D cells with either 100 nM non-coding (NC) siRNA or a IP_3R SmartPool, followed by treatment with E_2 (+E2) or ethanol-vehicle (-E2) for 4 hours. IP_3R smartpool contained 33 nM siRNA directed against each isoform of IP_3R Ca^{2+}-channel. (**D**) Quantitation of cytosolic Ca^{2+} levels in response to E_2, following treatment of T47D cells with 100 nM non-coding (NC) siRNA or IP_3R siRNA SmartPools for 3 days (n = 10 cells) (**E**) Western blot analysis of PLCγ, BiP, and ATF6α protein levels after treatment of T47D cells with 100 nM non-coding (NC) siRNA or PLCγ siRNA SmartPool, followed by treatment with E_2 (+E2) or ethanol- vehicle (-E2) for 4 hours. (**F**) Quantitation of cytosolic Ca^{2+} levels in response to E_2, following treatment of T47D cells with 100 nM non-coding (NC) siRNA or PLCγ siRNA SmartPool for 3 days. (**G**) Western blot analysis of ERα protein levels after treating T47D cells with either 100 nM non-coding (NC) siRNA or ERα siRNA SmartPool, followed by treatment with E_2 (+E2) or ethanol-vehicle (-E2) for 4 hours. (**H**) Visualization and quantitation of cytosolic Ca^{2+} levels in response to E_2 after ERα knockdown in T47D cells. Concentrations: E_2, 300 nM (A, B, D, F, H), 1 nM (C, E, G); 2- APB, 200 μM (A, B); ryanodine, 200 μM (A, B). Graphical data is mean ± SE (n = 10)). **I designed and performed research experiments, and analyzed data for the panel A, B, D, F and H.**

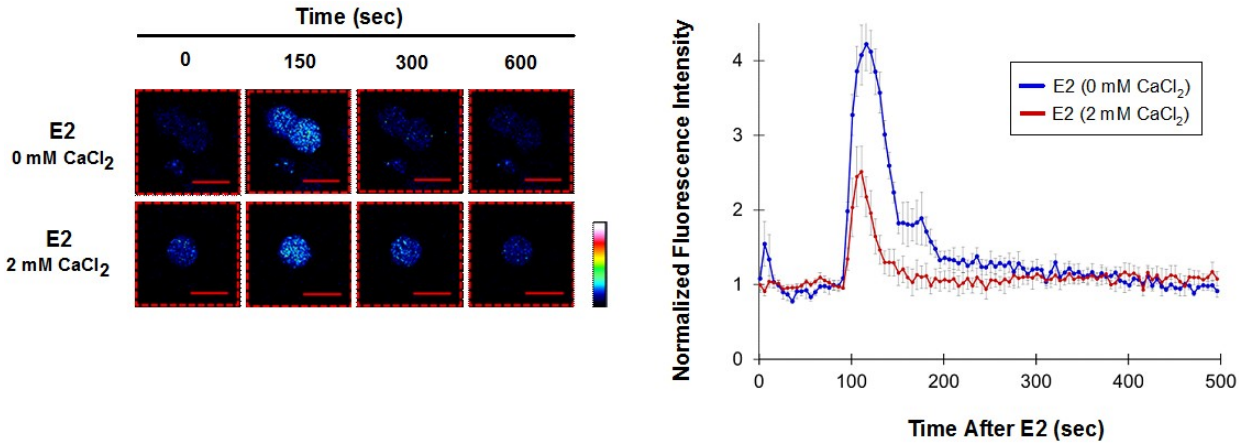

Figure 2.6. Estrogen increases intracellular calcium levels in ERα⁺ PEO4 ovarian cancer cells. Effect of 300 nM E_2 on intracellular calcium levels in ERα⁺ PEO4 ovarian cells. Cells visualized with the Ca^{2+} sensitive dye Fluor-4. Low levels of basal [Ca^{2+}] are blue and then green, whereas higher levels of [Ca^{2+}] are seen as red, with the highest levels white. The trace represents relative signal intensity averaged from 10 cells. E_2 was added at 60 sec, and fluorescence intensity prior to 60 sec was set to 1. Data is mean ± S.E.). **I designed and performed research experiments, and analyzed data for the entire figure.**

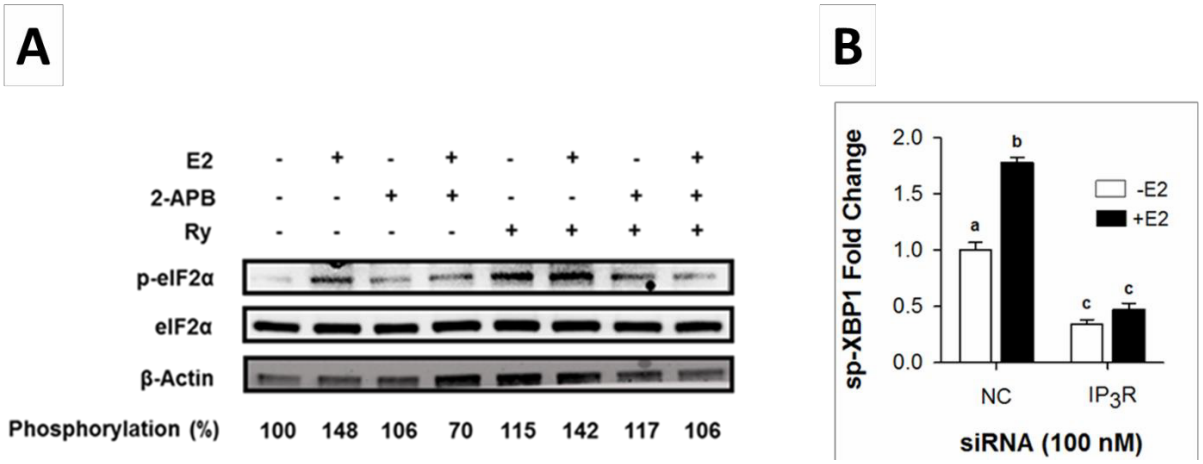

Figure 2.7. **Blocking Ca^{2+}-release from the EnR through the IP_3R Ca^{2+} channel prevents estrogen-dependent activation of the IRE1α and PERK arms of the UPR. (A)** Pre-blocking the IP_3R Ca^{2+}-channel with 2-APB prevents estrogen-dependent activation of the PERK arm of the UPR in T47D cells. Western blot analysis showing p-eIF2α and total eIF2α levels in T47D breast cancer cells pre-treated for 30 minutes with 2-APB and/or ryanodine (Ry) or a vehicle control, followed by treatment with E_2 for 30 minutes. Numbers below each lane are the ratio of p-eIF2α/eIF2α with the vehicle- treated control set at 100. **(B)** IP_3R knockdown abolishes E_2-induction of sp-XBP1 mRNA in T47D cells. Cells were treated with non-coding control (NC) or IP_3R siRNA SmartPools for 3 days, followed by E_2 treatment for 4 hours. Data is mean ± SEM. Letters indicate a significant difference among groups ($p < 0.05$) using one-way ANOVA followed by Tukey's post hoc test. Concentrations: E_2, 10 nM; 2-APB, 200 μM; Ryanodine, 200 μM.

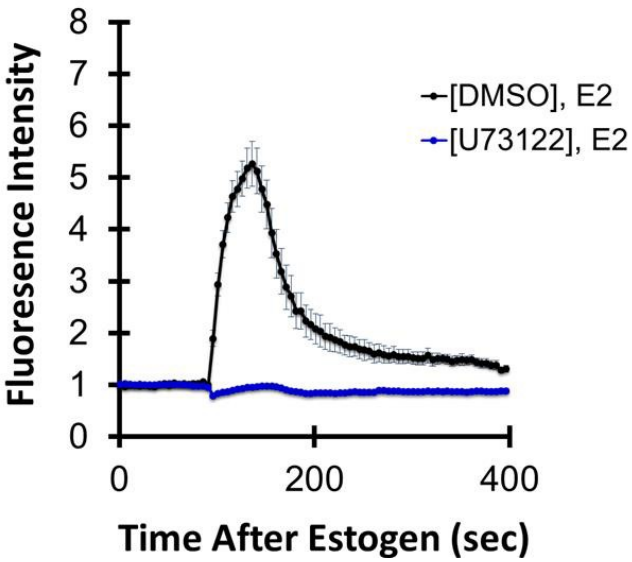

Figure 2.8. Treatment of T47D cells with the PLCγ inhibitor, U73122, blocks E_2-stimulated calcium release. Graph depicts quantitation of cytosolic calcium levels in ERα^+ T47D breast cancer cells pre-treated with DMSO vehicle or U73122, followed by treatment with 300 nM E_2 in the absence of extracellular calcium (n = 10 cells). E_2 was added at 60 sec, and fluorescence intensity prior to 60 sec was set to 1. Data is mean ± S.E.). **I designed and performed research experiment, and analyzed data for the figure.**

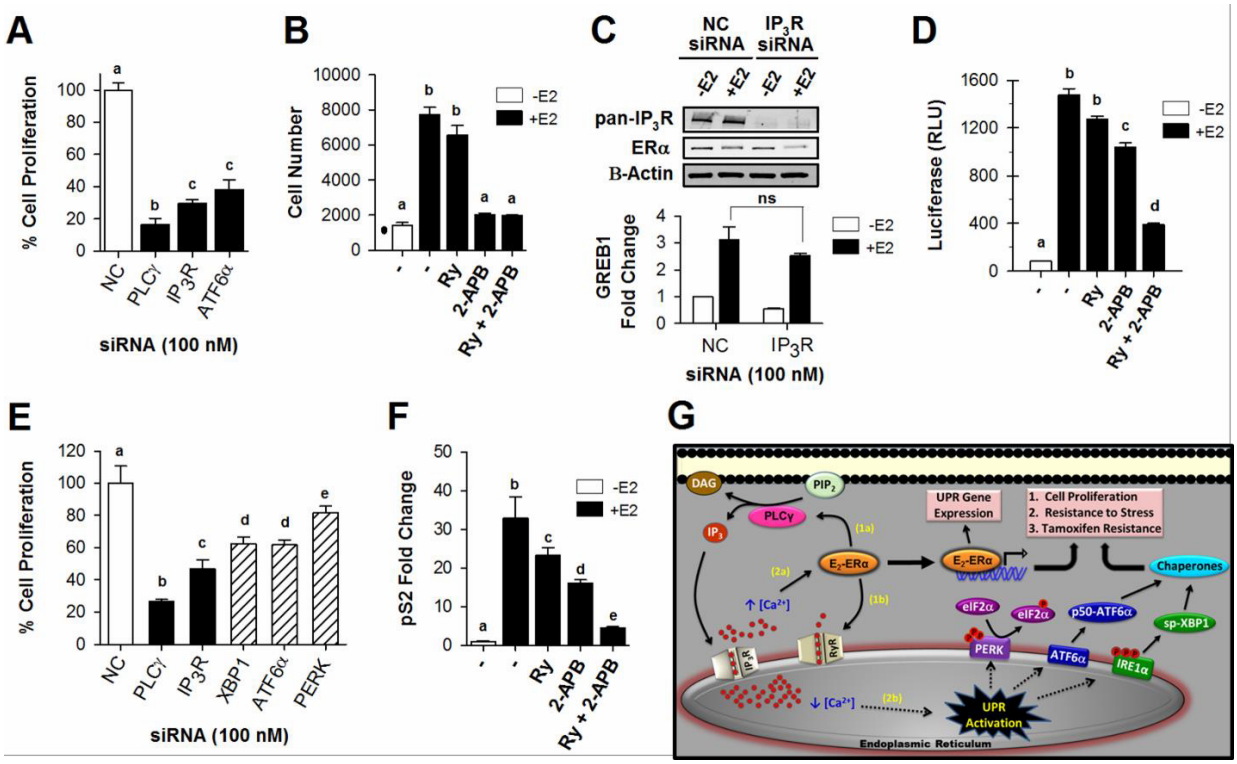

Figure 2.9. E_2-ERα induced calcium release from the EnR into the cytosol is important for E_2-ERα mediated gene expression and E_2-ERα stimulated cell proliferation. (**A**) E_2-ERα stimulated proliferation of T47D breast cancer cells treated 100 nM non-coding (NC), PLCγ, IP_3R, or ATF6α siRNA SmartPools (n = 6). (**B**) E_2-ERα stimulated proliferation of T47D breast cancer cells treated with ryanodine (Ry), 2-APB, or both inhibitors (Ry + 2-APB) for 4 days (n = 5). (**C**) qRT-PCR analysis of effects of IP_3R knockdown on E_2-ERα induction of GREB1 mRNA in T47D cells (n = 3). Western blot shows ERα protein levels after treatment of T47D cells with 100 nM non-coding (NC) siRNA or IP_3R siRNA, followed by treatment with E_2 (+E2) or ethanol-vehicle (-E2) for 4 hours. (**D**) ERE-luciferase activity in kBluc-T47D breast cancer cells treated with E_2 and either ryanodine (Ry), 2-APB, or both inhibitors for 24-hours (Ry + 2-APB) (n = 4). (**E**) E_2-ERα stimulated proliferation of MCF-7 breast cancer cells treated 100 nM non- coding (NC), PLCγ, IP_3R, ATF6α, XBP1, or PERK siRNA (n = 6). (**F**) qRT-PCR analysis of effects of ryanodine (Ry), 2-APB, or both inhibitors (Ry + 2-APB) on E_2-ERα induction of pS2 mRNA in MCF-7 cells (n = 3). (**G**) Model of E_2-ERα acting through the UPR to influence breast tumorigenesis. "•" denotes cell number at day 0. Concentrations: E_2, 100 pM (A-F); 2-APB, 200 μM (B, D, F); Ryanodine, 100 μM (B, D, F). Data is mean ± SEM. Different letters indicate a significant difference among groups ($p < 0.05$) using one-way ANOVA followed by Tukey's post hoc test. ns, not significant ($p > 0.05$).

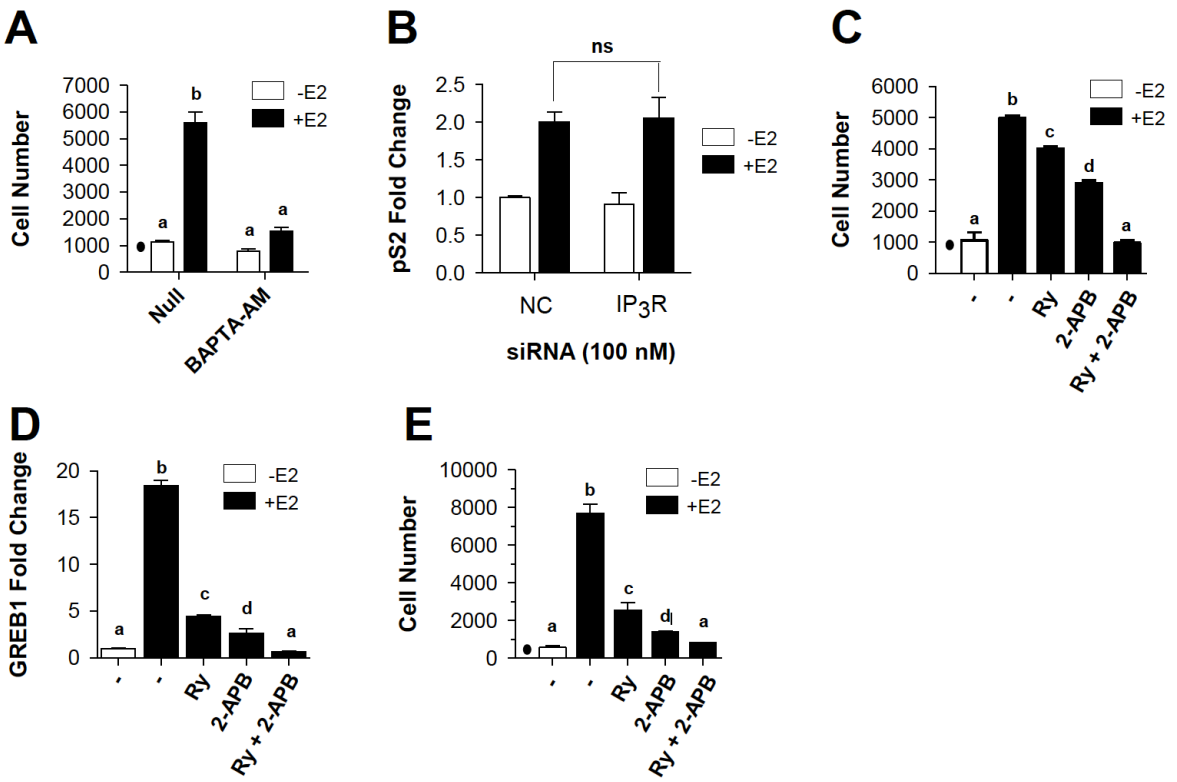

Figure 2.10. E_2-ERα induced calcium release from the EnR into the cytosol is important for E_2-ERα mediated gene expression and E_2-ERα stimulated cell proliferation. (**A**) Effects of the intracellular calcium chelator BAPTA-AM on E_2-ERα stimulated cell proliferation (n = 5). MCF-7 cells were treated with 10 μM BAPTA-AM for 3 days. (**B**) qRT-PCR analysis of effects of IP_3R knockdown on E_2-ERα induction of pS2 mRNA in T47D cells (n = 3). (**C**) E_2-ERα stimulated proliferation of MCF-7 breast cancer cells treated with ryanodine (Ry), 2-APB, or both inhibitors (Ry + 2-APB) for 4 days (n = 5). (**D**) qRT-PCR analysis of effects of ryanodine (Ry), 2-APB, or both inhibitors (Ry + 2- APB) on E_2-ERα induction of GREB1 mRNA in MCF-7 cells (n = 3). (**E**) E_2-ERα stimulated proliferation of BG-1 ovarian cancer cells treated with ryanodine (Ry), 2-APB, or both inhibitors (Ry + 2-APB) for 4 days (n = 5). "•" denotes cell number at day 0. Data is mean ± SEM. Letters indicate a significant difference among groups ($p < 0.05$) using one-way ANOVA followed by Tukey's post hoc test. * $P < 0.05$; ** $P < 0.01$; *** $P < 0.001$; ns, not significant. Concentrations: E_2, 100 pM; 2-APB, 200 μM; Ryanodine, 200 μM.

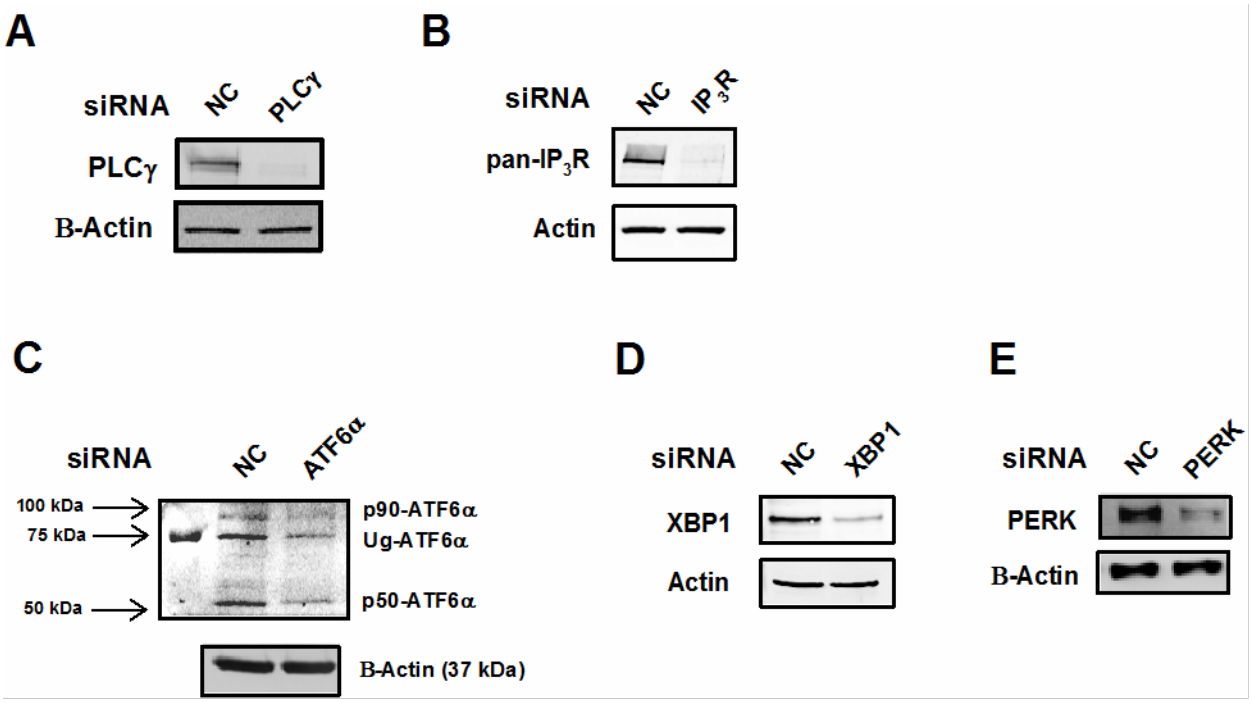

Figure 2.11. Western blot analysis of UPR proteins following siRNA knockdown in MCF-7 cells. Western blot analysis of (**A**) PLCγ, (**B**) pan-IP_3R, (**C**) ATF6α, (**D**) XBP1, and (**E**) PERK protein levels following treatment of MCF-7 cells with either 100 nM non- coding SmartPool siRNA or 100 nM SmartPool siRNA directed against the protein of interest. The IP_3R SmartPool consisted of three individual siRNAs SmartPools targeting each isoform of the IP_3R Ca^{2+}-channel (ITPR1, ITPR2, ITPR3).

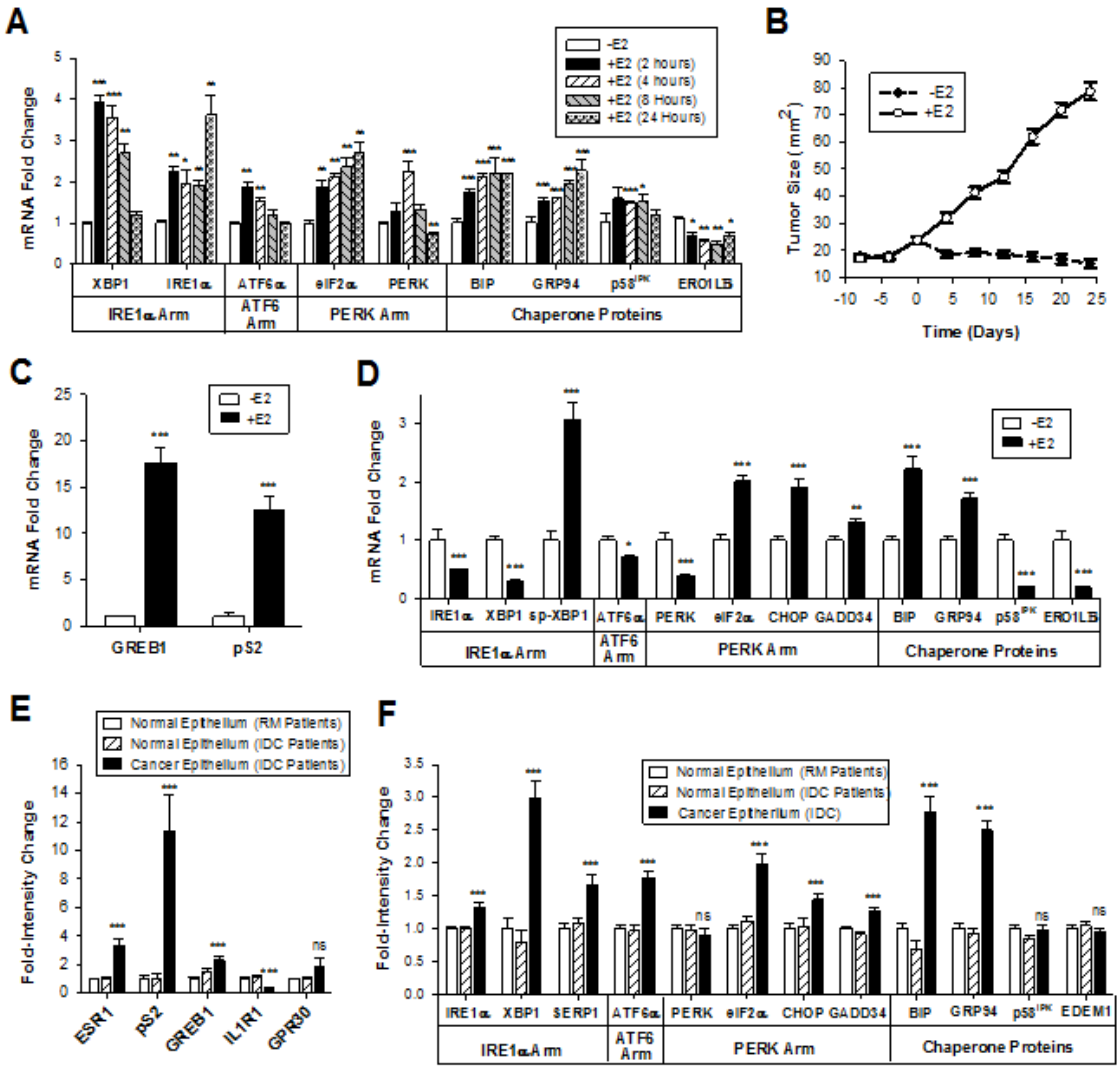

Figure 2.12. E_2-ERα activity and UPR activity are correlated *in vivo*. (**A**) qRT-PCR analysis of levels of mRNAs for each arm of the UPR after treatment of MCF-7 cells with 10 nM E_2 for the indication times (n = 3). (**B**) MCF-7 tumor growth in the presence or absence of estrogen in athymic mice. All mice were treated with estrogen to induce tumor formation. On "Day 0", E_2 in silastic tubes was replaced with silastic tubes containing only cholesterol in the $–E_2$ group (n = 15), while silastic tubes were retained in the $+E_2$ treatment group (n = 15). qRT-PCR analysis of (**C**) classical E_2-ERα regulated genes and (**D**) the UPR in mouse tumors collected after 24 days of exposure to estrogen (+E2) or vehicle-control (-E2) (n = 15). Relative mRNA levels of (**E**) classical E_2-ERα regulated genes and (**F**) the UPR pathway in patient samples of normal breast epithelium taken from patients undergoing reduction mammoplasty (RM) (n = 18), istologically normal breast epithelium taken from patients diagnosed with invasive ductal carcinoma (IDC) (n = 9), and carcinoma epithelium taken from IDC patients (n = 20). p-values represent comparisons to –E2 groups (A, C, D) or to histologically normal breast epithelium from patients who underwent reduction mammoplasty (e, f). Data is mean ± SEM. * $P < 0.05$; ** $P < 0.01$; ***$P < 0.001$; ns, not significant.

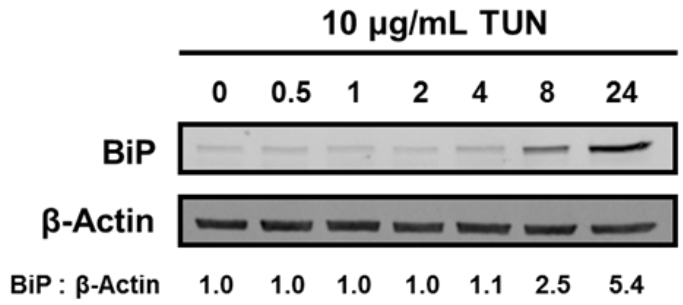

Figure 2.13 The UPR Activator, tunicamycin, induces BiP. Time course analysis of BiP protein levels following tunicamycin (TUN) treatment. Densiometric analysis performed by normalizing BiP protein levels to Actin.

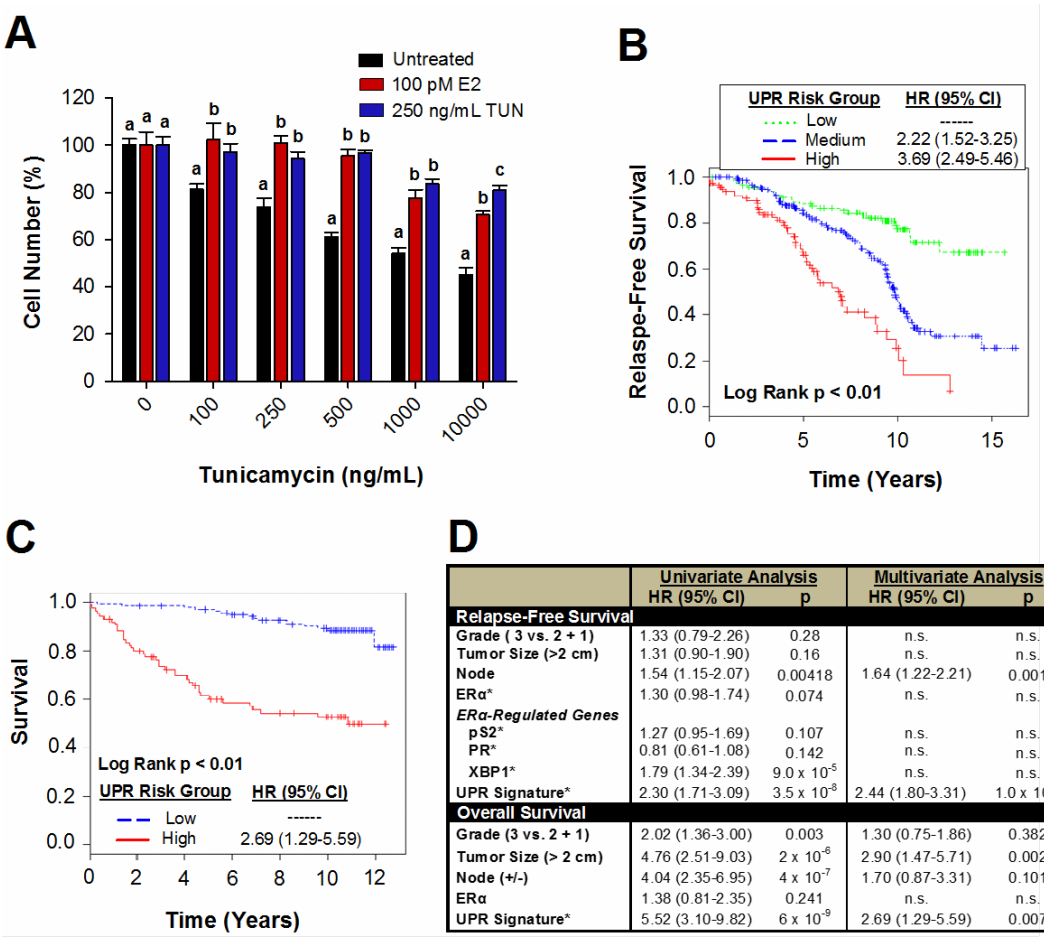

	Univariate Analysis HR (95% CI)	p	Multivariate Analysis HR (95% CI)	p
Relapse-Free Survival				
Grade (3 vs. 2 + 1)	1.33 (0.79-2.26)	0.28	n.s.	n.s.
Tumor Size (>2 cm)	1.31 (0.90-1.90)	0.16	n.s.	n.s.
Node	1.54 (1.15-2.07)	0.00418	1.64 (1.22-2.21)	0.001
ERα*	1.30 (0.98-1.74)	0.074	n.s.	n.s.
ERα-Regulated Genes				
pS2*	1.27 (0.95-1.69)	0.107	n.s.	n.s.
PR*	0.81 (0.61-1.08)	0.142	n.s.	n.s.
XBP1*	1.79 (1.34-2.39)	9.0×10^{-5}	n.s.	n.s.
UPR Signature*	2.30 (1.71-3.09)	3.5×10^{-8}	2.44 (1.80-3.31)	1.0×10^{-8}
Overall Survival				
Grade (3 vs. 2 + 1)	2.02 (1.36-3.00)	0.003	1.30 (0.75-1.86)	0.382
Tumor Size (> 2 cm)	4.76 (2.51-9.03)	2×10^{-6}	2.90 (1.47-5.71)	0.002
Node (+/-)	4.04 (2.35-6.95)	4×10^{-7}	1.70 (0.87-3.31)	0.101
ERα	1.38 (0.81-2.35)	0.241	n.s.	n.s.
UPR Signature*	5.52 (3.10-9.82)	6×10^{-9}	2.69 (1.29-5.59)	0.007

Figure 2.14. Anticipatory activation of the UPR by estrogen protects cells from subsequent cell stress, and expression of the UPR gene signature predicts relapse-free and overall survival in ERα positive breast tumor cohorts. (**A**) Weak anticipatory activation of the UPR with estrogen or tunicamycin protects cells from subsequent UPR stress. T47D cells were maintained in 10% CD-FBS for 8 days and treated with either 250 ng/ml tunicamycin (TUN), 100 pM E_2, or ethanol/DMSO-vehicle (Untreated). E_2, TUN, or the vehicle control were removed from medium, and cells were harvested in 10% CD-calf serum and treated with the indicated concentrations of tunicamycin. Data is mean ± SEM (n = 6). Different letters indicate a significant difference among groups ($p < 0.05$) using one-way ANOVA followed by Fisher's LSD post hoc test. (**B**) Relapse-free survival as a function of the UPR gene signature for patients with ERα$^+$ breast cancer who subsequently received tamoxifen alone for 5 years. Interquartile range used to assign tumors to risk groups, representing UPR activity from high to low. Hazard ratios are between low and medium and low and high UPR groups (n = 474). (**C**) Overall survival as a function of the UPR signature and clinical covariates (node status, tumor grade, ERα-status, tumor size). p-value is testing for significance between the combined model (UPR gene signature and clinical covariates) versus the covariates only model (multivariate analysis) (n = 236). (**D**) Univariate and multivariate Cox regression analysis of the UPR signature, clinical covariates, and classical estrogen-induced genes for time to recurrence and survival (n.s., not significant). Median used to classify tumors into high and low risk groups.

A

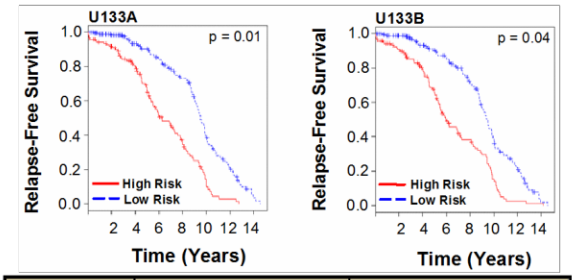

	Univariate Analysis		Multivariate Analysis	
	HR (95% CI)	p	HR (95% CI)	p
Grade	2.02 (1.36-3.00)	0.0005	1.18 (0.75-1.86)	0.441
Tumor Size	4.76 (2.51-9.03)	<0.0001	2.86 (1.44-5.68)	0.002
Node	4.04 (2.35-6.95)	<0.0001	1.70 (0.87-3.31)	0.101
ERα	1.38 (0.81-2.35)	0.241	1.30 (0.75-2.25)	0.345
UPR Signature	5.52 (3.10-9.82)	<0.0001	2.41 (1.12-5.25)	0.012

B

UPR Genes Predictive of Tumor Relapse (GSE6532)					
GeneChip	UPR Pathway	Gene	HUGO Gene	Hazard Ratio	p-Value
U133A	ATF6	ATF6	ATF6	1.91	$<1.0 \times 10^{-7}$
	PERK	eIF2α	EIF2S1	2.82	2.6×10^{-6}
		PERK	EIF2AK3	1.34	0.037
		ATF4	ATF4	1.53	0.033
		CHOP	DDIT3	3.36	5.0×10^{-7}
	Chaperones	$p58^{IPK}$	DNAJC3	1.99	8.0×10^{-7}
		BiP	HSPA5	1.73	3.3×10^{-4}
		GRP94	HSP90B1	0.54	6.6×10^{-4}
U133B	ATF6	ATF6	ATF6	1.62	$<1.0 \times 10^{-7}$
	IRE1α	RAMP4	SERP1	2.14	0.008
	Chaperones	$p58^{IPK}$	DNAJC3	2.14	2.7×10^{-6}
		BiP	HSPA5	1.70	1.4×10^{-6}
	ERAD	EDEM1	EDEM1	1.37	0.004
		HRD1	SYVN1	2.41	5.2×10^{-6}

C

UPR Genes Predictive of Tumor Relapse (GSE6532, GSE17705)					
GeneChip	UPR Pathway	Gene	HUGO Gene	Hazard Ratio	p-Value
U133A	ATF6	ATF6	ATF6	2.05	$<1.0 \times 10^{-7}$
	IRE1α	RAMP4	SERP1	1.73	2.0×10^{-7}
	PERK	eIF2α	EIF2S1	2.72	1.0×10^{-7}
		PERK	EIF2AK3	2.54	$<1.0 \times 10^{-7}$
		ATF4	ATF4	2.15	5.5×10^{-5}
		GADD34	PPP1R15A	0.46	3.2×10^{-5}
	Chaperones	$p58^{IPK}$	DNAJC3	1.49	0.009
		BiP	HSPA5	1.89	1.0×10^{-7}
		GRP94	HSP90B1	0.62	2.6×10^{-6}
	ERAD	EDEM1	EDEM1	1.59	0.021
		HERPUD1	HERPUD1	1.76	2.7×10^{-4}

D

UPR Genes Predictive of Survival (GSE3494)					
GeneChip	UPR Pathway	Gene	HUGO Gene	Hazard Ratio	p-Value
U133A	IRE1α	XBP1	XBP1	1.854	0.012
	PERK	PERK	EIF2AK3	2.043	0.027
U133B	ATF6	ATF6	ATF6	1.941	0.030
	Chaperones	BiP	HSPA5	2.108	0.022

Figure 2.15. The UPR genomic index is a new biomarker that predicts relapse free and overall survival of breast cancer patients. (**A**) Relapse rate of 261 ERα positive breast tumors, classified by expression levels of the UPR gene signature, plotted by the Kaplan-Meier method. Tumor samples were analyzed on both, U133A and U133B gene chips. The table below denotes univariate and multivariate Cox regression hazard ratios and p-values for the UPR gene signature and other clinical covariates (tumor grade, tumor size, node status). (**B**) UPR genes independently predictive of relapse ($p < 0.05$) in gene expression profiles obtained from 277 $ER\alpha^+$ positive breast cancers (27). Kaplan-Meier plots and Cox regression hazard analysis for this tumor cohort is displayed in Figure 15A. (**C**) UPR genes independently predictive of relapse in 474 gene expression microarrays taken from ERα-positive breast cancer patients prior to the initiation of tamoxifen-therapy (27, 28). Kaplan-Meier analysis and Cox regression hazard analysis for this tumor cohort are displayed in Figure 2.14B and Figure 2.14D, respectively. (**D**) UPR genes predictive of survival in 236 gene expression microarrays from breast cancer patients (29). All Kaplan-Meier plots assessing UPR risk prediction were computed using leave-one- out cross-validation. UPR signature genes shown in the tables are listed with their respective univariate Cox hazard ratio and p-value test the hypothesis if expression data is predictive of relapse or overall survival.

		ERα		ESR1		pS2		GREB1	
		Correlation Coefficient	p-Value	Correlation Coefficient	p-Value	Correlation Coefficient	p-Value	Correlation Coefficient	p-Value
IRE1α	XBP1	0.608	$<1 \times 10^{-7}$	0.817	$<1 \times 10^{-7}$	0.638	$<1 \times 10^{-7}$	0.618	$<1 \times 10^{-7}$
	SERP1	0.178	0.008	0.347	1×10^{-7}	0.213	0.006	0.371	$<1 \times 10^{-7}$
ATF6α	ATF6α	0.282	2×10^{-5}	0.397	$<1 \times 10^{-7}$	0.276	4×10^{-5}	0.341	2×10^{-7}
PERK	PERK	0.169	0.012	0.314	2×10^{-6}	0.222	0.0009	0.364	$<1 \times 10^{-7}$
	eIF2α	0.156	0.021	0.175	0.009	0.140	0.019	0.231	0.0006
	TRIB3	0.270	5×10^{-5}	0.358	$<1 \times 10^{-7}$	0.323	1×10^{-6}	0.420	$<1 \times 10^{-7}$
ERAD	EDEM	0.274	4×10^{-5}	0.387	$<1 \times 10^{-7}$	0.344	2×10^{-7}	0.274	4×10^{-5}
	HERPUD1	0.196	0.003	0.208	0.002	n.s.	n.s.	0.199	0.003
Chaperone	HSPA5	n.s.	n.s.	0.143	0.03	n.s.	n.s.	0.275	4×10^{-5}

Table 2.1. Expression of UPR genes is positively correlated with expression of ERα and ERα-regulated target-genes. Correlations between the UPR and ERα protein levels (ERα), ERα mRNA levels (ESR1), or transcriptional activity of E_2-ERα. E_2-ERα transcriptional activity was assessed using downstream target genes of E_2-ERα (pS2, GREB1) (38, 48, 50). Analysis carried out on a cohort of 278 breast cancer patients (GSE20194) (26), which consisted of 164 ERα positive tumors and 114 ERα negative tumors. Quantitation of ERα protein was by IHC. Pearson correlation coefficients and parametric p-values are shown in the table. "n.s." indicates that no significant correlation was observed. While expression of UPR genes is correlated with ERα levels and expression of ERα-regulated genes, the UPR index is not simply a surrogate marker for ERα activity. In multivariate analysis, the UPR index, but not ERα, or classical ERα-regulated genes, exhibits a statistically significant increase in hazard ratio (Figure 14D). Also, UPR index exhibits predictive power to stratify patients into high and low risk groups above ERα status (Figure 14C). Thus, while active ERα is important for expression of the UPR signature, it's the UPR signature not ERα level or activity that is predictive of reduced time to recurrence and reduced survival.

Genes Comprising UPR Gene Index		
UPR Pathway	**Pathway Components**	**Genes Indicative of UPR Arm Activation**
ATF6α	ATF6α (ATF6)	BiP (HSPA5) GRP94 (HSP90B1)
IRE1α	IRE1α (ERN1) XBP1 (XBP1)	ERDJ (DNAJB9) SERP1(RAMP4)
PERK	PERK (EIF2AK3) eIF2α (EIF2S1) ATF4 (ATF4)	CHOP (DDIT3) ERO1Lα (ERO1L) GADD34 (PPP1R15A)
EnR-Resident Chaperones	BiP (HSPA5), ERO1Lβ (ERO1LB), GRP94 (HSP90B1), $p58^{IPK}$ (DNAJC3)	
ERAD Machinery	EDEM1 (EDEM1), HERPUD1 (HERPUD1), HRD1 (SYVN1)	

Table 2.2. UPR gene signature. The table shows the genes used to construct the UPR gene signature. HUGO Gene Nomenclature Committee (HGNC) approved names for each gene are shown in parenthesis. UPR genes independently predictive either of relapse free or overall survival ($p < 0.05$) were used to construct the UPR gene signature, which was then used to carry out risk prediction analysis.

REFERENCES

1. Korach K.S. DBJ. (2006) Estrogen receptors and human disease. J Clin Inv. 116(3): 561-71.
2. Musgrove EA, Sutherland RL. (2009) Biological determinants of endocrine resistance in breast cancer. Nat Rev Cancer. 9(9): 631-43.
3. Yue W, Yager JD, Wang JP, Jupe ER, Santen RJ. (2013) Estrogen receptor-dependent and independent mechanisms of breast cancer carcinogenesis. Steroids. 78(2): 161-70.
4. (EBCTCG). EBCTCG. (2005) Effects of chemotherapy and hormonal therapy for early breast cancer on recurrence and 15-year survival: an overview of the randomised trials. Lancet. 365(9472): 1687-717.
5. Jensen EV, Jordan VC. (2003) The estrogen receptor: a model for molecular medicine. Clin Cancer Res. 9(6): 1980-9.
6. Ron D, Walter P. (2007) Signal integration in the endoplasmic reticulum unfolded protein response. Nat Rev Mol Cell Biol. 8(7): 519-29.
7. Walter P, Ron D. (2012) The unfolded protein response: from stress pathway to homeostatic regulation. Science. 334(6059): 1081-6.
8. Ma Y, Hendershot LM. (2004) The role of the unfolded protein response in tumour development: friend or foe? Nat Rev Cancer. 4(12): 966-77.
9. Luo B, Lee AS. (2013) The critical roles of endoplasmic reticulum chaperones and unfolded protein response in tumorigenesis and anticancer therapies. Oncogene. 32(7): 805-18.
10. Dong D, Ni M, Li J, Xiong S, Ye W, Virrey JJ, et al. (2008) Critical role of the stress

chaperone GRP78/BiP in tumor proliferation, survival, and tumor angiogenesis in transgene-induced mammary tumor development. Cancer Res. 68(2): 498-505.

11. Lee E, Nichols P, Spicer D, Groshen S, Yu MC, Lee AS. (2006) GRP78 as a novel predictor of responsiveness to chemotherapy in breast cancer. Cancer Res. 66(16): 7849-53.
12. Fu Y, Li J, Lee AS. (2007) GRP78/BiP inhibits endoplasmic reticulum BIK and protects human breast cancer cells against estrogen starvation-induced apoptosis. Cancer Res. 67(8): 3734-40.
13. Hu CC, Dougan SK, McGehee AM, Love JC, Ploegh HL. (2009) XBP-1 regulates signal transduction, transcription factors and bone marrow colonization in B cells. EMBO J. 28(11): 1624-36. PMCID**:** PMC2684024.
14. van Anken E, Romijn EP, Maggioni C, Mezghrani A, Sitia R, Braakman I, et al. (2003) Sequential waves of functionally related proteins are expressed when B cells prepare for antibody secretion. Immunity. 18(2): 243-53.
15. Perou CM, Sorlie T, Eisen MB, van de Rijn M, Jeffrey SS, Rees CA, et al. (2000) Molecular portraits of human breast tumours. Nature. 406(6797): 747-52.
16. Wang DY, Fulthorpe R, Liss SN, Edwards EA. (2004) Identification of estrogen-responsive genes by complementary deoxyribonucleic acid microarray and characterization of a novel early estrogen-induced gene: EEIG1. Mol Endocrinol. 18(2): 402-11.
17. Ding L, Yan J, Zhu J, Zhong H, Lu Q, Wang Z, et al. (2003) Ligand-independent activation of estrogen receptor alpha by XBP-1. Nucleic Acids Res. 31(18): 5266-74. PMCID**:** PMC203316.

18. Gomez BP, Riggins RB, Shajahan AN, Klimach U, Wang A, Crawford AC, et al. (2007) Human X-box binding protein-1 confers both estrogen independence and antiestrogen resistance in breast cancer cell lines. Faseb J. 21(14): 4013-27.
19. Andruska N, Mao C, Cherian M, Zhang C, Shapiro DJ. (2012) Evaluation of a luciferase-based reporter assay as a screen for inhibitors of estrogen-ERalpha-induced proliferation of breast cancer cells. J Biomol Screen. 17(7): 921-32.
20. Cherian MT, Wilson EM, Shapiro DJ. (2012) A competitive inhibitor that reduces recruitment of androgen receptor to androgen-responsive genes. J Biol Chem. 287(28): 23368-80. PMCID: PMC3390614.
21. Kretzer NM, Cherian MT, Mao C, Aninye IO, Reynolds PD, Schiff R, et al. (2010) A noncompetitive small molecule inhibitor of estrogen-regulated gene expression and breast cancer cell growth that enhances proteasome-dependent degradation of estrogen receptor {alpha}. J Biol Chem. 285(53): 41863-73. PMCID: PMC3009914.
22. Dong S, Teng Z, Lu FH, Zhao YJ, Li H, Ren H, et al. (2010) Post-conditioning protects cardiomyocytes from apoptosis via PKC(epsilon)-interacting with calcium-sensing receptors to inhibit endo(sarco)plasmic reticulum-mitochondria crosstalk. Mol Cell Biochem. 341(1-2): 195-206.
23. Spiller DG, Wood CD, Rand DA, White MR. (2010) Measurement of single-cell dynamics. Nature. 465(7299): 736-45.
24. Ju YH, Doerge DR, Allred KF, Allred CD, Helferich WG. (2002) Dietary genistein negates the inhibitory effect of tamoxifen on growth of estrogen-dependent human breast cancer (MCF-7) cells implanted in athymic mice. Cancer Res. 62(9): 2474-7.

25. Graham K, de las Morenas A, Tripathi A, King C, Kavanah M, Mendez J, et al. (2010) Gene expression in histologically normal epithelium from breast cancer patients and from cancer-free prophylactic mastectomy patients shares a similar profile. Br J Cancer. 102(8): 1284-93. PMCID: PMC2855998.
26. Shi L, Campbell G, Jones WD, Campagne F, Wen Z, Walker SJ, et al. (2010) The MicroArray Quality Control (MAQC)-II study of common practices for the development and validation of microarray-based predictive models. Nat Biotechnol. 28(8): 827-38.
27. Loi S, Haibe-Kains B, Desmedt C, Lallemand F, Tutt AM, Gillet C, et al. (2007) Definition of clinically distinct molecular subtypes in estrogen receptor-positive breast carcinomas through genomic grade. J Clin Oncol. 25(10): 1239-46.
28. Symmans WF, Hatzis C, Sotiriou C, Andre F, Peintinger F, Regitnig P, et al. (2010) Genomic index of sensitivity to endocrine therapy for breast cancer. J Clin Oncol. 28(27): 4111-9.
29. Miller LD, Smeds J, George J, Vega VB, Vergara L, Ploner A, et al. (2005) An expression signature for p53 status in human breast cancer predicts mutation status, transcriptional effects, and patient survival. Proc Natl Acad Sci U S A. 102(38): 13550-5.
30. Bolstad BM, Irizarry RA, Astrand M, Speed TP. (2003) A comparison of normalization methods for high density oligonucleotide array data based on variance and bias. Bioinformatics. 19(2): 185-93.
31. Bair E, Tibshirani R. (2004) Semi-supervised methods to predict patient survival from gene expression data. PLoS Biol. 2(4): E108.

32. Lee AH, Iwakoshi NN, Glimcher LH. (2003) XBP-1 regulates a subset of endoplasmic reticulum resident chaperone genes in the unfolded protein response. Mol Cell Biol. 23(21): 7448-59.
33. Wu J, Rutkowski DT, Dubois M, Swathirajan J, Saunders T, Wang J, et al. (2007) ATF6alpha optimizes long-term endoplasmic reticulum function to protect cells from chronic stress. Dev Cell. 13(3): 351-64.
34. Okada T, Yoshida H, Akazawa R, Negishi M, Mori K. (2002) Distinct roles of activating transcription factor 6 (ATF6) and double-stranded RNA-activated protein kinase-like endoplasmic reticulum kinase (PERK) in transcription during the mammalian unfolded protein response. Biochem J. 366(Pt 2): 585-94. PMCID: PMC1222788.
35. Rutkowski DT, Arnold SM, Miller CN, Wu J, Li J, Gunnison KM, et al. (2006) Adaptation to ER stress is mediated by differential stabilities of pro-survival and pro- apoptotic mRNAs and proteins. PLoS Biol. 4(11): e374. PMCID: PMC1634883.
36. Divekar SD, Storchan GB, Sperle K, Veselik DJ, Johnson E, Dakshanamurthy S, et al. (2011) The role of calcium in the activation of estrogen receptor-alpha. Cancer Res. 71(5): 1658-68.
37. Frasor J, Danes JM, Komm B, Chang KC, Lyttle CR, Katzenellenbogen BS. (2003) Profiling of estrogen up- and down-regulated gene expression in human breast cancer cells: insights into gene networks and pathways underlying estrogenic control of proliferation and cell phenotype. Endocrinology. 144(10): 4562-74.
38. Rae JM, Johnson MD, Scheys JO, Cordero KE, Larios JM, Lippman ME. (2005) GREB 1 is a critical regulator of hormone dependent breast cancer growth. Breast

Cancer Res Treat. 92(2): 141-9.

39. Rutkowski DT, Kaufman RJ. (2007) That which does not kill me makes me stronger: adapting to chronic ER stress. Trends Biochem Sci. 32(10): 469-76.
40. Rao RV, Peel A, Logvinova A, del Rio G, Hermel E, Yokota T, et al. (2002) Coupling endoplasmic reticulum stress to the cell death program: role of the ER chaperone GRP78. FEBS Lett. 514(2-3): 122-8. PMCID: PMC3971841.
41. Ariazi EA, Cunliffe HE, Lewis-Wambi JS, Slifker MJ, Willis AL, Ramos P, et al. (2011) Estrogen induces apoptosis in estrogen deprivation-resistant breast cancer through stress responses as identified by global gene expression across time. Proc Natl Acad Sci U S A. 108(47): 18879-86.
42. Teske BF, Wek SA, Bunpo P, Cundiff JK, McClintick JN, Anthony TG, et al. (2011) The eIF2 kinase PERK and the integrated stress response facilitate activation of ATF6 during endoplasmic reticulum stress. Mol Biol Cell. 22(22): 4390-405. PMCID: PMC3216664.
43. Ma Y, Hendershot LM. (2004) Herp is dually regulated by both the endoplasmic reticulum stress-specific branch of the unfolded protein response and a branch that is shared with other cellular stress pathways. J Biol Chem. 279(14): 13792-9.
44. Yamamoto K, Sato T, Matsui T, Sato M, Okada T, Yoshida H, et al. (2007) Transcriptional induction of mammalian ER quality control proteins is mediated by single or combined action of ATF6alpha and XBP1. Dev Cell. 13(3): 365-76.
45. Novoa I, Zeng H, Harding HP, Ron D. (2001) Feedback inhibition of the unfolded protein response by GADD34-mediated dephosphorylation of eIF2alpha. J Cell Biol. 153(5): 1011-22.

46. van Huizen R, Martindale JL, Gorospe M, Holbrook NJ. (2003) P58IPK, a novel endoplasmic reticulum stress-inducible protein and potential negative regulator of eIF2alpha signaling. J Biol Chem. 278(18): 15558-64.
47. Yan W, Frank CL, Korth MJ, Sopher BL, Novoa I, Ron D, et al. (2002) Control of PERK eIF2alpha kinase activity by the endoplasmic reticulum stress-induced molecular chaperone P58IPK. Proc Natl Acad Sci U S A. 99(25): 15920-5.
48. Mohammed H, D'Santos C, Serandour AA, Ali HR, Brown GD, Atkins A, et al. (2013) Endogenous purification reveals GREB1 as a key estrogen receptor regulatory factor. Cell Rep. 3(2): 342-9.
49. Park HR, Tomida A, Sato S, Tsukumo Y, Yun J, Yamori T, et al. (2004) Effect on tumor cells of blocking survival response to glucose deprivation. J Natl Cancer Inst. 96(17): 1300-10.
50. Shang Y, Hu X, DiRenzo J, Lazar MA, Brown M. (2000) Cofactor dynamics and sufficiency in estrogen receptor-regulated transcription. Cell. 103(6): 843-52.

CHAPTER 3

AN ESTROGEN RECEPTOR α INHIBITOR ACTIVATES THE UNFOLDED PROTEIN RESPONSE, BLOCKS PROTEIN SYNTHESIS AND INDUCES TUMOR REGRESSION [2]

ABSTRACT

Recurrent estrogen receptor α (ERα) positive breast and ovarian cancers are often therapy-resistant. Using screening and functional validation, we identified BHPI, a potent non-competitive small molecule ERα biomodulator that selectively blocks proliferation of drug-resistant ERα positive breast and ovarian cancer cells. In a mouse xenograft model of breast cancer, BHPI induced rapid and substantial tumor regression. While BHPI potently inhibits nuclear estrogen-ERα-regulated gene expression, BHPI is effective because it elicits sustained ERα-dependent activation of the endoplasmic reticulum (EnR) stress sensor, the unfolded protein response (UPR) and persistent inhibition of protein synthesis. BHPI distorts a newly described action of estrogen-ERα, mild and transient UPR activation. In contrast, BHPI elicits massive and sustained UPR activation, converting the UPR from protective to toxic. In $ERα^+$ cancer cells, BHPI rapidly hyperactivates plasma membrane PLCγ, generating IP_3, which opens EnR IP_3R calcium channels, rapidly depleting EnR Ca^{2+} stores. This leads to activation of all three arms of the UPR. Activation of the PERK arm, stimulates phosphorylation of eukaryotic initiation

[2] This chapter appeared in its entirety in the *Proceedings of the National Academy of Sciences.* Neal D Andruska, **Xiaobin Zheng**, Xujuan Yang, Chengjian Mao, Mathew M Cherian, Lily Mahapatra, William G Helferich, David J Shapiro. (2015) Estrogen receptor α inhibitor activates the unfolded protein response, blocks protein synthesis, and induces tumor regression. PNAS. DOI: 10.1073/pnas.1403685112. **My contributions to the research are denoted under the figure legends**.

factor 2α (eIF2α), resulting in rapid inhibition of protein synthesis. The cell attempts to restore EnR Ca^{2+} levels, but the open EnR IP_3R calcium channel leads to an ATP-depleting futile cycle, resulting in activation of the energy sensor AMPK and phosphorylation of eukaryotic elongation factor 2 (eEF2). eEF2 phosphorylation inhibits protein synthesis at a second site. BHPI's novel mode of action, high potency, and effectiveness in therapy-resistant tumor cells, make it an exceptional candidate for further mechanistic and therapeutic exploration.

SIGNIFICANCE

Late-stage estrogen receptor α (ERα)-positive breast and ovarian cancers exhibit many regulatory alterations and therefore resist therapy. Our novel ERα inhibitor, BHPI, stops growth and often kills drug-resistant $ER\alpha^+$ cancer cells and induces rapid and substantial tumor regression in a mouse model of human breast cancer. BHPI distorts a normally protective estrogen-ERα-mediated activation of the unfolded protein response (UPR) and elicits sustained UPR activation. The UPR cannot be deactivated because BHPI, acting at a second site, inhibits production of proteins that normally help turn it off. This persistent activation converts the UPR from protective to lethal. Targeting therapy-resistant ERα positive cancer cells by converting the UPR from cytoprotective to cytotoxic may hold significant therapeutic promise.

INTRODUCTION

Estrogens, acting via estrogen receptor α (ERα), stimulate tumor growth (1-3). Approximately 70% of breast cancers are ERα positive and most deaths due to breast

cancer are in patients with ERα$^+$ tumors (2, 4). Endocrine therapy using aromatase inhibitors to block estrogen production, or tamoxifen and other competitor antiestrogens, often results in selection and outgrowth of resistant tumors. Although 30-70% of epithelial ovarian tumors are ERα positive (1), endocrine therapy is largely ineffective (5-7). After several cycles of chemotherapy, tumors recur as resistant ovarian cancer (5), and most patients die within 5 years (8).

Non-competitive ERα inhibitors targeting this unmet therapeutic need including DIBA, TPBM, TPSF, and LRH-1 inhibitors that reduce ERα levels, show limited specificity, require high concentrations (>5 μM) and usually have not advanced through preclinical development (9-12). These non-competitive ERα inhibitors and competitor antiestrogens are primarily cytostatic and act by preventing estrogen-ERα action; therefore, they are largely ineffective in therapy-resistant ERα containing cancer cells that no longer require estrogens and ERα for growth.

To target the estrogen-ERα axis in therapy-resistant cancer cells, we developed (13) and implemented an unbiased pathway-directed screen of ~150,000 small molecules. We identified ~2,000 small molecule biomodulators of 17β-estradiol (E_2)-ERα induced gene expression, evaluated these biomodulators for inhibition of E_2-ERα-induced cell proliferation and performed simple follow-on assays to identify inhibitors with a novel mode of action. Here, we describe BHPI, our most promising small molecule ERα biomodulator.

In response to stress cancer cells often activate the endoplasmic reticulum (EnR) stress sensor, the unfolded protein response (UPR). We recently showed that as an essential component of the E_2-ERα proliferation program, estrogen induces a different

mode of UPR activation, a weak anticipatory activation of the UPR prior to increased protein folding loads that accompany cell proliferation. This weak and transient E_2-ERα-mediated UPR activation is protective (14). BHPI distorts this normal action of E_2-ERα and induces a massive and sustained ERα-dependent activation of the UPR, converting UPR activation from cytoprotective to cytotoxic. Moreover, independent of its effect on the UPR and protein synthesis, BHPI rapidly suppresses E_2-ERα-regulated gene expression.

RESULTS

BHPI IS EFFECTIVE IN DRUG-RESISTANT ERα^+ BREAST AND OVARIAN CANCER CELLS.

We investigated BHPI's effect on proliferation in therapy-sensitive and therapy-resistant cancer cells. BHPI (Figure 3.1*A* and *B*) completely inhibited proliferation of ERα^+ breast (Figure 3.2 *A, E, F* and *G*), endometrial (Figure 3.2*C*) and ovarian (Figure 3.2*B*, *H*, and *I*) cancer cells, and had no effect in counterpart ERα^- cell lines (Figure 3.2*D*). At 100-1,000 nM, BHPI completely blocked proliferation in diverse drug-resistant cell lines: 4-hydroxytamoxifen (4-OHT)-resistant ZR-75-1 breast cancer cells (Figure 3.2*E*); tamoxifen and fulvestrant/ICI 182,780 (ICI)-resistant BT-474 cells (Figure 3.2*F*) (15); epidermal growth factor (EGF) stimulated T47D breast cancer cells, which are resistant to 4-OHT, ICI and raloxifene (RAL) (Figure 3.2*G*); Caov-3 ovarian cancer cells, which are resistant to 4-OHT, ICI and cisplatin (Figure 3.2*H*) (16), and multidrug resistant OVCAR-3 ovarian cancer cells, which are resistant to 5 μM ICI (Figure 3.2*I*) and to paclitaxel, cisplatin and other anticancer drugs (17, 18). BHPI blocked proliferation in all 15 ERα^+ cell lines and at

10 μM had no effect on proliferation in all 12 ERα$^-$ cell lines tested (Figure 3.3). Furthermore, BHPI blocked anchorage-independent growth of MCF-7 cells in soft agar (Figure 3.4).

BHPI INDUCES TUMOR REGRESSION.

We next evaluated BHPI in a mouse xenograft model using MCF-7 cell tumors (19). For each tumor, cross-sectional area at Day 0 (~45 mm^2) is set to 0%. Control (vehicle injected) and BHPI treated mice were continuously exposed to estrogen. After daily IP injections for 10 days, the tumors in the vehicle treated mice exhibited continued robust growth (Figure 3.5, red bars). While BHPI at 1 mg/kg every other day was ineffective (Figure 3.6*A*), initiation of 15 mg/kg daily BHPI treatment resulted in rapid regression of 48/52 tumors (Figure 3.5, blue bars). BHPI easily exceeded the goal of >60% tumor growth inhibition proposed as a benchmark more likely to lead to clinical response (20). Furthermore, BHPI, at 10 mg/kg every other day, ultimately stopped tumor growth and final tumor weight was reduced ~60% compared to controls (Figure 3.6*A* and *B*). BHPI was well tolerated; BHPI-treated and control mice exhibited similar food intake and weight gain (Figure 3.6*C* and *D*).

BHPI IS AN ERα-DEPENDENT INHIBITOR OF PROTEIN SYNTHESIS.

Surprisingly, BHPI greatly reduced protein synthesis in ERα$^+$ cancer cells (Figure 3.7*A* and Figure 3.8). If BHPI inhibits protein synthesis through ERα, it should only work in ERα$^+$ cells, and ERα overexpression should increase its effectiveness. BHPI inhibited protein synthesis in all 14 ERα$^+$ cell lines, with no effect on protein synthesis in all 12

ERα$^-$ cell lines (Figure 3.7*A* and Figure 3.8*A* and *B*). BHPI does not inhibit protein synthesis in ERα negative MCF-10A breast cells, but gains the ability to inhibit protein synthesis when ERα is stably expressed in isogenic MCF10A$_{ER\ In9}$ cells (Figure *3.7B*) (21). Notably, BHPI loses the ability to inhibit protein synthesis when ERα in the stably transfected cells is knocked down with siRNA (Figure *3.7C* and Figure 3.9*A*), or is degraded by ICI (Figure *3.7D*). Furthermore, increasing the ERα level in MCF7ERαHA cells (22), stably transfected to express doxycycline-inducible ERα, progressively increased BHPI inhibition of protein synthesis (Figure *3.7E*). BHPI does not work by activating the estrogen binding protein GPR30. BHPI has no effect on cell proliferation (Figure 3.3) or protein synthesis (Figure 3.8*A*) in HepG2 cells that contain functional GPR30 (23) and activating GPR30 with G1, did not inhibit protein synthesis (Figure 3.9*B* and *C*). Thus, ERα is necessary and sufficient for BHPI to inhibit protein synthesis.

BHPI RAPIDLY INHIBITS PROTEIN SYNTHESIS BY A PLCγ-MEDIATED OPENING OF THE INOSITOL TRIPHOSPHATE RECEPTOR (IP_3R) CA^{2+} CHANNEL, ACTIVATING THE PERK ARM OF THE UPR.

Inhibiting mechanistic target of rapamycin (mTOR) signaling did not strongly inhibit protein synthesis (Figure 3.9*D*), suggesting BHPI is unlikely to work through mTOR. We next investigated whether initial inhibition of protein synthesis by BHPI is due to activation of the UPR. There are three UPR arms. The transmembrane kinase PERK is activated by autophosphorylation. P-PERK phosphorylates eukaryotic initiation factor 2α (eIF2α), inhibiting translation of most mRNAs (Figure 3.10*A*) (24, 25). The other arms of the UPR initiate with ATF6α activation (Figure 3.10*B*), leading to increased protein folding capacity

and activation of IRE1α, which alternatively splices XBP1, producing active spliced (sp)-XBP1 (Figure 3.10*C*) (24, 25). In ERα$^+$ MCF-7 and T47D cells, but not in ERα$^-$ MDA-MB-231 cells, BHPI rapidly inhibited protein synthesis (Figure 3.11*A*) and in parallel increased eIF2α phosphorylation (Figure 3.7*F* and Figure 3.11*B* and *C*). Downstream readouts of eIF2α phosphorylation, CHOP and GADD34 mRNAs, were rapidly induced by BHPI (Figure 3.11*D* and *E*). Consistent with BHPI inhibiting protein synthesis through eIF2α-Ser51 phosphorylation, transfecting cells with a dominant-negative eIF2α-S51A mutant largely prevented BHPI from inhibiting protein synthesis (Figure 3.11*F*). We next evaluated whether increases in eIF2α phosphorylation and rapid inhibition of protein synthesis occur through activation of PERK. p-PERK was increased 30 minutes after BHPI treatment (Figure 3.7*F* and Figure 3.11*G),* and pre-treating cells with a PERK inhibitor (PERKi) abolished rapid BHPI inhibition of protein synthesis (Figure 3.12*A*). RNAi knockdown of PERK abolished BHPI inhibition of protein synthesis at 30 minutes and strongly inhibited BHPI-stimulated eIF2α phosphorylation (Figure 3.7*G* and Figure 3.12*B*). Since PERK knockdown blocks rapid eIF2α phosphorylation, BHPI is not inhibiting translation by activating other upstream kinases that phosphorylate eIF2α. Furthermore, BHPI rapidly activates the ATF6α and IRE1α arms of the UPR, as shown by increased cleaved p50-ATF6α and sp-XBP1 (Figure 3.7*H*).

To explore how BHPI activates the UPR, we examined inhibition of protein synthesis by known UPR activators. Thapsigargin and Ionomycin, which activate the UPR by release of Ca^{2+} from the lumen of the EnR into the cytosol (24, 25), but not UPR activators that work by other mechanisms, elicited the rapid and near quantitative inhibition of protein synthesis seen with BHPI (Figure 3.13*A*).

To test whether BHPI alters intracellular Ca^{2+}, we monitored intracellular Ca^{2+} with the calcium sensitive dye Fluo-4 AM. In MCF-7 cells, BHPI produced a large and sustained increase in intracellular Ca^{2+} in the presence of extracellular Ca^{2+}, and a large transient increase in intracellular Ca^{2+} in the absence of extracellular calcium (Figure 3.7*I* and Figure 3.13*B*). Time-dependent changes in cytosol calcium in BHPI-treated MCF-7 cells were quantitated (Figure *3.13B*). Since BHPI elicits a large increase in cytosol Ca^{2+} when there is no extracellular Ca^{2+}, BHPI is acting by depleting the Ca^{2+} store in the EnR. BHPI had no effect on intracellular Ca^{2+} in ERα^- HeLa cells (Figure 3.13*C*).

We next identified the EnR Ca^{2+} channel that opens after BHPI treatment. The inositol triphosphate receptor (IP_3R) and ryanodine (RyR) receptors are the major EnR Ca^{2+} channels. Treatment with 2-APB, which locks the IP_3R Ca^{2+} channels closed, but not closing the RyR Ca^{2+} channels with high concentration ryanodine (Ry), abolished the rapid BHPI-ERα-mediated increase in cytosol Ca^{2+} and inhibition of protein synthesis (Figure 3.7*I* and *J*). Furthermore, RNAi knockdown of IP_3R (Figure 3.14*A*) abolished the BHPI-mediated increase in cytosol Ca^{2+} and inhibition of protein synthesis (Figure 3.7*K* and *L*). IP_3R Ca^{2+} channels are also modulated through protein kinase A (PKA), but BHPI did not induce PKA-dependent IP_3R-Ser^{1756} phosphorylation (26) (Figure 3.14*B*).

BHPI STRONGLY ACTIVATES PHOSPHOLIPASE C γ, PRODUCING INOSITOL 1,4,5-TRIPHOSPHATE.

Inositol 1,4,5-triphosphate (IP_3) is produced when the activated phosphorylated plasma membrane enzyme, PLCγ, hydrolyzes PIP_2 to diacylglycerol (DAG) and IP_3. Supporting a role for PLCγ, siRNA knockdown of PLCγ (Figure 3.14*C*) abolished the

BHPI-mediated increase in cytosol Ca^{2+} (Figure 3.14*C*) and BHPI inhibition of protein synthesis (Figure 3.7*L*), and the PLCγ inhibitor U73122 abolished the BHPI-ERα increase in cytosol Ca^{2+} (Figure 3.14*C*). Confirming PLCγ's role, BHPI induces rapid PLCγ-Tyr^{783} phosphorylation (Figure 3.14*D*), and strongly increased IP_3 levels (Figure 3.7*M*). Supporting the idea that BHPI acts by distorting the newly described weak E_2-ERα activation of the UPR (14), BHPI induced a much larger increase in IP_3 levels than E_2 (Figure 3.7*M*).

Rapid BHPI activation of plasma membrane PLCγ indicates UPR activation is an extranuclear action of BHPI-ERα. PLCγ and ERα coimmunoprecipitate (27), and overexpression of ERα in MCF7ERαHA cells further increased IP_3 levels in response to BHPI (Figure 3.14*E*). Consistent with extranuclear ERα-dependent activation of the UPR, an estrogen-dendrimer conjugate (EDC) that cannot enter the nucleus (28), induced sp-XBP1, but not nuclear estrogen-regulated genes (Figure 3.15). A model depicting BHPI action is presented in Figure 3.7*N*.

BHPI INHIBITS E_2-ERα-REGULATED GENE EXPRESSION AND LIKELY INTERACTS WITH ERα.

Consistent with BHPI binding to E_2-ERα, BHPI, but not an inactive close relative, Compound 8 (Figure 3.1*B*), significantly altered the fluorescence emission spectrum of purified ERα (Figure 3.16*A*). We also tested whether BHPI alters the sensitivity of purified ERα ligand-binding domain (LBD) to protease digestion. Addition of BHPI followed by cleavage with proteinase K revealed a 15 kDa band in BHPI treated ERα LBD that was nearly absent in the LBD treated with DMSO or Compound 8 (Figure 3.16*B*).

Because BHPI interacts with ERα and distorts an extranuclear action of E_2-ERα, we tested whether, independent of its ability to inhibit protein synthesis and activate the UPR, BHPI would also modulate nuclear E_2-ERα-regulated gene expression. At early times when BHPI inhibited E_2-ERα induction of pS2 mRNA, neither inhibiting protein synthesis with CHX, nor activating the UPR with TUN or THG (Figure 3.17*A*), inhibited induction of pS2 mRNA (Figure 3.16*C*). BHPI inhibited E_2-ERα induction of pS2, GREB1, XBP1, CXCL2, and ERE-luciferase in ERα$^+$ MCF-7 and T47D cells (Figure 3.17*B-F),* and blocked E_2-ERα down-regulation of IL1-R1 and EFNA mRNA (Figure *3.17E* and *G*). BHPI is not a competitive ERα inhibitor. Increasing the concentration of E_2 by 1,000-fold had no effect on BHPI inhibition of E_2 induction of pS2 mRNA (Figure 3.16*D*). Moreover, BHPI did not compete with E_2 for binding to ERα (Figure 3.18*A*). Since BHPI inhibits E_2-ERα induction and repression of gene expression, BHPI acts at the level of ERα and not by a general inhibition or activation of transcription.

BHPI did not alter ERα protein levels or nuclear localization (Figure 3.18*B* and *C*). Chromatin immunoprecipitation (ChIP) showed that BHPI strongly inhibited E_2-stimulated recruitment of ERα and RNA polymerase II to the pS2 and GREB1 promoter regions (Figure 3.16*E* and Figure 3.18*D*). Consistent with BHPI inducing an ERα conformation exhibiting reduced affinity for gene regulatory regions, ten-fold overexpression of ERα in MCF7ERαHA cells abolished BHPI inhibition of induction of GREB1 mRNA (Figure 3.16*F*). BHPI still kills these cells because ERα overexpression enhances BHPI inhibition of protein synthesis (Figure 3.7*E*). Taken together, our data provides compelling evidence BHPI is a new type of biomodulator, altering both nuclear and extranuclear actions of

ERα.

BHPI RAPIDLY DEPLETES INTRACELLULAR ATP STORES AND ACTIVATES AMPK.

BHPI treatment results in rapid depletion of EnR Ca^{2+}. To restore EnR Ca^{2+}, the cell activates SERCA (Sarco/Endoplasmic Reticulum Ca^{2+}-ATPase) pumps, which catalyze ATP-dependent transfer of Ca^{2+} from the cytosol into the lumen of the EnR. Since BHPI opens the IP_3R Ca^{2+} channel, Ca^{2+} pumped back into the EnR lumen by SERCA flows back into the cytosol (model in Figure 3.7*N*). This futile cycle rapidly depletes intracellular ATP, resulting in activation of AMP-activated protein kinase (AMPK) by AMPKα-Thr^{172} phosphorylation (Figure 3.19*A* and *B*). Moreover, the AMPK target, acetyl CoA-carboxylase (ACC) is rapidly phosphorylated (Figure 3.19B). Since Thapsigargin, which depletes EnR Ca^{2+} by inhibiting SERCA pumps, had no effect on ATP levels (Figure 3.19*A*) and did not increase levels of p-AMPKα and p-ACC (Figure 3.20*A*), ATP depletion, rather than increased cytosol Ca^{2+} is responsible for AMPK activation. Importantly, pre-blocking SERCA-pumps with Thapsigargin, abolished the BHPI-induced decline in ATP levels and phosphorylation of AMPKα (Figure 3.19*A*).

BHPI BLOCKS UPR INACTIVATION BY TARGETING A SECOND SITE OF PROTEIN SYNTHESIS INHIBITION.

In $ERα^+$, but not $ERα^-$ cells, after ~2 hours, BHPI phosphorylates and inactivates eukaryotic elongation factor 2, (eEF2) (Figure 3.19*C* and Figure 3.20*B* and *C*). eEF2 phosphorylation is regulated by a single Ca^{2+}/calmodulin-dependent kinase, eukaryotic

elongation factor 2 kinase (CAMKIII/eEF2K). eEF2K is inhibited by mTORC1-p70^{S6K} and ERK-p90^{RSK} through eEF2K-Ser^{366} phosphorylation and activated by Ca^{2+}/calmodulin and AMPK (29, 30). BHPI increases cytosol Ca^{2+} and activates AMPK, but inhibiting AMPK did not inhibit eEF2 phosphorylation (Figure 3.20*D*). BHPI also rapidly induces a transient increase in ERK1/2 activation (Figure 3.20*E* and *F*), which stimulates ERK-p90^{RSK} and mTORC1-p70^{S6K} activation (31). Together, these pathways induce eEF2K-Ser^{366} phosphorylation (Figure 3.19*D*), and prevent increases in p-eEF2 for ~1 hour after BHPI treatment (Figure 3.19*C* and Figure 3.20*G*). Consistent with this, blocking ERK activation with U0126 prevented BHPI from producing transient declines in eEF2 phosphorylation through inactivation of eEF2K (Figure 3.20*G*).

UPR activation with conventional UPR activators produces transient eIF2α phosphorylation and inhibition of protein synthesis (Figs. 3.20A, 3.21*A,* and 3.21*B*) in part because they induce BiP and p58^{IPK} chaperones (Figure 3.21*C* and *D*). The chaperones help resolve UPR stress and inactivate the UPR. In contrast, BHPI blocks induction and reduces levels of BiP and p58^{IPK} protein (Figure 3.19*E*), leading to sustained eIF2α phosphorylation and inhibition of protein synthesis (Figure 3.8 and 3.11*B*). BHPI failed to increase p58 protein despite inducing p58 mRNA (Figure 3.19*E*), and at later times PERK inhibition failed to prevent BHPI from inhibiting protein synthesis (Figure 3.12*A)*. This is consistent with BHPI targeting protein synthesis at a second site at later times.

DISCUSSION

BHPI and estrogen share the same ERα-dependent pathway for UPR activation: Activation of PLCγ producing IP_3, opening of the IP_3R Ca^{2+} channels, release of EnR

Ca^{2+}, and activation of the PERK, IRE1α and ATF6α arms of the UPR (model in Figure 3.7*N*). We recently reported that as an early component of the proliferation program, E_2-ERα weakly and transiently activates the UPR. We showed that E_2-ERα elicits a mild and transient activation of the PERK arm of the UPR, while simultaneously increasing chaperone levels and protein folding capacity by activating the IRE1α and ATF6α arms of the UPR (14). BHPI distorts this normal action of E_2-ERα by increasing the amplitude and duration of UPR activation. Compared to E_2, BHPI hyperactivates PLCγ, producing much higher IP_3 levels, Ca^{2+}-release from the EnR, and UPR activation. BHPI initially inhibits protein synthesis by strongly activating the PERK arm of the UPR. Knockdown of ERα, PLCγ, IP_3R and PERK blocked rapid BHPI inhibition of protein synthesis. While BHPI activates the IRE1α and ATF6α UPR arms, by acting at later times to inhibit protein synthesis at a second site, BHPI prevents the synthesis of chaperones required to inactivate the UPR. Because the cell attempts to restore EnR Ca^{2+} while the IP_3R Ca^{2+} channels remain open, BHPI rapidly depletes ATP (Figure 3.7*N*), resulting in activation of AMPK. Several actions of BHPI, including strong elevation of intracellular calcium, sustained UPR activation, long-term inhibition of protein synthesis, ATP depletion and AMPK activation can potentially contribute to BHPI's ability to block cell proliferation. How the cascade of events initiated by BHPI enables BHPI to block cell proliferation, and often kill, ERα^+ cancer cells requires further exploration. Supporting BHPI targeting PLCγ and the UPR through ERα, independent of its effects on the UPR, BHPI inhibits E_2-ERα-mediated induction and repression of gene expression.

BHPI and E_2 activation of plasma membrane-bound PLCγ, resulting in increased IP_3, is an extranuclear action of ERα. Increasing the level of ERα, increased IP_3 levels.

Consistent with ERα and PLCγ interaction, they coimmunoprecipitate (27). BHPI and E_2 induce Ca^{2+} release in 1 min., too rapidly for action by regulating nuclear gene expression (14). Furthermore, a membrane-impermeable estrogen-dendrimer induces the UPR marker sp-XBP1, but not nuclear E_2-ERα-regulated genes.

The UPR plays important roles in tumorigenesis, therapy resistance, and cancer progression (14, 32). Moderate and transient UPR activation by E_2 and other activators promotes an adaptive stress response, which increases UPR expression and confers protection from subsequent exposure to higher levels of cell stress (14, 33). In contrast, sustained UPR activation triggers cell death. Since most current anticancer drugs inhibit a pathway or protein important for tumor growth or metastases, most UPR targeting efforts focus on inactivating a protective stress response by inhibiting UPR components (34). UPR overexpression in cancer is associated with a poor prognosis (14), suggesting that sustained lethal hyperactivation of the UPR by BHPI represents a novel alternative anticancer strategy.

BHPI can selectively target cancer cells, because its targets, ERα and the UPR, are both overexpressed in breast and ovarian cancers (14, 22, 32, 35). Cells expressing low levels of ERα, more typical of non-transformed ERα containing cells, such as PC-3 prostate cancer cells, were less sensitive to BHPI inhibition of protein synthesis (Figure 3.3), while doxycycline-treated MCF7ERαHA cells expressing very high levels of ERα exhibited near complete inhibition of protein synthesis (Figure 3.7*E*). Consistent with low toxicity, in the xenograft study, BHPI-treated mice showed no evidence of gross toxicity. Most gynecological cancers show little dependence on estrogens for growth and other non-competitive ERα inhibitors have not demonstrated effectiveness in these cells. BHPI

is highly effective in several breast and ovarian cancer drug-resistance models and extends the reach of ERα biomodulators to gynecologic cancers that do not respond to current endocrine therapies. BHPI's effectiveness in ERα-containing breast, ovarian and endometrial cancer cells is consistent with the finding that female reproductive cancers exhibit common genetic alterations and might respond to the same drugs (36), and with our finding that E_2-ERα weakly activates the UPR in breast and ovarian cancer cells (14).

With its submicromolar potency, effectiveness in a broad range of therapy resistant cancer cells, ability to induce substantial tumor regression and unique mode of action, BHPI is a promising small molecule for therapeutic evaluation and mechanistic studies.

MATERIALS AND METHODS

Cell Culture and Reagents

MCF-7, T47D, T47D-kBluc, HCC-1500, ZR-75-1, MCF10A, MDA MB-231, CAOV-3, OVCAR-3, IGROV-1, ES2, ECC-1, HeLa, PC-3, DU145, H1793, A549, MEF, and HepG2 cells wereobtained from the ATCC. Dr. E. Wilson provided HeLa-AR13 cells, Dr. K. Korach provided BG-1/MCF-7 cells, Dr. B.H. Park provided MCF10AER IN9 cells, Dr. R. Schiff provided BT-474 cells, and E. Alarid provided MCF7ERαHA cells. Prior to experiments, to deplete cells of estrogens in the serum and medium, ERα positive cell lines were maintained for 4 days in medium supplemented with phenol red-free charcoal-dextran (CD) treated serum.

Chemical Libraries and Screening

The small molecule libraries screened were: The ~150,000 small molecule Chembridge

MicroFormat small molecule library, the ~10,000 small molecule University of Illinois Marvel library developed by Drs. K. Putt and P. Hergenrother (37), and the ~2,000 small molecule NCI diversity set obtained from NIH. High throughput screening for small molecule inhibitors of endogenous E_2-ERα induced expression of the stably transfected $(ERE)_3$-luciferase reporter in T47D-KBluc cells, was carried out using the assay we recently described (38).

Cell Proliferation Assays

Cells were resuspended in the following media and plated in 96 well plates at the indicated densities: MCF-7 (10% CD-calf, 1,000 cells); MCF7ERαHA (10% CD-calf, 1,000); T47D (10% CD-calf, 2,000); T47D- kBluc (10% CD-FBS, 1,000); HCC-1500 (10% CD-FBS, 1,000); BT-474 (10% CD-calf, 2,000); ZR-75-1 (10% CD-calf 2,000); MCF10AER IN9 (2% CD-FBS, 1,000); MCF10A (2% CD-FBS, 1,000); MDA MB-231 (10% FBS, 1,000); BG-1/MCF-7 (5% FBS, 250); CaOV-3 (10% CD-CALF, 2,000); OVCAR-3 (10% CD-FBS, 2,000); IGROV-1 (10% FBS, 1,000); ES2 (10% FBS, 1,000); ECC-1 (5% CD-FBS, 1,000); Ishikawa (10% CD-calf, 2,000); HeLa (10% FBS, 1,000); PC-3 (10% CD-FBS, 1,000); DU145 (10% FBS, 1,000); 201T (10% FBS, 2,000); 273T (10% FBS, 1,000); H1793 (5% FBS, 2,000); A549 (10% FBS, 1,000); HepG2 (10% CD-FBS, 1,000), MEF (10% FBS, 2,000). The medium was replaced with treatment medium the following day, and plates were incubated at 37^{o} C in 5% CO_2 for 4 days except for BT-474, BG-1/MCF-7 and Ishikawa which were incubated for 6 days and ZR-75-1 cells which were incubated for 7 days. Treatment solutions were replaced every two days. Cell number was determined from MTS assays using CellTiter 96 Aqueous One Solution Reagent (Promega). For each

cell line, cell number was calculated from a standard curve of the number of plated cells versus A490.

ATP Measurements

To measure ATP levels, cells were lysed and ATP luminescence levels were measured using an ATPlite Luminesence Assay kit (PerkinElmer, MA). ATP released from cells was quantified from a standard curve of ATP standards versus luminescence.

Luciferase Assays

Reporter gene assays were carried out, as previously described (38, 39). Briefly, cells were switched to 10% CD-FBS for four days prior to experiments, and plated at a density of 50,000 cells/well in 24-well plates. The medium was replaced the next day with medium containing the test compounds, with or without hormone, incubated for 24 hours and luciferase assays were performed using Bright Glow reagent (Promega, WI).

qRT-PCR

RNA was extracted using a QiaShredder kit (Qiagen) for cell homogenization, and purified with the RNAeasy mini-kit (Qiagen, CA). cDNA was prepared from 0.5 μg of RNA by reverse transcription using a DyNAmo cDNA synthesis kit (Finnzymes, Finland). Quantitative PCR assays were performed on samples from 3 independent sets of cells (biological triplicate). Reactions contained 10 ng of cDNA and 50 nM forward and reverse primers in 15 μl and were carried out using Power SYBR Green PCR Mastermix (Applied Biosystems). The fold change in expression of each gene was calculated using the ΔΔCt

method with the ribosomal protein 36B4 used as the internal control, as described previously (38, 40, 41).

Chromatin Immunoprecipitation

MCF-7 cells were stripped of estrogens for 3 days in 5% CD-FBS. Cells were pretreated with 1 μM BHPI or DMSO (0.1%) as a control for 105 minutes, and then were treated with either 10 nM E_2 or an ethanol-vehicle control (0.1%) for 45 minutes. ChIP was carried out essentially, as previously described (39).

Transfections

siRNA knockdowns were performed using DharmaFECT1 Transfection Reagent and 100 nM ON-TARGETplus non-targeting pool or SMARTpools for ERα (ESR1), PLCγ (PLCG1), PERK (EIF2AK3), or pan-IP3R (Dharmacon). The pan-IP3R SmartPool consisted of three individual SmartPools, each at 33 nM, directed against each isoform of the IP3R (ITPR1, ITPR2, and ITPR3). To knockdown ERα, MCF10AERα IN9 cells were treated for 16 hours with either human ERα SMARTpool (ESR1) siRNA or Non-targeting Control Pool siRNA. Cells were treated with transfection complex for 16 hours, and medium was replaced with DMEM/F12, supplemented with 2% CD-FBS. ERα knockdown at the mRNA and protein level was assessed every 24 hours following transfection. The effects of BHPI on protein synthesis following ERα knockdown were assessed 3-days post-knockdown by treating cells with either 0.1% DMSO loading control or 100 nM BHPI for the indicated times and protein synthesis was then assessed

by measuring ^{35}S-Methionine incorporation. Knockdowns of PERK, IP3R, and PLCγ were performed by maintaining MCF-7 cells in MEM containing 5% CD-FBS for 4 days prior to plating cells in serum-free MEM. Cells were treated with transfection complexes for 16 hours and medium was replaced with MEM, supplemented with 10% CD-calf serum. The effects of BHPI on protein synthesis or calcium signaling were assessed 3-days post-knockdown. The eIF2α S51A plasmid was a gift from Dr. David Ron (Addgene plasmid # 21808). ECC-1 cells (4×10^3) were transfected with either 0.2 μg of eIF2α S51A plasmid DNA or empty expression vector. Transfections were performed using Lipofectamine 3000, according to manufacture instructions. Cells were treated with 100 nM BHPI 30 hours after transfection, and protein synthesis was evaluated by measuring ^{35}S-Methionine incorporation.

Immunoblotting

Western blotting was carried out as previously described (38, 40, 42). The following antibodies were used: ERα [6F11] antibody (Biocare Medical, CA), Phospho-eIF2α (Ser51) (#3398; Cell Signaling Technology), eIF2α (#5324; Cell Signaling Technologies, MA), Phospho-eEF2 (#2331; Cell Signaling Technology, MA), eEF2 (#2332; Cell Signaling Technology, MA), Phospho-p44/42 MAPK (#4370; Cell Signaling Technology, MA), p44/42 MAPK (#4695; Cell Signaling Technology, MA), Phospho-PERK (#3179; Cell Signaling Technology, MA), PERK (#5683; Cell Signaling Technology, MA), ATF6α (Imgenex, CA), Phospho-AMPKα (#2535; Cell Signaling Technology, MA), AMPKα (#2603; Cell Signaling Technology, MA), Phospho-AMPKβ1 (#4181; Cell Signaling

Technology, MA), AMPKβ1/2 (#4150, Cell Signaling Technology, MA), Phospho-Acetyl-CoA Carboxylase (#3661; Cell Signaling Technology, MA), Acetyl-CoA Carboxylate (#3676; Cell Signaling Technology, MA), Phospho-IP3R (#8548; Cell Signaling Technology, MA), IP3R (#8568; Cell Signaling Technology, MA), Pan-IP3R (sc-28613; Santa Cruz, CA), Phospho-PLCγ (#2821; Cell Signaling Technology, MA), PLCγ (#5690; Cell Signaling Technology, MA), BiP (#3177; Cell Signaling Technology, MA), $p58^{IPK}$ (#2940; Cell Signaling Technology, MA), laminin A/C (Santa Cruz, CA), β-Actin (Sigma, MO), and α- Tubulin (Sigma, MO). Bound antibodies were detected using horseradish peroxidase-conjugated secondary antibodies and chemiluminescent immunodetection with an ECL Detection Kit (GE Healthcare, NJ), and were visualized using a PhosphorImager.

Nuclear-cytoplasmic Distribution of ER

MCF-7 cells were pre-treated with 1 μM BHPI or DMSO (0.1%) for 30 minutes, followed by 2 hours with or without E2. Nuclear and cytoplasmic extraction was carried out on ~6 million cells/treatment using a NE-PER Nuclear and Cytoplasmic Extraction Reagents (ThermoScientific). Lamin A/C and α-Tubulin, were used as nuclear and cytoplasmic markers, respectively.

Protein Synthesis

Protein synthesis rates were evaluated by measuring incorporation of ^{35}S-Methionine into newly synthesized protein. Cells were plated at a density of 10,000 cells/well in 96-

well plates. Cells were incubated for 30 minutes with 3 μCi of ^{35}S methionine (PerkinElmer, MA) per well at 37^{o} C. Cells were washed two times with PBS, and lysed using 30 μL of RIPA buffer. Cell lysates were collected in microfuge tubes and clarified by centrifugation at 13,000 x g for 10 min at 4^{o} C. Samples were normalized to total protein, and the appropriate volume of sample was spotted onto Whatman 540 filter paper discs and immersed in cold 10% TCA. The filters were washed once in 10% TCA and 3 times in 5% TCA and air dried. Trapped protein was then solubilized and the filters were counted.

Calcium Imaging

Cytoplasmic Ca^{2+} concentrations were measured using the calcium-sensitive dye, Fluo-4 AM. The cells were grown on 35 mm-fluorodish cell culture plates (#FD35-100, World Precision Instruments) for two days prior to imaging experiments. The cells were loaded with 5 μM Fluo-4 AM (Life Technologies, CA) in HEPES-based buffer (140 mM NaCl, 4.7 mM KCl, 1.13 mM $MgCl_2$, 10 mM HEPES, 10 mM Glucose, pH = 7.4) for 30 minutes at 37^{o} C before measurement of intracellular calcium. The cells were washed three times with HEPES buffer to remove extracellular Fluo4-AM dye and incubated with either 2 mM $CaCl_2$ or 0 mM $CaCl_2$ for 10 minutes to complete de-esterification of the dye. Confocal images were obtained for one minute to determine basal fluorescence intensity, and then the appropriate treatment was added. Confocal images were captured using a Zeiss LSM 700 confocal system, Plan-Four 20X objective (N.A. = 0.8) and scanned at a resolution of 512x512 pixels (780ms/min). To minimize photo-bleaching and photo-

toxicity of samples, the laser power was reduced to 7%. For fluorescence measurements, the cells were excited at 488 nm, and the emission was collected at 525 nm. Images were acquired and analyzed with AxioVision and Zen software (Zeiss). Calcium traces were generated by normalizing fluorescence to basal fluorescence intensity. Data presented as mean ± standard error (n = 10 individual cells).

Protease Sensitivity Assays

ERα LBD (N304-S554) containing an N-terminal 6-His tag, was expressed and purified as described previously (43), and stored in Tris-HCl buffer (50 mM Tris-HCl pH 8.0, 10% glycerol, 2 mM DTT, 1 mM EDTA, and 1 mM Na_3VO_4). Purified ERα LBD protein (10 µg) was incubated with 500 nM E_2 for 20 min at 37^{o} C. Samples were then treated with either DMSO vehicle, BHPI (1 µM) or inactive Compound 8 (1 µM) and incubated for 20 min at 37^{o} C. For partial protease cleavage, the binding mixture was added with/without protease K at a concentration of 7.5 ng protease K per µg protein. After incubation for 10 min at 22^{o} C, the digestions were terminated by addition of SDS sample buffer buffer. The denatured samples were analyzed on a 15% SDS-PAGE gel and visualized by coomassie blue staining.

Intrinsic Fluorescence Spectroscopy

The stock solution of full-length ERα was diluted to 400 nM in a Tris- Buffer (50 mM Tris/HCl pH8.0, 150 mM KCl, 2 mM DTT, 1 mM EDTA, and 10% glycerol). The intrinsic fluorescence measurements were carried out in a 10 mm quartz cuvette using a Varian

Cary Eclipse Fluorescence Spectrophotometer. The excitation and emission slits were set at 5 nm. Tryptophan fluorescence was measured using an excitation wavelength of 295 nm. Emission spectra were collected from 310-380 nm. All spectra were collected at 37 ^{o}C E_2 (500 nM), BHPI (500 nM), or inactive compound 88 (500 nM) was added and incubated at 37 ^{o}C for 10 min, and then the ERα emission spectra were recorded. All the spectra were corrected for baseline in the absence of E_2.

Colony Formation Assays

Assays to assess anchorage-independent cell proliferation in soft agar were carried out as previously described (39). Each treatment condition was evaluated on five independent sets of cells. Culture medium was changed every 3 days. Colonies were visible after 2 weeks, and total colonies were counted at Day 21 using a dissecting microscope. Photographs of colonies were taken using a Zeiss AxioImager2 imaging system at 5X magnification.

Mouse xenograft

All experiments were approved by the Institutional Animal Care Committee (IACUC) of the University of Illinois at Urbana-Champaign. The MCF-7 cell mouse xenograft model has been described previously (44). At least 12 animals, with 2-4 tumors per mouse, were required per experimental group to maintain significant statistical power to detect >25% difference in tumor growth rates. Briefly, estrogen pellets (1 mg:19 mg estrogen:cholesterol) were implanted into 60 athymic female OVX mice, which were 7 weeks of age. Three days after E2 pellet implantation 1 million MCF-7, human breast

cancer cells per site in matrigel were subcutaneously injected at 2 sites in each flank for a total of 4 potential tumors per mouse. When the average tumor size reached 17.6 mm^2 (4.7 by 4.7 mm), E_2 pellets were removed and a lower dose of E_2 in sealed silastic tubing (1:31 estrogen:cholesterol, 3 mg total weight) was implanted in the same site. When the average tumor size reached 23.5 mm^2 (5.5 by 5.5 mm), mice were divided into 4 groups with tumor size normalized: E_2 group, no treatment control (NC) group, B_10 group and B_1/B_15 group. E_2 silastic tubes in the NC group were removed, while E_2 silastic tubes in the E2, B_10, and B_1/B_15 groups were retained. The E_2 and NC group received intraperitoneal injection every other day with 10 ml/kg vehicle (2% DMSO, 10% Tween-20, and 88% PBS). The B_10 group received 10 mg/kg BHPI by intraperitoneal injection every other day. The B_1/B_15 group received 1 mg/kg BHPI by intraperitoneal injection every other day for 14 days. Since this extremely low BHPI dose had no effect, (average tumor cross-sectional area ~45 mm^2) they then received 15 mg/kg BHPI every day for another 10 days. Food intake and body weight were measured every 4 days and food intake is presented as grams/day. Tumors were measured every 4 days with a caliper. Tumor cross sectional area was calculated as (a/2)*(b/2)*3.14, where a and b were the measured diameters of each tumor. On termination of the experiments mice were euthanized and the tumors were excised and weighed. 2 of 60 mice were removed during the course of the study, one that failed to form tumors and the other due to unrelated illness. No tumors were excluded from analysis, and blinding was not performed.

IP_3 Quantitation

MCF-7 cells were incubated for 10 minutes in 100 nM E_2, 10 μM BHPI or vehicle.

Intracellular IP_3 levels were determined by extracting the cells, and determining IP_3 levels in an assay based on competition with radiolabeled IP_3 for binding to a recombinant fragment of IP_3R containing the IP_3 binding site. Unlabeled IP_3 provided a standard for the competition assays. $1.5x10^6$ MCF-7 cells were incubated with ice-cold 1 M trichloroacetic acid (TCA) containing 1 mM EDTA on ice for 15 min. After centrifugation, the supernatant was collected and incubated for 15 min. at room temperature. The TCA solution was removed by adding two volumes of 1,1,2-Trichloro-1,2,2-trifluoroethane (TCTFE)-triocylamine solution. The TCTFE-solution was prepared by mixing 3:1 (v/v) of TCTFE and trioctylamine (Sigma). Unlabeled IP_3, labeled, IP_3 and the unlabeled IP_3R fragment were from Perkin Elmer (Waltham, MA) and were used largely according to the supplier's directions. Briefly, unlabeled IP_3 standards or cell extracts were incubated with the working receptor/tracer solution at 1:4 (v/v) for 1 hr. at 4^oC. The samples were sedimented by centrifugation at 2,000xg for 20 min and the supernatant was discarded. The pellet was suspended in 0.15 M NaOH. After 15 min. at room temperature, the samples were mixed with 5 ml of Pico-Fluor Plus scintillation fluid (Perkin Elmer, Watham, MA) and radioactivity determined by scintillation counting. IP_3 levels in biological samples were calculated from the standard curve generated using a range of unlabeled IP_3 concentrations.

EDC Dendrimer

The EDC dendrimer was prepared and used as previously described (45).

Statistical Analysis

Calcium measurements reported as mean ± S.E. All other pooled measurements are represented as mean ± S.E.M. Two-tailed student t-tests or one-way ANOVA with post-hoc Fisher's LSD tests were used to test for statistical significance ($p < 0.05$).

FIGURES

A

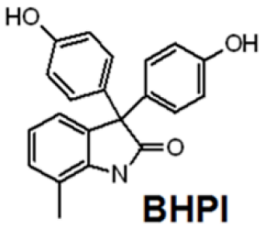

BHPI

B

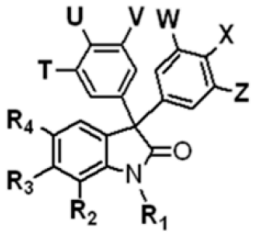

Comp.	R_1	R_2	R_3	R_4	T	U	V	W	X	Z	IC_{50} (μM)
BHPI	-H	-Me	-H	-H	-H	-OH	-H	-H	-OH	-H	.015
1	-H	-Me	-Cl	-H	-H	-OH	-H	-H	-OH	-H	.015
2	-H	-H	-H	-H	-H	-OH	-H	-H	-OH	-H	.150
3	-H	-H	-H	-Br	-H	-OH	-H	-H	-OH	-H	.300
4	-H	-H	-H	-H	-F	-OH	-H	-F	-OH	-H	.300
5	-Me	-H	-H	-H	-H	-OH	-H	-H	-OH	-H	.750
6	-Me	-Me	-H	-Br	-H	-OH	-H	-H	-OH	-H	1.5
7	-H	-H	-H	-H	-Me	-OH	-H	-H	-OH	-Me	7.5
8	-H	-H	-H	-H	-H	-OH	-Me	-H	-OH	-Me	7.5
9	-H	-Me	-H	-Me	-H	-OH	-Me	-H	-OH	-Me	>10

Figure 3.1. BHPI and structurally related compounds selectively inhibit estrogen-dependent cell proliferation. (*A*) Structure of BHPI (3,3-bis(4-hydroxyphenyl)-7-methyl-1,3,dihydro-2Hindol-2-one). (*B*) Inhibition of the proliferation of T47D cells by BHPI and by structurally related compounds (n = 6).

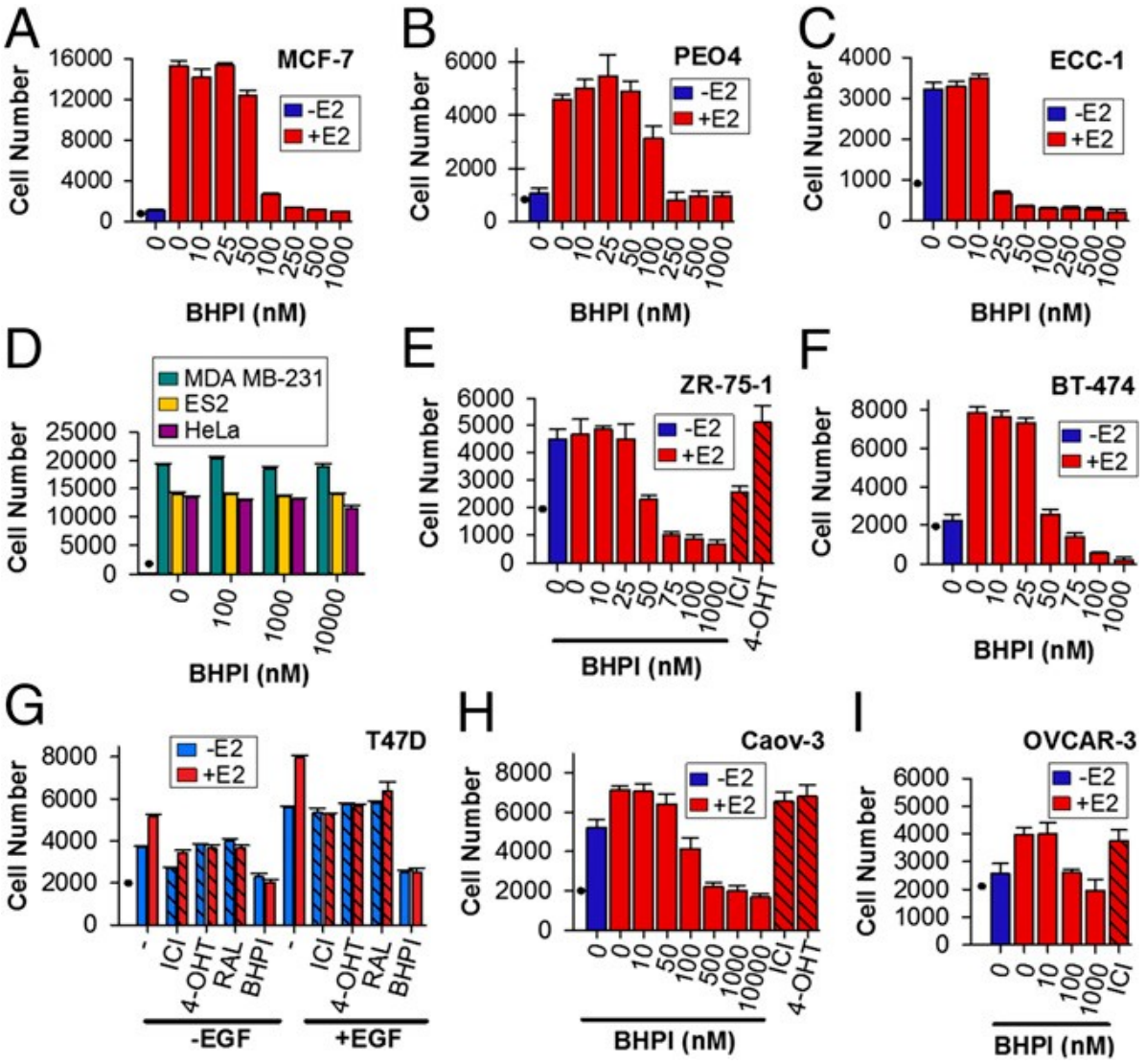

Figure 3.2. BHPI selectively inhibits proliferation of ERα$^+$ cancer cells sensitive or resistant to drug therapy. BHPI inhibits proliferation of ERα$^+$ (*A*) MCF-7 breast, (*B*) PEO4 ovarian, and (*C*) ECC-1 endometrial cancer cells with no effects on (*D*) counterpart ERα$^-$ cancer cells. Effects of BHPI on proliferation of drug-resistant cells**:** Tamoxifen- and ICI-resistant (*E*) ZR-75-1 cells and (*F*) BT-474 breast cancer cells. (*G*) T47D cells treated with 1 μM BHPI or competitor antiestrogens (4-OHT, RAL, ICI) in the presence or absence of E_2 and/or EGF. Proliferation of (*H*) cisplatin resistant Caov-3 ovarian cancer cells and (*I*) multi-drug resistant OVCAR-3 ovarian cancer cells treated with BHPI, or the antiestrogens 4-OHT or ICI. Concentrations: E_2, 1 nM (*E, G, H*) or 10 nM (*A*-*C*, *F*, *I*); EGF, 50 ng/mL (*G*); ICI, 1 μM (*E*, *G*, *H*), 5 μM (*I*); 4-OHT, 1 μM (*E*, *G*, *H*); RAL, 1 μM (*G*) "•" denotes cell number at day 0. Hatched bars denote antiestrogens (4-OHT, RAL, or ICI). Cell proliferation is expressed as mean ± SEM (n = 6).

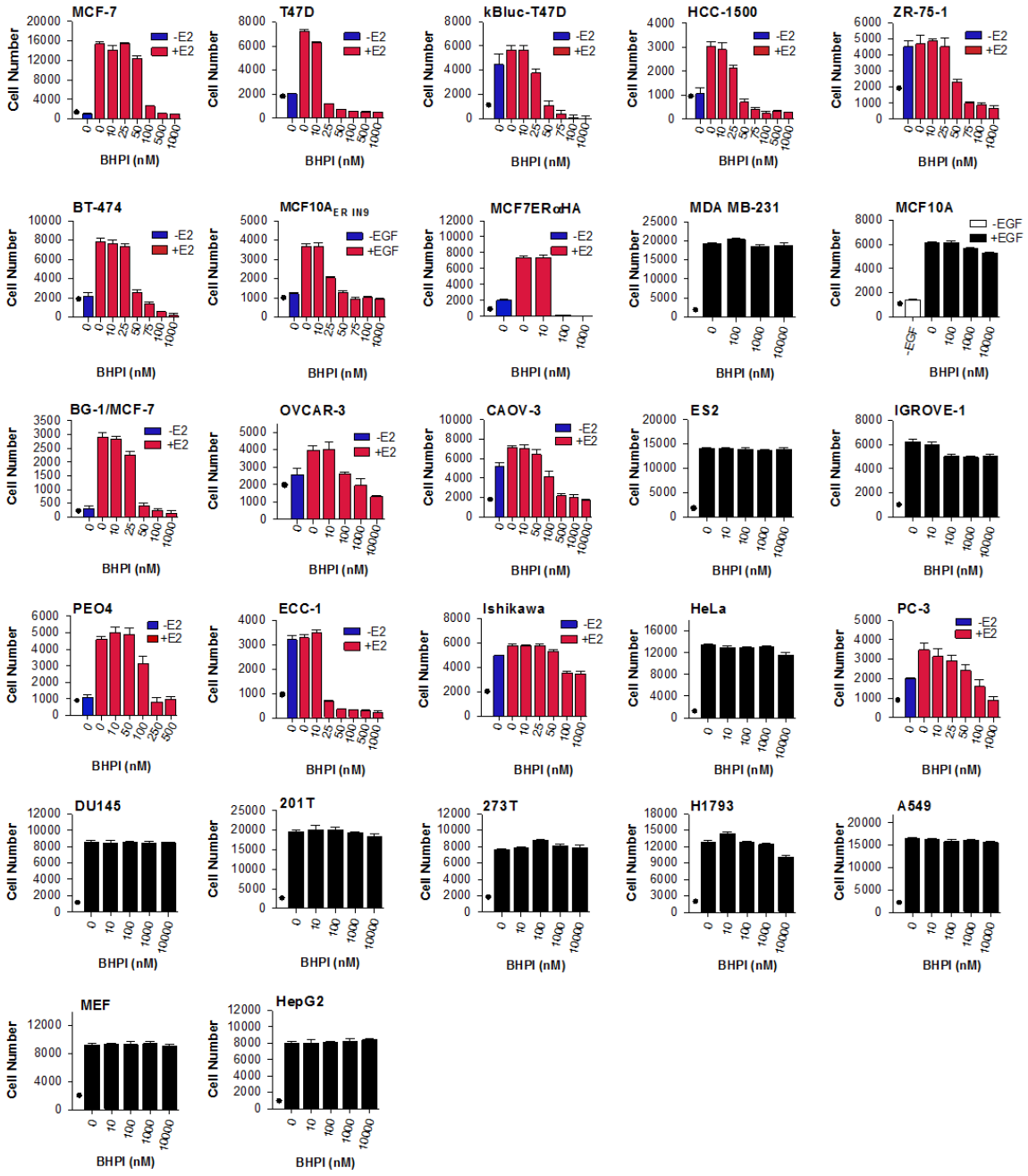

Figure 3.3. BHPI selectively inhibits cell proliferation in ERα positive cancer cells. Effects of BHPI on cell proliferation in 15 ERα positive (colored bars) and 12 ERα negative (black bars) cell lines. Cell lines are grouped by tissue of origin (breast, ovary, cervix, prostate, lung and liver). "•" on each graph denotes the number of cells at the start of the experiment. Most cell proliferation studies were for 3 or 4 days in 10 nM E2. Since we recently found that our BG-1 cells are genetically identical to MCF-7 cells, that data is presented as BG-1/MCF-7. Data is the mean ± SEM (n = 6).

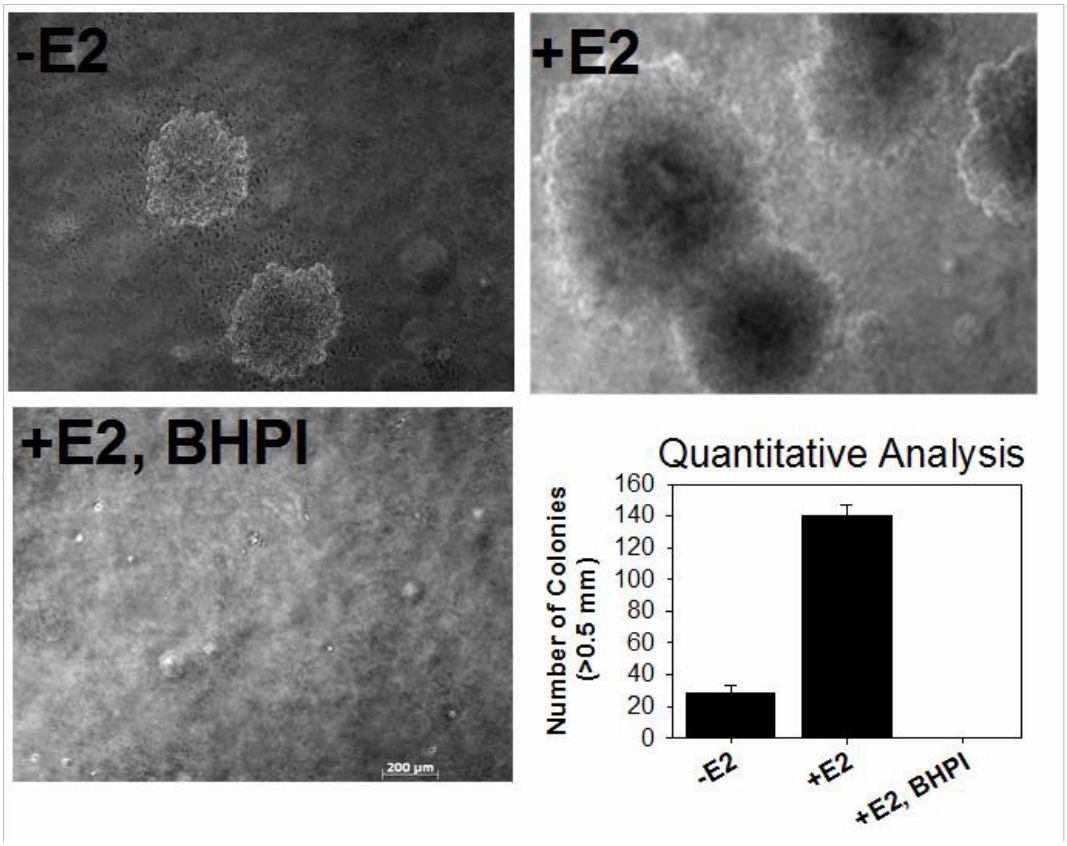

Figure 3.4. BHPI inhibits anchorage-independent growth of MCF-7 cells in soft agar. 5,000 MCF-7 cells were plated into top agar. Cells were treated with medium containing DMSO (vehicle) and either, 10 nM E2 (+E2) or Ethanol (vehicle) (-E2), or 1 μM BHPI and 10 nM E2 (+E2, BHPI). Medium was changed every 3 days. After 21 days, colonies were counted and photographed at 5x magnification. For each treatment, the bar graph represents the average of the total number colonies per well with a diameter >0.5 mm. Data is the mean ± SEM (n = 6).

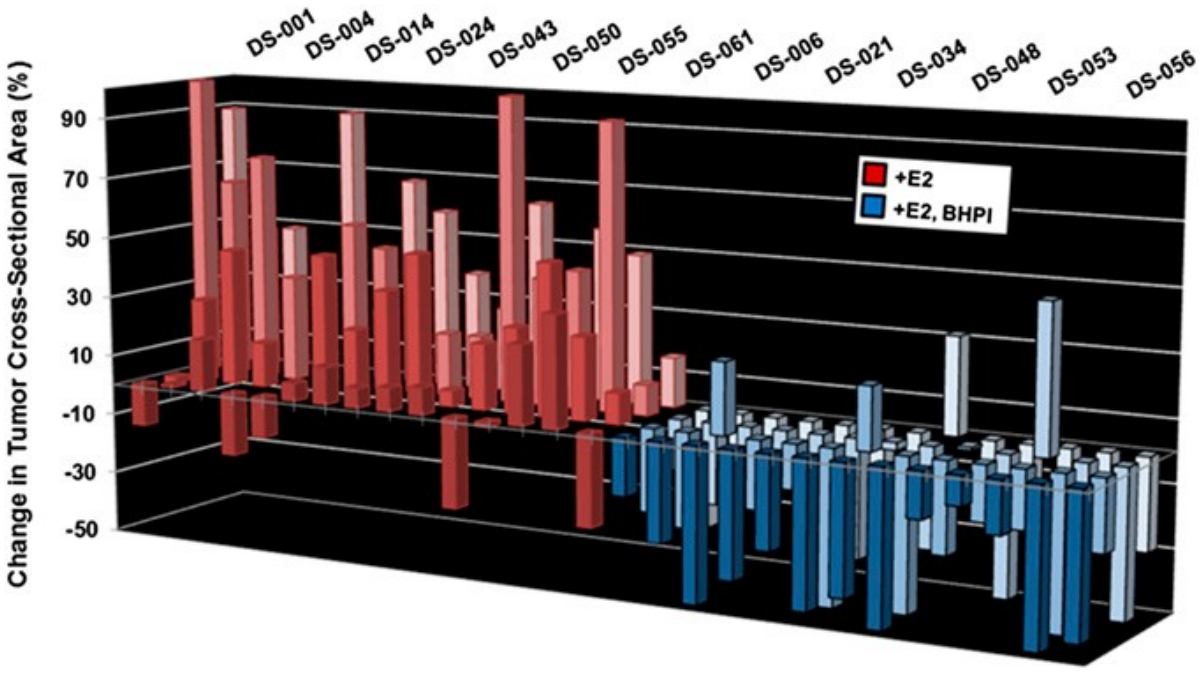

Figure 3.5. BHPI induces tumor regression in a mouse xenograft. Change in tumor cross sectional area in mouse MCF-7 xenografts after 10 days of daily IP injections of either 15 mg/kg BHPI (blue) or vehicle control (red). Tumors had an average starting cross-sectional area of ~45 mm^2. For each tumor, area at day 0 was set to 0% change.

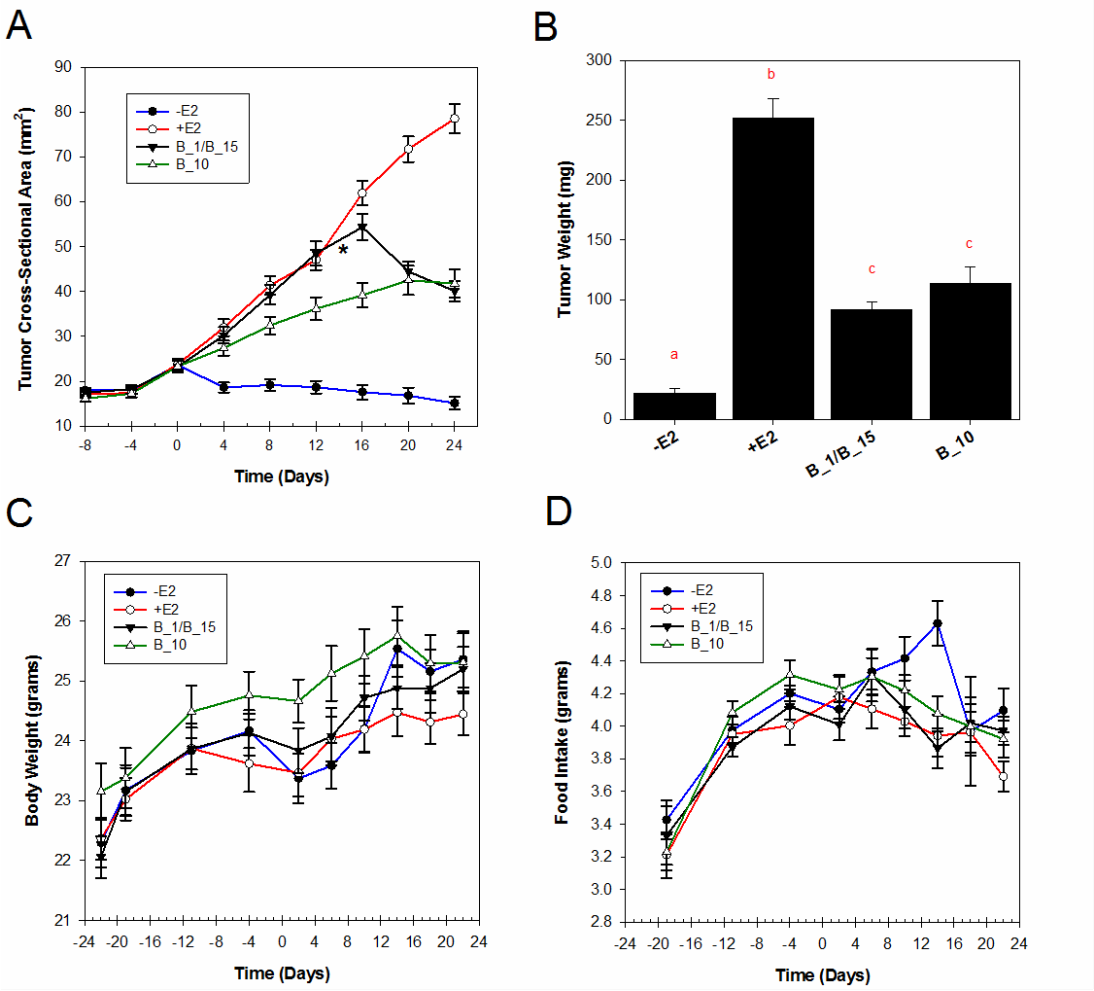

Figure 3.6. BHPI inhibits tumor growth in a mouse xenograft model of breast cancer and is not toxic. (*A*) MCF-7 tumor growth in athymic mice was monitored every 4 days by measuring tumor diameter with a caliper. The E2 and –E2 group received vehicle injection, while the B_10 group was injected with 10 mg/kg BHPI every other day. The B_1/B_15 group received the extremely low dose of 1 mg/kg BHPI every other day for 14 days. This very low dose of BHPI had no effect on tumor growth. They then received 15 mg/kg BHPI every day until the end of the study (* denotes change in dosage). Tumor size was represented as tumor cross sectional area (mm^2). Each tumor was analyzed individually, and data are expressed as mean ± SEM (n = 52). (*B*) Mice were sacrificed and tumor weights were recorded. Data is expressed as mean ± SEM (n = 52) and analyzed using one way ANOVA with post hoc Fisher's LSD test. Different letters indicate significant differences between groups ($p < 0.05$). (*C*) Mouse body weight was measured every 4 days after initiation of drug injection. Data is expressed as mean ± SEM (n = 13). (*D*) Mouse food intake was measured every 4 days after initiation of drug injection. Data expressed as mean ± SEM (n = 13). BHPI treatment had no effect on body weight or food intake and was therefore not overtly toxic.

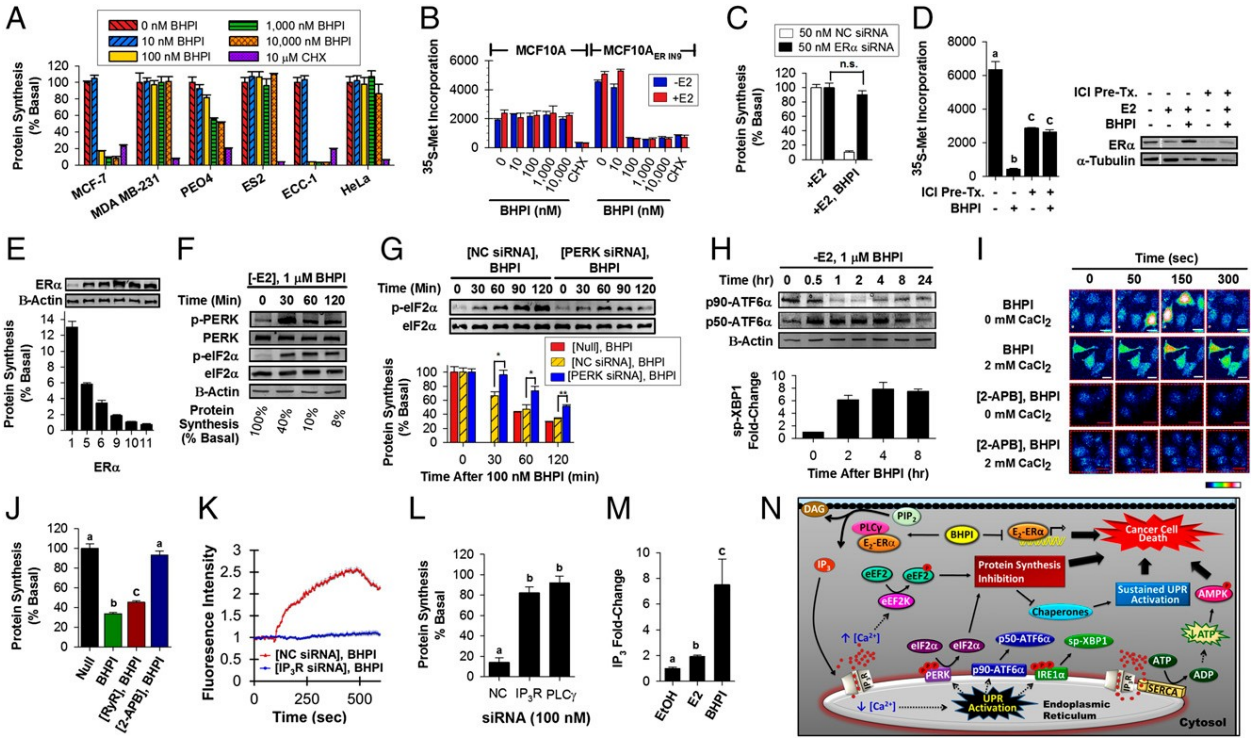

Figure 3.7. BHPI selectively inhibits protein synthesis in ERα positive cancer cells by activating PLCγ, depleting endoplasmic reticulum Ca^{2+}, and activating the UPR. (*A*) Protein synthesis in BHPI-treated $ER\alpha^{+}$ and $ER\alpha^{-}$ cells (n = 4). CHX, cycloheximide. (*B*) ERα is sufficient to make a cell sensitive to BHPI inhibition of protein synthesis. Protein synthesis in parental $ER\alpha^{-}$ MCF10A cells and ERα expressing $MCF10A_{ER\ IN9}$ cells (*n = 4*). (*C*) RNAi knockdown of ERα abolishes BHPI inhibition of protein synthesis. Protein synthesis in $MCF10A_{ER\ IN9}$ cells treated with non-coding (NC) siRNA or ERα siRNA SmartPool followed by 100 nM BHPI (*n = 4*). (*D*) Protein synthesis and immunoblot analysis of ERα protein levels in $MCF10A_{ER\ IN9}$ cells pre-treated with 1 μM ICI for 24 hours to degrade ERα, followed by treatment with 100 nM BHPI (*n = 4*). (*E*) Residual protein synthesis (untreated cells are set to 100%) after treatment with 1 μM BHPI in Doxycycline-treated MCF7ERαHA cells expressing increasing levels of ERα (n = 6). Western blot shows ERα levels in each sample. (*F*) Time course of phosphorylation of PERK and eIF2α following BHPI treatment of MCF-7 cells. (G) eIF2α phosphorylation and protein synthesis after 4-day treatment of MCF-7 cells with either 50 nM non-coding (NC) siRNA or PERK siRNA, followed by treatment with BHPI (n = 4). (H) Western blot analysis showing full-length (p90-ATF6α) and cleaved p50-ATF6α in BHPI-treated cells and effect of BHPI on levels of spliced-XBP1 mRNA (sp-XBP1). (I) BHPI increases intracellular calcium levels. Visualization of intracellular Ca^{2+} using Fluo-4 AM; BHPI (1 μM) was added to MCF-7 cells at 30 sec. Color scale from basal Ca^{2+} to highest Ca^{2+}: blue, green, red, white. (*J*) Inhibiting opening of the endoplasmic reticulum IP_3R Ca^{2+} channel abolishes BHPI inhibition of protein synthesis. The ryanodine and IP_3R Ca^{2+} channels were pre-blocked with 100 μM ryanodine (RyR) and 100 μM 2-amino propyl-benzoate (2-APB), respectively, followed by 70 nM BHPI for 3 hours (n = 4). (*K*) Quantitation of cytosolic Ca^{2+} levels after treating MCF-7 cells with either 50 nM non-coding (NC) siRNA,

Figure 3.7 (cont.)

pan IP_3R siRNA SmartPool, followed by treatment with BHPI (n = 10). IP_3R SmartPool contained equal amounts of three individual SmartPools directed against each isoform of IP_3R. (*L*) Effects of BHPI on protein synthesis in MCF-7 cells treated with either 100 nM NC siRNA, pan-IP_3R siRNA, or PLCγ siRNA SmartPool (n = 4). (*M*) Quantitation of intracellular IP_3 levels following treatment of MCF-7 cells for 10 min. with E2 or BHPI (n=3) (*N*) Model of BHPI acting through the UPR, eEF2 and AMPK to kill ERα^+ cancer cells. Data is mean ± S.E.M. Different letters indicate a significant difference among groups ($p < 0.05$) using one-way ANOVA followed by Tukey's post hoc test. ns, not significant. ***$P < 0.001$, compared with NC control. ns, not significant. **I designed and performed research experiments, and analyzed data for the panel I, J, K, and M.**

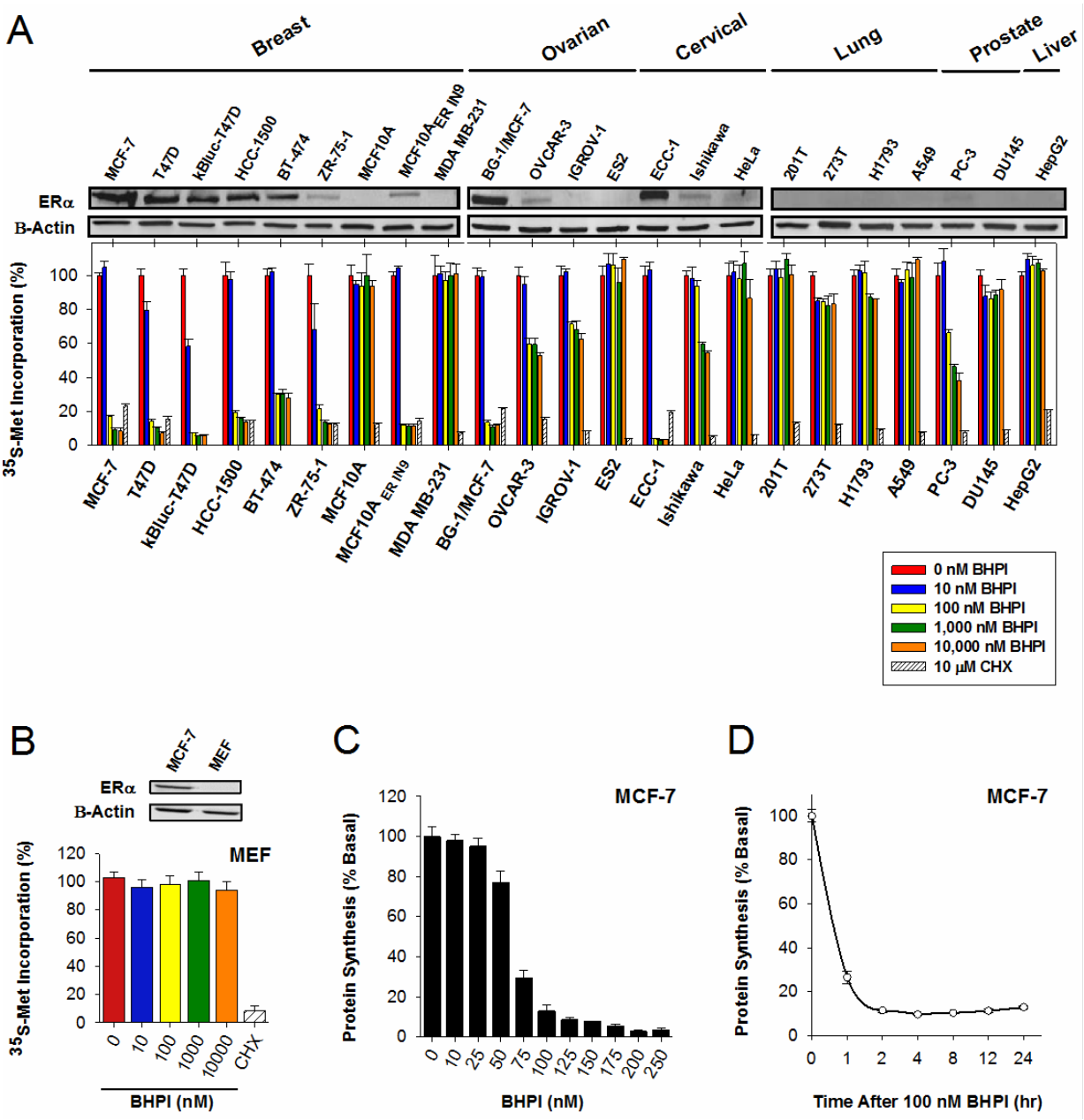

Figure 3.8. BHPI selectively inhibits protein synthesis in ERα positive cells in 26 cells lines. (*A*) Comparison of ERα protein levels and the effects of BHPI treatment on protein synthesis in 23 cell lines. The number of samples was too large to run on a single gel and the data is from 3 identically processed gels. (*B*) Effects of BHPI on protein synthesis in ERα$^-$ Mouse Embryo Fibroblast (MEF) cells. Incorporation with no added BHPI was set to 100%. In general, protein synthesis in cells expressing moderate or high levels of ERα was robustly inhibited by 100 nM BHPI (yellow bars), while 10,000 nM BHPI (orange bars), the highest concentration tested, had very little or no effect on protein synthesis in ERα negative cells. Cells expressing low levels of ERα, more typical of non-transformed ERα containing cells, such as PC-3 prostate cancer cells, were much less

Figure 3.8 (cont.)

sensitive to BHPI inhibition of protein synthesis. Western blot of ERα protein levels in MEF cells. (*C*) Dose-response curve, which shows the effects of increasing concentrations of BHPI on protein synthesis in MCF-7 cells following 24-hour treatment. The narrow dose-response curve is consistent with either activation of the autoactivated kinase PERK, or with a threshold level of calcium required for PERK activation (*D*) Time course showing the effect of 100 nM BHPI on protein synthesis in MCF-7 cells. Data is the mean ± SEM (n = 4). **I designed and performed research experiment, and analyzed data for the panel B.**

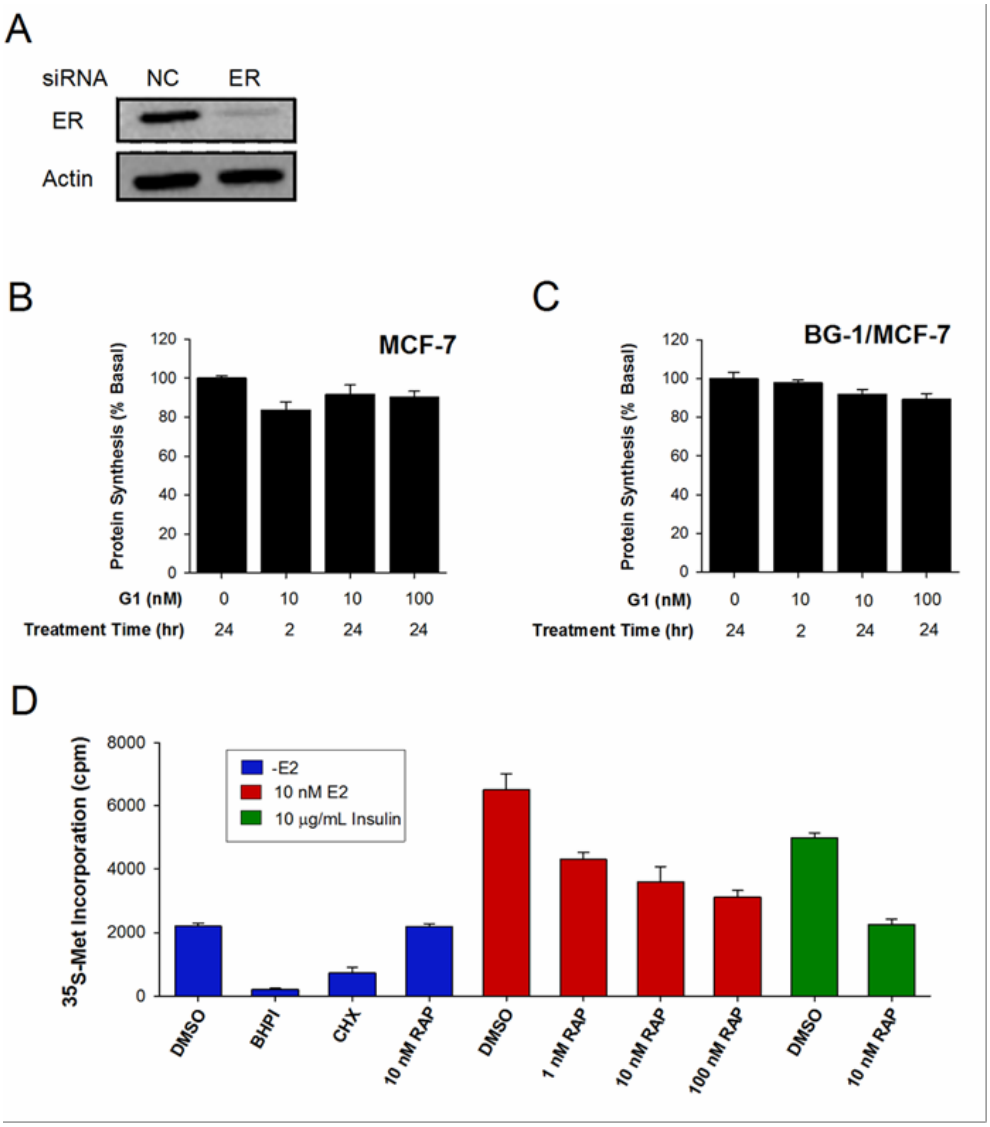

Figure 3.9. Activation of the estrogen binding protein, GPR30, or inhibition of mTOR, have minimal effects on protein synthesis. (*A*) Western blot analysis of ERα levels after treatment of MCF-7 cells with either 100 nM non-coding SmartPool siRNA or 100 nM SmartPool ERα siRNA. Effects of the GPR30 activator, G1, on (*B*) MCF-7 and (*C*) BG-1/MCF-7 cells. Cells were plated at 10,000 cells/well, the indicated concentrations of G1 (0- 100 nM) were added for the times indicated, and ^{35}S-Methionine incorporation was used to assess rates of protein synthesis. Protein synthesis with no added G1 was set to 100%. (*D*) The effects of rapamycin (RAP) on protein synthesis in MCF-7 cells in the absence of growth factors (blue bars), or in the presence of 10 nM E2 (red bars) or 10 µg/ml Insulin (green bars). Inhibition of mTORC1 with rapamycin blocks insulin-dependent increases in protein synthesis (green bars) and substantially blocks estrogen-dependent increases in protein synthesis (red bars). In contrast, BHPI and cycloheximide (CHX) treatment elicit near-quantitative inhibition of protein synthesis, far below baseline levels of protein synthesis (blue bars). Data is mean ± SEM (n = 4).

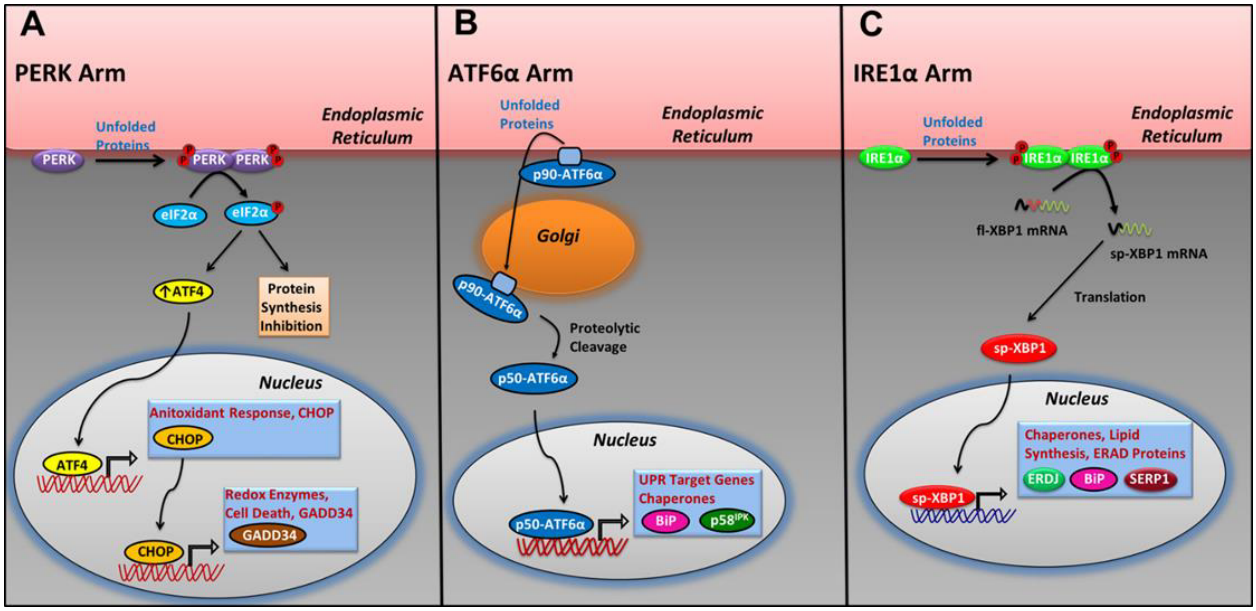

Figure 3.10. Endoplasmic reticulum (EnR) stress activates the three arms of the UPR. (*A*) EnR stress induces the oligomerization and phospho-activation of the transmembrane kinase PERK. P-PERK phosphorylates eukaryotic initiation factor 2α (eIF2α), leading to inhibition of protein synthesis and a reduction in the endoplasmic reticulum protein folding load (46, 47). Reduced protein synthesis increases levels of the transcription factor, ATF4. ATF4 induces the transcription factor CHOP, which induces GADD34 and several pro-apoptotic genes. (*B*) EnR stress promotes the translocation of the transmembrane protein, p90-ATF6α, from the EnR to the Golgi Apparatus, where it encounters proteases that liberate the N-terminal fragment of ATF6α (p50-ATF6). p50-ATF6 increases the protein-folding capacity of the EnR by inducing EnR-resident chaperones, including BiP and GRP94 (47-48). (*C*) EnR stress induces the oligomerization and phospho- activation of the transmembrane protein, IRE1α (46, 47, 49). Activated IRE1α removes an intron from full- length XBP1 (fl-XBP1) mRNA, producing spliced (sp)-XBP1 mRNA, which is subsequently translated into sp- XBP1 protein (sp-XBP1). sp-XBP1 increases the protein-folding capacity of the EnR and turnover of misfolded proteins by inducing EnR resident-chaperone protein genes (BiP, HEDJ, SERP1), EnR-associated degradation (ERAD) genes and alters mRNA decay and translation (36, 47).

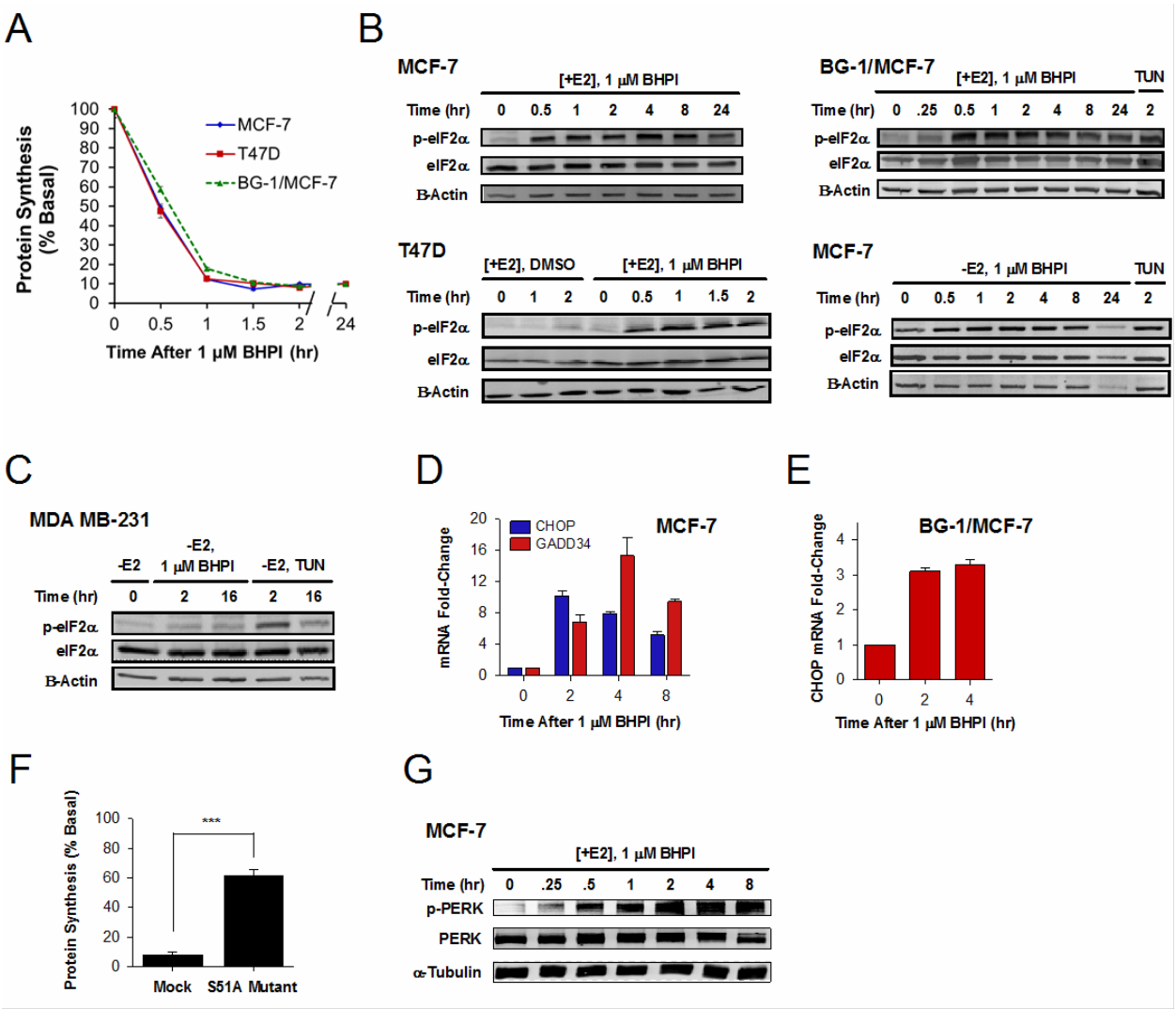

Figure 3.11. In ERα positive cell lines, BHPI rapidly inhibits protein synthesis by activating the PERK arm of the UPR. (*A*) Time course of BHPI inhibition of protein synthesis. ERα positive MCF-7, T47D, and BG-1/MCF-7 cells were incubated for the indicated times with 1 μM BHPI. Set to 100% was incorporation of ^{35}S-methionine into protein at time = 0. Data is mean ± SEM (n = 4). At 30 min. with BHPI, ^{35}S-methionine incorporated into protein was reduced by ~50%. (*B*) In the presence [+E2], BHPI increases p-eIF2α (Ser-51) in ERα^{+} MCF-7, BG-1/MCF-7, and T47D cells. In the absence of estrogen (-E2), BHPI increases eIF2α phosphorylation in ERα^{+} MCF-7 cells. (*C*) BHPI does not increase p-eIF2α in ERα negative MDA MB-231 cells. Since the UPR activator Tunicamycin (TUN) increased p-eIF2α in these cells, the absence of BHPI induced phosphorylation of eIF2α in the MDA-MB-231 cells was not due to the inability of UPR activation to induce eIF2α phosphorylation. (*D*) Induction of CHOP and GADD34 mRNA in MCF-7 cells following treatment with 1 μM BHPI, as determined by qRT-PCR. (*E*) Induction of CHOP mRNA in BG-1/MCF-7 cells following treatment with 1 μM BHPI. Increased levels of ATF4 induce the transcription factor, CHOP, which then induces GADD34. Increased phosphorylation of eIF2α results in translational upregulation of the

Figure 3.11 (cont.)

transcription factor, ATF4. ATF4 contains short, inhibitory upstream open reading frames (uORFs), which normally inhibit translation of ATF4 mRNA (46). Under conditions of reduced eIF2α availability, the inhibitory uORFs are skipped, allowing ATF4 translation. (*F*) Effects of 100 nM BHPI on protein synthesis following transfection of ECC-1 endometrial cells with either a dominant-negative eIF2αS51A mutant or empty vector. Data is the mean ± SEM (n = 4). *** p <0.001. (*G*) Time course of phosphorylation of PERK (Thr-980) and total PERK protein levels following treatment with BHPI in MCF-7 cells. PERK-Thr^{980} phosphorylation serves as a marker of PERK activation.

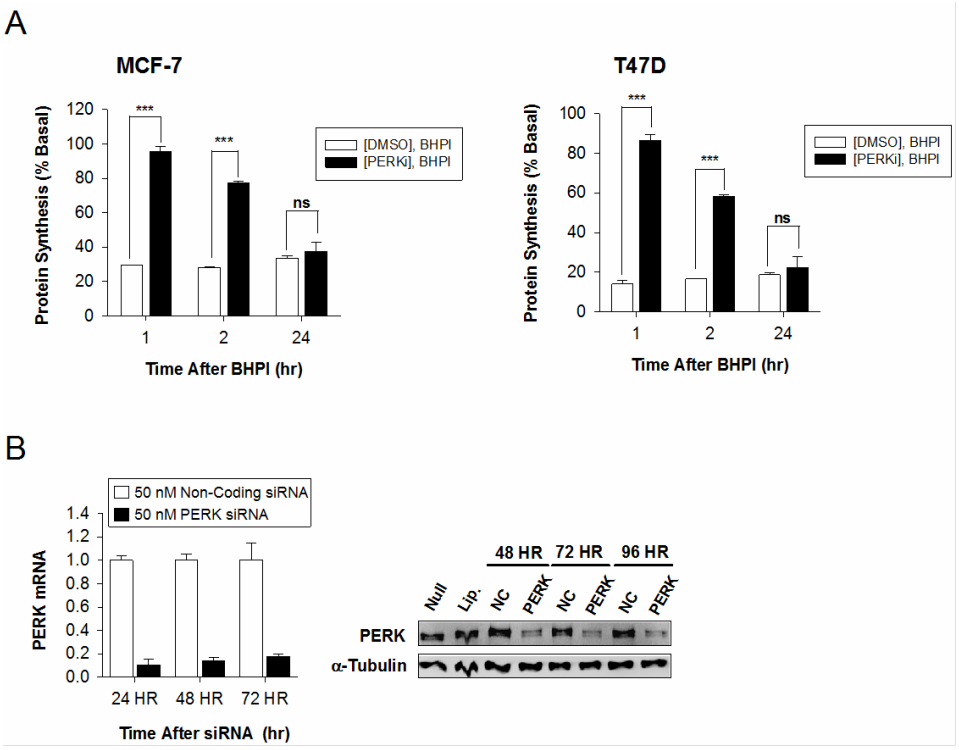

Figure 3.12. Blocking PERK activation or PERK knockdown largely blocks inhibition of protein synthesis at early times after BHPI treatment, but does not prevent BHPI from inhibiting protein synthesis at later times. (*A*) Inhibiting PERK activation with the PERK inhibitor, GSK2606414 (PERKi) (50, 51), blocks rapid BHPI inhibition of protein synthesis in MCF-7 and T47D cells (n = 4). Cells were pre-treated for 1 hour with DMSO-vehicle or 1 μM GSK2606414, followed by treatment with 100 nM BHPI for the indicated times. (*B*) RNAi knockdown of PERK mRNA and protein. MCF-7 cells were transfected with either 50 nM PERK siRNA SmartPool (PERK) or with 50 nM of a control non-coding SmartPool (NC). PERK mRNA levels were determined by qRT-PCR with 36B4 as internal standard. Set to 1 at each time was the level of PERK mRNA in cells transfected with the Non-coding control (NC) siRNA. Shown is a Western blot of PERK protein levels after transfection with PERK siRNA and control siRNA (NC). Null: control cells, no transfection; Lip: liposome only no siRNA. Data is the mean ± SEM. *** $p < 0.001$; ns, not significant ($p > 0.05$). **I designed and performed research experiment, and analyzed data for the panel A.**

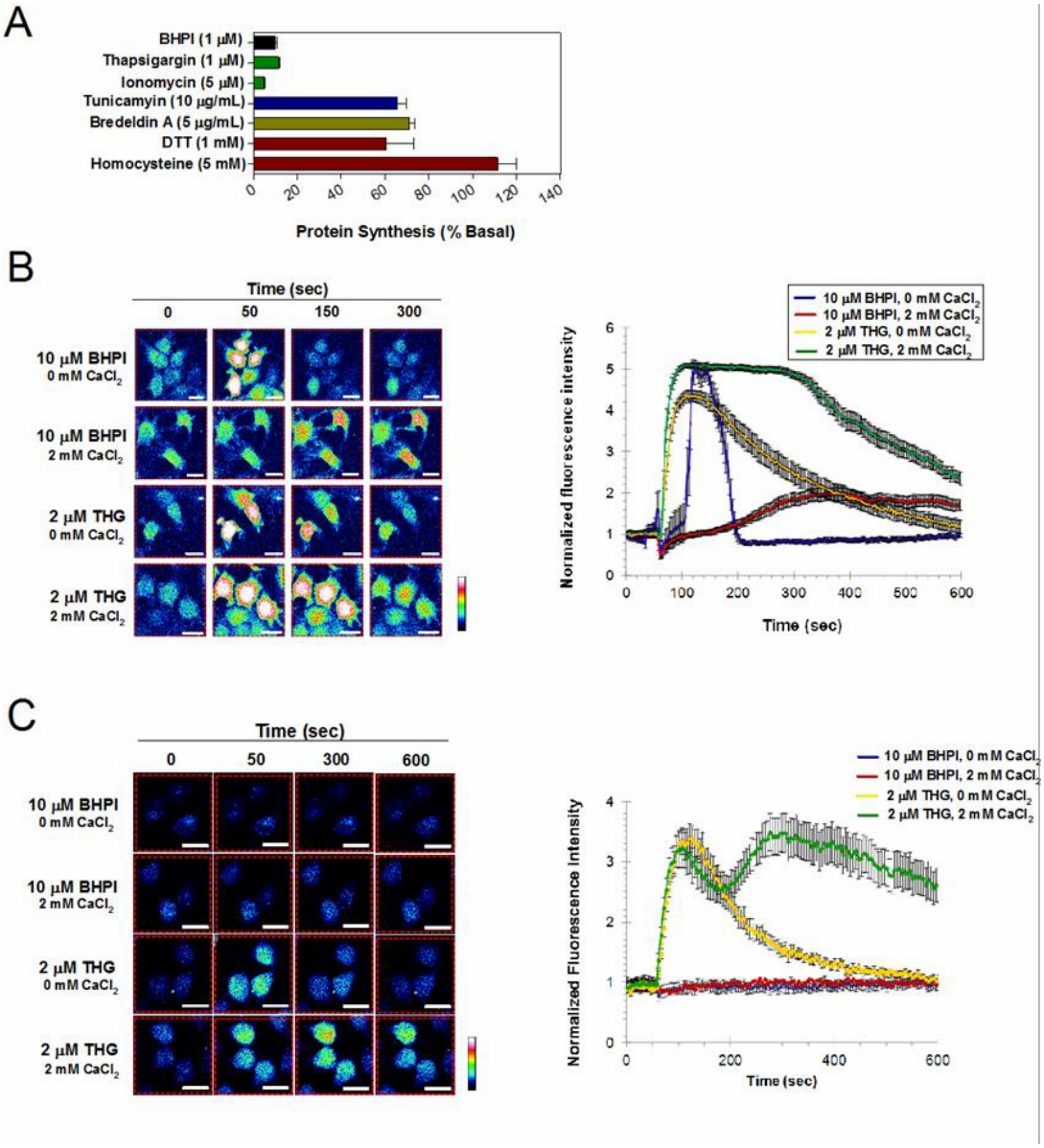

Figure 3.13. BHPI activates the UPR through depletion of endoplasmic reticulum calcium stores in ERα$^+$ MCF-7 breast cancer cells, but not in ERα$^-$ HeLa cervical cancer cells. (*A*) Protein synthesis in MCF-7 cells treated for 2 hours with UPR activators (n = 6). Effect of BHPI and Thapsigargin (THG) on intracellular calcium levels in (*B*) ERα$^+$ MCF-7 breast cancer cells and (*C*) ERα$^-$ HeLa cervical cells. Although BHPI has no effect, HeLa cells remain sensitive to Thapsigargin. Cells visualized with the Ca^{2+}sensitive dye Fluo-4 AM. Low levels of basal [Ca^{2+}] are blue and then green, whereas higher levels of [Ca^{2+}] are seen as red, with the highest levels white. Trace represents calcium following treatment with Thapsigargin or BHPI. Intensity was normalized to the basal signal, which was set to 1. Data is mean ± SEM (n = 10). **I designed and performed research experiments, and analyzed data for the entire figure.**

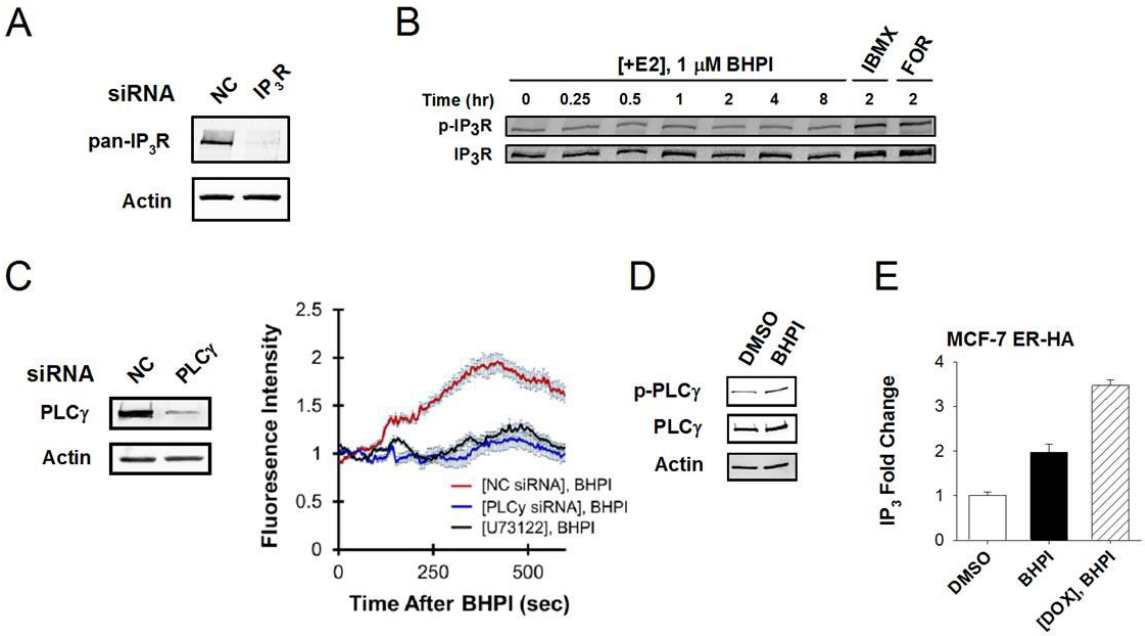

Figure 3.14. Effects of BHPI on IP3R, IP3, and PLCγ. (*A*) Western blot analysis of pan-IP3R protein levels after treatment of MCF-7 cells with either 100 nM non-coding (NC) SmartPool siRNA or 100 nM SmartPool IP3R siRNA. Data in panel *A* is from ([40]). (*B*) Time course of phosphorylation of the IP3R Ca^{2+}-channel and total IP3R following treatment with BHPI. Phosphorylation of IP3R at Ser-1756 by cyclic AMP- dependent protein kinase A (PKA) regulates the activity of the IP3R Ca^{2+} channel. While BHPI had no effect, the MCF-7 cells contain a functional protein kinase A pathway since the protein kinase A activators, IBMX and Forskolin, increased phosphorylation of IP3R. (*C*) Effects of BHPI on cytosol Ca^{2+} following either PLCγ knockdown or blocking PLCγ activation with U73122. Western blot shows PLCγ protein levels following treatment of MCF-7 cells with either 100 nM non-coding SmartPool siRNA or 100 nM SmartPool PLCγ siRNA. (*D*) Effects of BHPI on phosphorylation and activation of PLCγ. Phosphorylation of PLCγ at Tyr-1756 regulates the activity of PLCγ. MCF-7 cells were treated for 10 min. with 1 μM BHPI. (*E*) Effects of overexpressing ERα on BHPI-induced increases in IP3 levels. ERα in MCF7ERαHA cells was induced with DOX as described in Figure 3*E*. IP3 levels were determined 10 min. after treatment with 1 μM BHPI. Data is mean ± SEM (n=3). **I designed and performed research experiments, and analyzed data for the panel C and E.**

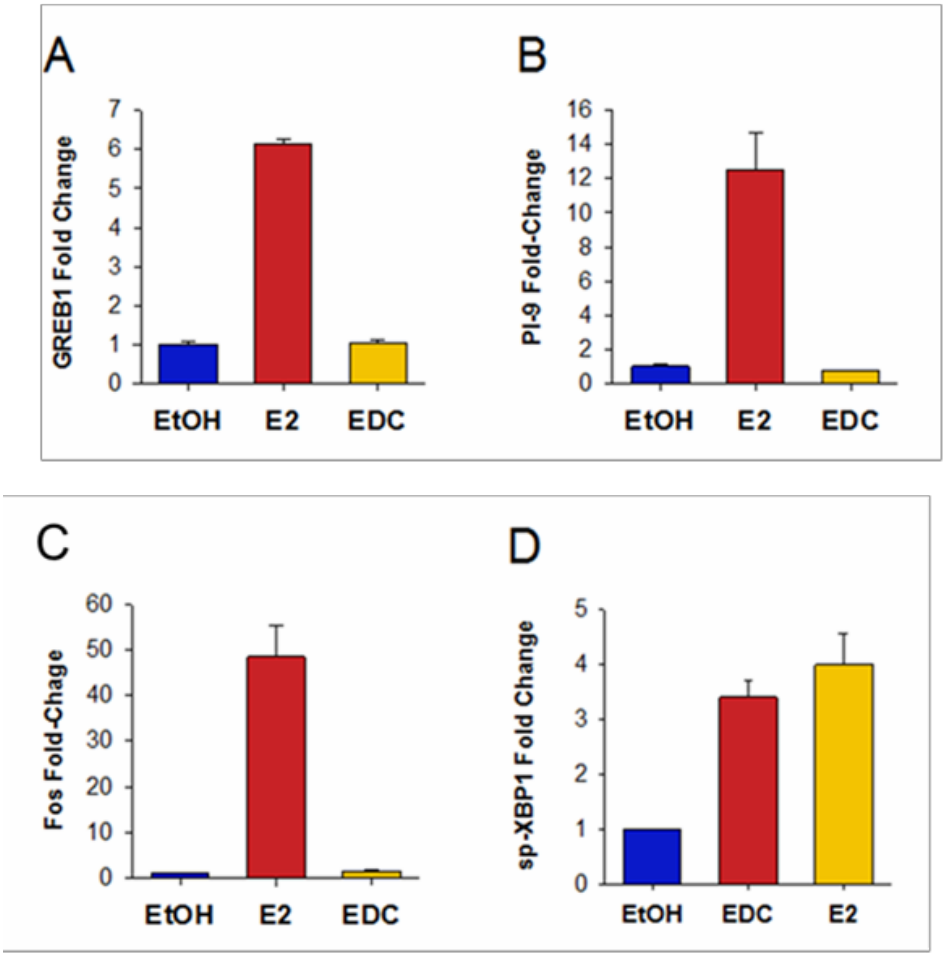

Figure 3.15. Comparison of effects of 17β-estradiol (E2) and estrogen-dendrimer-conjugate (EDC) on the ability of ERα to activate (*A*) GREB1, (*B*) PI-9, and (*C*) Fos expression. These are classical estrogen-regulated genes. (*D*) Comparison of the effects of E2 and EDC on the ability to induce spliced-XBP1 (sp-XBP1), which is a widely used marker of UPR activation. **I designed and performed research experiments, and analyzed data for the entire figure.**

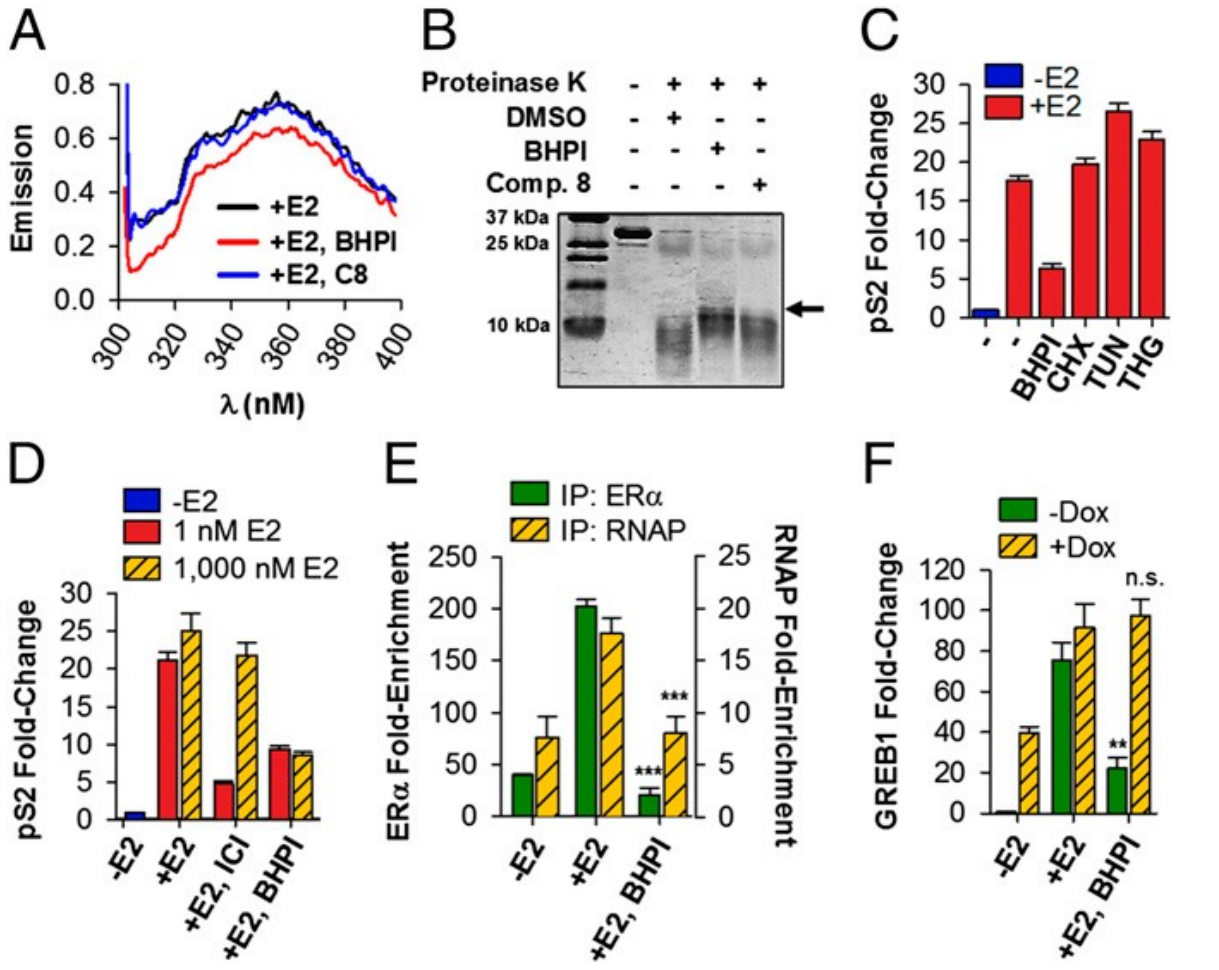

Figure 3.16. BHPI interacts with ERα and inhibits E_2-ERα regulated gene expression. (*A*) Fluorescence emission spectra of full-length ERα in the presence of E_2 and either DMSO, 500 nM BHPI, or 500 nM of the BHPI-related inactive Compound 8 (C8). (*B*) ERα LBD was subjected to proteinase K digestion in the presence of DMSO vehicle, C8, or BHPI. Bands were visualized by Coomassie-staining. (*C*) qRT-PCR showing pS2 mRNA in MCF-7 cells pre-treated for 0.5 hours with BHPI, cycloheximide (CHX), Tunicamycin (TUN), Thapsigargin (THG), or DMSO, followed by treatment with or without E_2 for 2 hours. (*D*) BHPI is a non-competitive ERα inhibitor. qRT-PCR showing pS2 mRNA in MCF-7 cells treated with BHPI or the competitive inhibitor ICI, and low (1 nM) or high (1,000 nM) E_2. (*E*) ChIP showing effect of BHPI on recruitment of E_2-ERα (green bars) and RNA polymerase II (RNAP, yellow hatched bars) to the promoter region of pS2. (*F*) qRT-PCR showing GREB1 mRNA levels in MCF7ERαHA cells after 1 day + or – doxycycline (DOX), pre-treated for 30 minutes with BHPI or DMSO, followed by 4 hours with or without E_2. Concentrations: E_2, 500 nM (*A* and *B*), 10 nM (*C*-*F*); BHPI, 500 nM (*A*) or 1 μM (*B*-*F*); C8, 500 nM (*A*) or 1 μM (*B*); CHX, 10 μM; THG, 1 μM; TUN, 10 μg/ml. Data is mean ± SEM (n = 3). * $P < 0.05$, ** $P < 0.01$, ***$P < 0.001$, compared with +E_2 samples. n.s., not significant. **I designed and performed research experiments, and analyzed data for the panel A and B**.

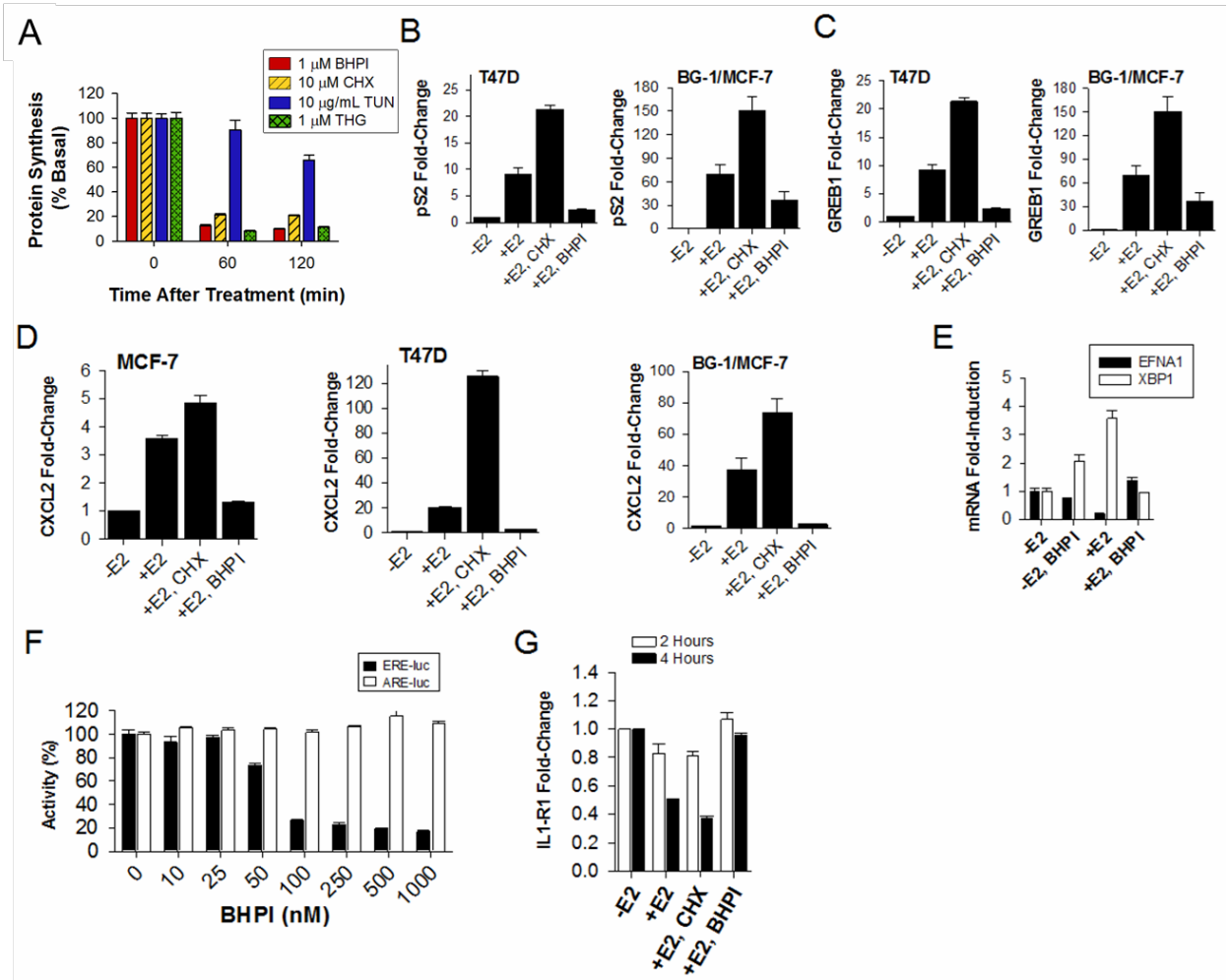

Figure 3.17. BHPI inhibits E2-ERα regulated gene expression. (*A*) Comparison of the effects of BHPI, the protein synthesis inhibitor cycloheximide (CHX), and the UPR activators Tunicamycin (TUN) or thapsigargin (THG) on protein synthesis. Since protein synthesis was robustly inhibited by CHX after 120 minutes, this time was used in the gene expression studies. Effects of BHPI on E2-ERα induction of (*B*) pS2, (*C*) GREB1 and (*D*) CXL2 mRNAs and (*E*) XBP1 in MCF-7, T47D and BG-1/MCF-7 cells. Cells were pretreated with either 1 μM BHPI (+E2, BHPI), 10 μM cycloheximide (+E2, CHX), or 0.1% DMSO (+E2; -E2) for 30 minutes, followed by treatment with either 10 nM E2 (+E2; +E2, BHPI; +E2, CHX) or 0.1% ethanol-vehicle control (-E2) for 2 hours. (*F*) Dose response studies of the effect of BHPI on E2-ERα induction of ERE-luciferase activity in ERα positive T47D-kBluc breast cancer cells (black bars) and for dihydrotestosterone-androgen receptor (DHT-AR) induction of prostate specific antigen (PSA)-luciferase in ERα negative HeLaA6 cells (open bars). HeLaA6 cells are stably transfected to express AR and a PSA-luciferase reporter. Supporting specificity of BHPI, it did not inhibit DHT-AR induction of ARE-luciferase. BHPI blocks E2-ERα down-regulation of EFNA1 in MCF-7 cells(*E*) and IL1-R1 in T47D cells (*G*). Data is mean ± SEM (n = 3).

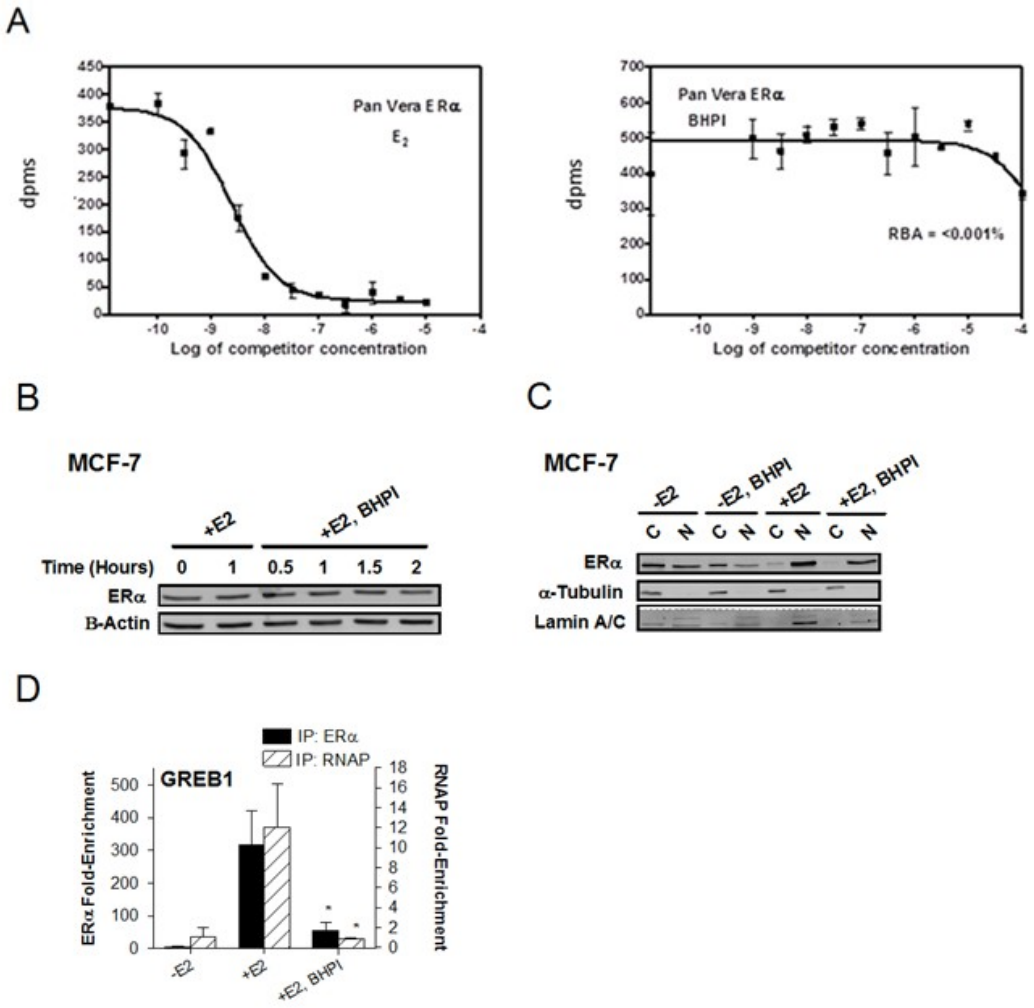

Figure 3.18. BHPI is a non-competitive inhibitor that reduces binding of E2-ERα to gene regulatory regions. BHPI does not compete with estrogens for binding to ERα. (*A*) Competitive radioligand binding assay comparing the ability of E2 and BHPI to compete with [^{3}H] estradiol (E2) for binding to ERα. The relative binding affinity (RBA) of BHPI for the estrogen-binding pocket of ERα was determined using 0.2 nM [^{3}H] E2 and a range of BHPI concentrations. RBA values were determined from the competitive radiometric binding assay (43, 52). Values are expressed as percentages relative to the affinity of the standard, E2 = 100%. (*B*) Western blots showing that at early times after treatment with 1 μM BHPI, ERα protein levels are nearly unchanged. (*C*) Western blot showing that treatment of MCF-7 cells with 1 μM BHPI does not inhibit nuclear localization of ERα. α-Tubulin and lamin A/C were controls for the cytoplasmic and nuclear fractions, respectively. ERα protein levels and nuclear localization were assessed 2 hours after treatment, which was the same time used to assess endogenous mRNA levels of E2-ERα regulated genes via qRT-PCR. (*D*) ChIP shows that 1 μM BHPI BHPI inhibits recruitment of E2-ERα (black bars) and RNA polymerase II (RNAP, hatched bars) to the GREB1 promoter region. Data is mean ± SEM (n = 3). * Significant at ($p < 0.05$).

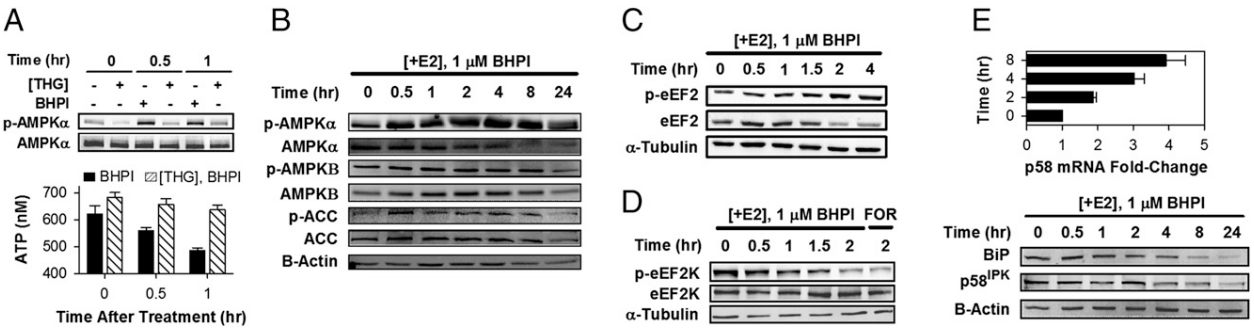

Figure 3.19. BHPI depletes intracellular ATP stores, activates AMPK, and inhibits protein synthesis at a second site. (*A*) Inhibiting SERCA pumps with Thapsigargin (THG) prevents BHPI from reducing intracellular ATP levels. Western blot showing effect of THG (1 μM) or BHPI (1 μM) treatment of MCF-7 cells on AMPKα-Thr^{172} phosphorylation. ATP levels in MCF-7 cells treated with 1 μM BHPI, or 1 μM BHPI and 1 μM THG (n = 5). (*B*) Western blot analysis of the time course of AMPKα (Thr-172), AMPKβ (Ser-108), acetyl CoA carboxylase (ACC) (Ser-79) phosphorylation in BHPI-treated MCF-7 cells. AMPKα-Thr^{172} and AMPKβ-Ser^{108} phosphorylation are required for AMPK activation. (*C*) Western blot analysis of eEF2 phosphorylation (Thr-56) over time in BHPI-treated ERα^{+} MCF-7 cells. (*D*) Western blot analysis showing the time course of decreasing eEF2K (Ser-366) phosphorylation in BHPI-treated MCF-7 cells. Ser-366 dephosphorylation activates eEF2K. (*E*) qRT-PCR analysis showing changes in p58^{IPK} mRNA and Western blot analysis showing p58^{IPK} and BiP protein after treatment with BHPI (n = 3). -E_2 set to 1.

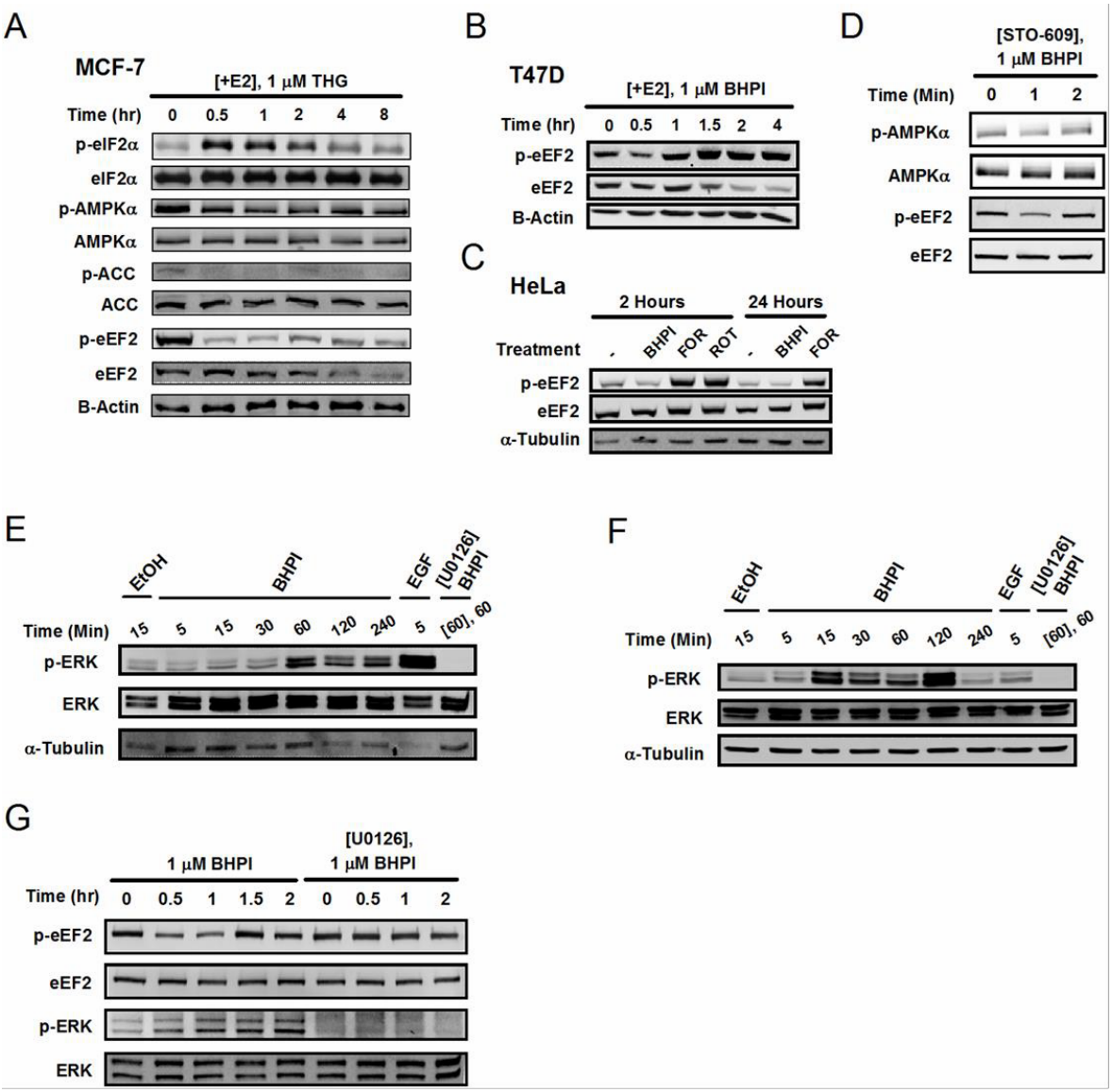

Figure 3.20. Conventional UPR activators do not induce phosphorylation of eEF2, but induces transient eIF2α phosphorylation, transient inhibition of protein synthesis, and induction of chaperones. (*A*) Analysis of the time course of Thapsigargin (THG) effects on phosphorylation of eIF2α (Ser-51), AMPKα (Thr-172), ACC (Ser-79), and eEF2 (Thr-56). Unlike BHPI, Thapisgargin does not induce phosphorylation of eEF2 but induces transient phosphorylation of eIF2α. Western blots of the time course of BHPI effects on phosphorylation of eEF2 (Thr-56) in (*B*) ERα positive T47D and (*C*) ERα negative HeLa cells. T47D Cells were pre-treated with 10 nM E2 for 24-hours. eEF2 is essential for protein synthesis, and eEF2-Ser^{56} phosphorylation inactivates eEF2, blocking the elongation step of protein synthesis. The positive controls, Forskolin (FOR) and Rottlerin (ROT) induce robust eEF2 phosphorylation, demonstrating eEF2 retains the capacity for phosphorylation in HeLa cells. (*D*) Inhibiting AMPK phosphorylation and activation with ST-609 did not block BHPI-stimulated phosphorylation of eEF2. Effects of BHPI on Thr-202/Thr-204 phosphorylation of p44/p42 MAPK (p-ERK) in ERα positive (*E*) MCF-7 cells and (*F*) T47D cells. Activation of p44/p42 MAPK promotes the

Figure 3.20 (cont.)

phosphorylation and inactivation of eEF2K. The classical ERK activator, EGF (20 ng/ml), served as a positive control for ERK1/2 phosphorylation. As a control, cells were treated with 10 μM UO126 for the indicated times. U0126 inhibits the upstream kinase MEK1/2, inhibiting ERK1/2 phosphorylation. UO126 pre-treatment was for 2 hours. (*G*) Effects of blocking ERK activation with U0126 on BHPI-induced phosphorylation of eEF2. By inhibiting the ERK pathway, UO126 allows eEF2K to be active and the reduced activation seen at 0.5 and 1 hours due to BHPI-induced ERK activation is abolished.

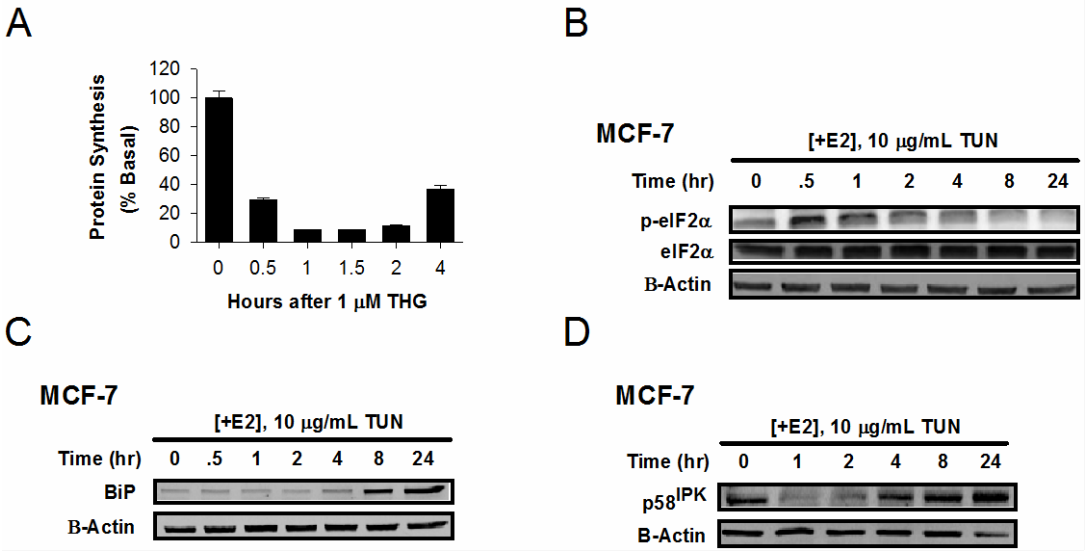

Figure 3.21. The UPR activators, Thapsigargin and Tunicamycin, reversibly activate the UPR. Induction of BiP and p58^{IPK} normally helps resolve UPR stress and reverses UPR activation. (*A*) Time course of THG inhibition of protein synthesis. Consistent with transient phosphorylation of eIF2α by THG (see Figure S15*A*) and resolution of UPR stress, protein synthesis begins to recover at 4 hours after treatment with THG. (*B*) Western blot analysis of phosphorylation of eIF2α following TUN treatment. TUN induces transient phosphorylation of eIF2α. Western blot analysis showing the time course of Tunicamycin (TUN) induction of BiP (*C*) and p58^{IPK} (*D*) in MCF-7 cells. Data in panel *C* is from ([40], supplementary figures). Data is mean ± SEM (n = 3). (*A*-*D*) 24-hour pre-treatment with 10 nM E_2.

REFERENCES

1. Korach K.S. DBJ (2006) Estrogen receptors and human disease. *J Clin Inv* 116(3):561-571.
2. Musgrove EA & Sutherland RL (2009) Biological determinants of endocrine resistance in breast cancer. *Nat Rev Cancer* 9(9):631-643.
3. Tyson JJ*, et al.* (2011) Dynamic modelling of oestrogen signalling and cell fate in breast cancer cells. *Nat Rev Cancer* 11(7):523-532.
4. Yu KD, Wu J, Shen ZZ, & Shao ZM (2012) Hazard of breast cancer-specific mortality among women with estrogen receptor-positive breast cancer after five years from diagnosis: implication for extended endocrine therapy. *J Clin Endocrinol Metab* 97(12):E2201-2209.
5. Emons G*, et al.* (2013) Phase II study of fulvestrant 250mg/month in patients with recurrent or metastatic endometrial cancer: A study of the Arbeitsgemeinschaft Gynakologische Onkologie. *Gynecol Oncol*.
6. Simpkins F*, et al.* (2012) Src Inhibition with saracatinib reverses fulvestrant resistance in ER-positive ovarian cancer models in vitro and in vivo. *Clin Cancer Res* 18(21):5911-5923.
7. Smyth JF*, et al.* (2007) Antiestrogen therapy is active in selected ovarian cancer cases: the use of letrozole in estrogen receptor-positive patients. *Clin Cancer Res* 13(12):3617-3622.
8. Jemal A*, et al.* (2004) Annual report to the nation on the status of cancer, 1975-2001, with a special feature regarding survival. *Cancer* 101(1):3-27.
9. Benod C*, et al.* (2013) Structure-Based Discovery of Antagonists of Nuclear

Receptor LRH-1. *J Biol Chem*.

10. Kretzer NM*, et al.* (2010) A noncompetitive small molecule inhibitor of estrogen-regulated gene expression and breast cancer cell growth that enhances proteasome-dependent degradation of estrogen receptor {alpha}. *J Biol Chem* 285(53):41863-41873.
11. Thiruchelvam PT*, et al.* (2011) The liver receptor homolog-1 regulates estrogen receptor expression in breast cancer cells. *Breast Cancer Res Treat* 127(2):385-396.
12. Wang LH*, et al.* (2006) Disruption of estrogen receptor DNA-binding domain and related intramolecular communication restores tamoxifen sensitivity in resistant breast cancer. *Cancer Cell* 10(6):487-499.
13. Andruska N, Mao C, Cherian M, Zhang C, & Shapiro DJ (2012) Evaluation of a luciferase-based reporter assay as a screen for inhibitors of estrogen-ERalpha-induced proliferation of breast cancer cells. *J Biomol Screen* 17(7):921-932.
14. Andruska N, Zheng X, Yang X, Helferich WG, & Shapiro DJ (2014) Anticipatory estrogen activation of the unfolded protein response is linked to cell proliferation and poor survival in estrogen receptor α-positive breast cancer. *Oncogene* 33(advance online publication, September 29, 2013).
15. Rimawi MF*, et al.* (2011) Reduced dose and intermittent treatment with lapatinib and trastuzumab for potent blockade of the HER pathway in HER2/neu-overexpressing breast tumor xenografts. *Clin Cancer Res* 17(6):1351-1361.
16. Ohta T*, et al.* (2006) Inhibition of phosphatidylinositol 3-kinase increases efficacy of cisplatin in in vivo ovarian cancer models. *Endocrinology* 147(4):1761-1769.

17. Ali AY, Abedini MR, & Tsang BK (2012) The oncogenic phosphatase PPM1D confers cisplatin resistance in ovarian carcinoma cells by attenuating checkpoint kinase 1 and p53 activation. *Oncogene* 31(17):2175-2186.
18. Vergara D*, et al.* (2012) Lapatinib/Paclitaxel polyelectrolyte nanocapsules for overcoming multidrug resistance in ovarian cancer. *Nanomedicine* 8(6):891-899.
19. Ju YH, Doerge DR, Allred KF, Allred CD, & Helferich WG (2002) Dietary genistein negates the inhibitory effect of tamoxifen on growth of estrogen-dependent human breast cancer (MCF-7) cells implanted in athymic mice. *Cancer Res* 62(9):2474-2477.
20. Wong H*, et al.* (2012) Antitumor activity of targeted and cytotoxic agents in murine subcutaneous tumor models correlates with clinical response. *Clin Cancer Res* 18(14):3846-3855.
21. Abukhdeir AM*, et al.* (2008) Tamoxifen-stimulated growth of breast cancer due to p21 loss. *Proc Natl Acad Sci U S A* 105(1):288-293.
22. Fowler AM, Solodin NM, Valley CC, & Alarid ET (2006) Altered target gene regulation controlled by estrogen receptor-alpha concentration. *Mol Endocrinol* 20(2):291-301.
23. Ikeda Y*, et al.* (2012) Estrogen regulates hepcidin expression via GPR30-BMP6-dependent signaling in hepatocytes. *PLoS One* 7(7):e40465.
24. Ron D & Walter P (2007) Signal integration in the endoplasmic reticulum unfolded protein response. *Nat Rev Mol Cell Biol* 8(7):519-529.
25. Walter P & Ron D (2012) The unfolded protein response: from stress pathway to homeostatic regulation. *Science* 334(6059):1081-1086.

26. DeSouza N*, et al.* (2002) Protein kinase A and two phosphatases are components of the inositol 1,4,5-trisphosphate receptor macromolecular signaling complex. *J Biol Chem* 277(42):39397-39400.
27. Li T*, et al.* (2009) SH2D4A regulates cell proliferation via the ERalpha/PLC-gamma/PKC pathway. *BMB Rep* 42(8):516-522.
28. Harrington WR*, et al.* (2006) Estrogen dendrimer conjugates that preferentially activate extranuclear, nongenomic versus genomic pathways of estrogen action. *Mol Endocrinol* 20(3):491-502.
29. Leprivier G*, et al.* (2013) The eEF2 kinase confers resistance to nutrient deprivation by blocking translation elongation. *Cell* 153(5):1064-1079.
30. Proud CG (2007) Signalling to translation: how signal transduction pathways control the protein synthetic machinery. *Biochem J* 403(2):217-234.
31. Ma L, Chen Z, Erdjument-Bromage H, Tempst P, & Pandolfi PP (2005) Phosphorylation and functional inactivation of TSC2 by Erk implications for tuberous sclerosis and cancer pathogenesis. *Cell* 121(2):179-193.
32. Luo B & Lee AS (2013) The critical roles of endoplasmic reticulum chaperones and unfolded protein response in tumorigenesis and anticancer therapies. *Oncogene* 32(7):805-818.
33. Rutkowski DT*, et al.* (2006) Adaptation to ER stress is mediated by differential stabilities of pro-survival and pro-apoptotic mRNAs and proteins. *PLoS Biol* 4(11):e374.
34. Healy SJ, Gorman AM, Mousavi-Shafaei P, Gupta S, & Samali A (2009) Targeting the endoplasmic reticulum-stress response as an anticancer strategy. *Eur J*

Pharmacol 625(1-3):234-246.

35. Thorpe SM, Christensen IJ, Rasmussen BB, & Rose C (1993) Short recurrence-free survival associated with high oestrogen receptor levels in the natural history of postmenopausal, primary breast cancer. *Eur J Cancer* 29A(7):971-977.
36. Getz G*, et al.* (2013) Integrated genomic characterization of endometrial carcinoma. *Nature* 497(7447):67-73.
37. Putt KS & Hergenrother PJ (2004) A nonradiometric, high-throughput assay for poly(ADP-ribose) glycohydrolase (PARG): application to inhibitor identification and evaluation. Anal Biochem 333(2):256- 264.
38. Andruska N, Mao C, Cherian M, Zhang C, & Shapiro DJ (2012) Evaluation of a luciferase-based reporter assay as a screen for inhibitors of estrogen-ERalpha-induced proliferation of breast cancer cells. J Biomol Screen 17(7):921-932.
39. Cherian MT, Wilson EM, & Shapiro DJ (2012) A competitive inhibitor that reduces recruitment of androgen receptor to androgen-responsive genes. J Biol Chem 287(28):23368-23380.
40. Andruska N, Zheng X, Yang X, Helferich WG, & Shapiro DJ (2014) Anticipatory estrogen activation of the unfolded protein response is linked to cell proliferation and poor survival in estrogen receptor α-positive breast cancer. Oncogene 33(advance online publication, September 29, 2013).
41. Kretzer NM, et al. (2010) A noncompetitive small molecule inhibitor of estrogen-regulated gene expression and breast cancer cell growth that enhances proteasome-dependent degradation of estrogen receptor {alpha}. J Biol Chem 285(53):41863-41873.

42. Cheng J, Zhang C, & Shapiro DJ (2007) A functional serine 118 phosphorylation site in estrogen receptor-alpha is required for down-regulation of gene expression by 17beta-estradiol and 4- hydroxytamoxifen. Endocrinology 148(10):4634-4641.
43. Carlson KE, Choi I, Gee A, Katzenellenbogen BS, & Katzenellenbogen JA (1997) Altered ligand binding properties and enhanced stability of a constitutively active estrogen receptor: evidence that an open pocket conformation is required for ligand interaction. Biochemistry 36(48):14897-14905.
44. Ju YH, Doerge DR, Allred KF, Allred CD, & Helferich WG (2002) Dietary genistein negates the inhibitory effect of tamoxifen on growth of estrogen-dependent human breast cancer (MCF-7) cells implanted in athymic mice. Cancer Res 62(9):2474-2477.
45. Harrington WR, et al. (2006) Estrogen dendrimer conjugates that preferentially activate extranuclear, nongenomic versus genomic pathways of estrogen action. Mol Endocrinol 20(3):491-502.
46. Ron D & Walter P (2007) Signal integration in the endoplasmic reticulum unfolded protein response. Nat Rev Mol Cell Biol 8(7):519-529.
47. Walter P & Ron D (2012) The unfolded protein response: from stress pathway to homeostatic regulation.
48. Science 334(6059):1081-1086.
49. Wu J, et al. (2007) ATF6alpha optimizes long-term endoplasmic reticulum function to protect cells from chronic stress. Dev Cell 13(3):351-364.
50. Hetz C, Martinon F, Rodriguez D, & Glimcher LH (2011) The unfolded protein response: integrating stress signals through the stress sensor IRE1alpha. Physiol

Rev 91(4):1219-1243.

51. Axten JM, et al. (2012) Discovery of 7-methyl-5-(1-{[3-(trifluoromethyl)phenyl]acetyl}-2,3-dihydro-1H- indol-5-yl)-7H-p yrrolo[2,3-d]pyrimidin-4-amine (GSK2606414), a potent and selective first-in-class inhibitor of protein kinase R (PKR)-like endoplasmic reticulum kinase (PERK). J Med Chem 55(16):7193- 7207.
52. Harding HP, Zyryanova AF, & Ron D (2012) Uncoupling proteostasis and development in vitro with a small molecule inhibitor of the pancreatic endoplasmic reticulum kinase, PERK. J Biol Chem 287(53):44338-44344.
53. Katzenellenbogen JA, Johnson HJ, Jr., & Myers HN (1973) Photoaffinity labels for estrogen binding proteins of rat uterus. Biochemistry 12(21):4085-4092.

CHAPTER 4

TARGETING MULTIDRUG-RESISTANT OVARIAN CANCER THROUGH ESTROGEN RECEPTOR α DEPENDENT ATP DEPLETION CAUSED BY HYPERACTIVATION OF THE UNFOLDED PROTEIN RESPONSE [3]

ABSTRACT

Ovarian cancers often recur and tumors acquire resistance to chemotherapy due to overexpression of the ATP-dependent efflux pump, multidrug resistance protein 1 (MDR1/P-glycoprotein/ABCB1). Nontoxic small molecule inhibitors targeting MDR1 have remained largely elusive. Instead, in a novel application of our recently described estrogen receptor α (ERα) biomodulator, BHPI, we targeted MDR1's substrate, ATP. BHPI depletes intracellular ATP and nearly blocks MDR1-mediated drug efflux in ovarian cancer cells by inducing toxic hyperactivation of the endoplasmic reticulum stress sensor, the unfolded protein response (UPR). BHPI increased sensitivity of MDR1 overexpressing multidrug resistant OVCAR-3 ovarian cancer cells to killing by paclitaxel by >1,000 fold. BHPI also restored doxorubicin sensitivity in OVCAR-3 cells and in MDR1 overexpressing breast cancer cells. In an orthotopic OVCAR-3 xenograft model, paclitaxel was ineffective and the paclitaxel-treated group was uniquely prone to form large secondary tumors in adjacent tissue. BHPI alone strongly reduced tumor growth. Notably, tumors were undetectable in mice treated with BHPI plus paclitaxel. Compared to control ovarian tumors, after the combination therapy, levels of the plasma ovarian cancer biomarker

[3] This chapter appeared in its entirety in the *Oncotarget*. **X Zheng**, N Andruska, MJ Lambrecht, S He, A Parissenti, PJ Hergenrother, ER Nelson, DJ Shapiro. (2016) Targeting multidrug-resistant ovarian cancer through estrogen receptor α dependent ATP depletion caused by hyperactivation of the unfolded protein response. Oncotarget. DOI: 10.18632/oncotarget.10819.

CA125 were at least several hundred folds lower; moreover, CA125 levels progressively declined to undetectable. Targeting MDR1 through UPR-dependent ATP depletion represents a promising therapeutic strategy.

INTRODUCTION

Ovarian cancer usually presents at an advanced stage and more than half of ovarian cancer patients die within 5 years [1-3]. Although 30-70% of ovarian tumors are estrogen receptor α (ERα) positive, endocrine therapy is largely ineffective [4-6]. Recurrent ovarian tumors are therefore treated with chemotherapy. Although initially responsive, after several cycles of treatment tumors often recur as resistant ovarian cancer, with few therapeutic options [7]. In ovarian cancer, the most common mechanism for resistance to paclitaxel and other chemotherapeutic agents is overexpression of ATP-dependent membrane efflux pumps of the ABC transporter family, especially Multidrug Resistance Protein 1 (MDR1)/P-glycoprotein/ABCB1 [8-13]. MDR1-mediated efflux reduces intracellular drug concentrations to levels at which the drugs are no longer effective at doses patients can tolerate [8, 12, 13]. Despite intensive efforts, clinically effective non-toxic small molecule MDR1 inhibitors have not been described [14]. Instead of inhibition of MDR1 we target its substrate, ATP. MDR1-mediated efflux is exquisitely sensitive to reductions in ATP levels [15-17]. However, selective depletion of ATP in cancer cells has been little studied and is difficult to achieve.

We recently described the novel non-competitive estrogen receptor α (ERα) biomodulator, BHPI, which is effective in models of ERα^+ breast cancer [18]. In cancer cells, BHPI, acting via ERα, induces sustained toxic hyperactivation of the endoplasmic

reticulum (EnR) stress sensor, the unfolded protein response (UPR) [18]. The UPR consists of three main branches that together balance the synthesis of new proteins with the availability of chaperones and other proteins to help fold and transport proteins within cells [19, 20]. In the classical reactive mode, EnR stress resulting from accumulation of unfolded or misfolded protein, or other stresses, triggers UPR activation [19-21]. In the recently unveiled anticipatory mode of UPR activation, estrogen or other mitogenic hormones pre-activate the UPR and anticipate a future need for increased protein folding capacity [22, 23]. BHPI distorts this normal anticipatory pathway by binding to a different site on ERα than estrogens and inducing a different ERα conformation [18]. This enables BHPI to act through ERα to hyperactivate the UPR, converting it from protective to toxic [18]. BHPI strongly activates phospholipase C γ (PLCγ), producing inositol triphosphate (IP_3), which binds to and opens endoplasmic reticulum IP_3 Receptor (IP_3R) calcium channels allowing rapid efflux of calcium from the lumen of the EnR into the cytosol.

Intracellular calcium levels are tightly regulated by EnR transport channels and pumps [24, 25]. Opening the IP_3Rs and ryanodine receptor (RyR) calcium channels allows efflux of the high concentrations of Ca^{2+} stored in the lumen of the EnR into the cytosol [26-28]. To produce this concentration gradient, powerful ATP-dependent sarcoplasmic/endoplasmic reticulum calcium-ATPase (SERCA) pumps in the EnR membrane pump calcium from the cytosol into the EnR lumen [29-31]. We show that BHPI elicits a sustained, IP_3R dependent, increase in cytosol calcium in ovarian cancer cells. Since the IP_3R calcium channels remain open after BHPI treatment, the calcium pumped into the EnR by the ATP-dependent SERCA pumps rapidly leaks back out. We hypothesized that sustained BHPI hyperactivation of the UPR creates a futile cycle

depleting intracellular ATP, and this ATP depletion might provide a novel way to inactivate MDR1.

Using cell-based and *in vivo* studies we evaluated the potential of this novel approach to restoring chemosensitivity of multidrug resistant ovarian tumors. Notably, in OVCAR-3 ovarian cancer cells, which are resistant to micromolar paclitaxel, BHPI restored sensitivity to therapeutically relevant low nanomolar concentrations of paclitaxel. We preformed what is perhaps the first orthotopic intra-ovarian mouse xenograft study using multidrug resistant OVCAR-3 cells. Surprisingly, paclitaxel was both ineffective and actually appeared to promote metastases, a result not seen in the other treatment groups. Notably, no ovarian tumors were detected in any of the mice treated with BHPI plus paclitaxel. Moreover, levels of the circulating ovarian cancer marker, CA125/mucin 16, declined from ~700 units/ml in control vehicle-treated mice to undetectable in all of the BHPI plus paclitaxel treated mice.

RESULTS

BHPI induces a sustained increase in intracellular calcium through activation of the ERα-PLCγ-IP_3R pathway

Using breast cancer cells, we previously showed E_2-ERα activates a PLCγ-IP_3R pathway to release calcium from EnR stores into the cytosol [32]. Activated PLCγ cleaves its substrate to produce IP_3. The non-competitive ERα biomodulator BHPI, that works by hyperactivating the UPR, produces much higher levels of IP_3 than E_2 [18]. If we were to use this pathway to target multidrug resistant ovarian cancer, we had to first show that the pathway functions in ovarian cancer cells. We initially quantitated IP_3 levels in $ERα^+$

PEO-4 ovarian cancer cells treated with E_2 or BHPI. E_2 induced a modest increase in IP_3 levels, while BHPI induced a much more robust 6-fold increase (Figure 4.1A).

To test whether E_2 and BHPI rapidly increase cytosolic Ca^{2+}, we monitored calcium levels using the fluorescent calcium sensor dye Fluo-4 AM. In <1 min., E_2 and BHPI increased cytosol Ca^{2+} in PEO-4 cells (Figure 4.1B, C). Notably, in the absence of extracellular calcium, E_2 elicited a transient ~3.5 fold increase in cytosolic Ca^{2+} with the Ca^{2+} signal rapidly returning to the basal level (Figure 4.1B). In contrast, BHPI elicited a sustained ~7 fold increase in cytosolic Ca^{2+} (Figure 4.1C). Since pretreatment with the PLCγ inhibitor U73122 abolished the calcium release observed with E_2 or BHPI, PLCγ activation was required for the increase in cytosolic Ca^{2+} (Figure 4.1B, C). BHPI induced a large increase in cytosolic Ca^{2+} even in the absence of extracellular Ca^{2+}, indicating that BHPI increases cytosolic Ca^{2+} by depleting the Ca^{2+} store in the EnR. Supporting this idea is our observation that inhibiting the IP_3R Ca^{2+} channel with 2-APB abolished the rapid E_2 and BHPI stimulated Ca^{2+} release (Figure 4.1B, C and Figure 4.2). In contrast, inhibition of RyR calcium channels with high concentration ryanodine (Ry) did not block E_2 or BHPI stimulated Ca^{2+} release in PEO-4 cells (Figure 4.1B, C). Confirming BHPI's structural specificity and the requirement for ERα, a control compound, C8, that is structurally related to BHPI, but does not bind ERα *in vitro* [18], failed to increase cytosolic Ca^{2+} (Figure 4.1C). These results demonstrate that BHPI strongly activates the ERα-PLCγ-IP_3R pathway in ovarian cancer cells, resulting in a sustained increase in cytosolic Ca^{2+}.

BHPI activates the UPR in ovarian cancer cells

Efflux of calcium stored in the lumen of the EnR into the cell body activates the UPR. The core UPR signaling cascade consists of 3 EnR sensors whose activation increases protein-folding capacity and temporarily reduces protein production (Figure 4.2). Activation of IRE1α, which alternatively splices the transcription factor XBP1, produces the widely used UPR marker, active spliced XBP1 (sp-XBP1) [33]. Supporting activation of the IRE1α branch of the UPR, in PEO-4 ovarian cancer cells, BHPI and E_2 robustly induced sp-XBP1 (Figure 4.3A and Figure 4.4A). Protein synthesis is regulated by autophosphorylation of PERK [34]. Phosphorylated PERK (p-PERK) phosphorylates of eukaryotic initiation factor 2 α (eIF2α), which leads to transient inhibition of protein synthesis (Figure 4.2). E_2 induced a weak and transient phosphorylation of eIF2α in ovarian cells (Figure 4.4B), while BHPI elicited robust phosphorylation of PERK and eIF2α (Figure 4.3B, C), resulting in inhibition of most protein synthesis (Figure 4.3D) and a decline in total PERK and eIF2α protein (Figure 4.3B, C). Consistent with their inhibitors' ability to block calcium efflux (Figure 4.1B, C), inhibition of PLCγ with U73122 and locking the IP_3R calcium channels with 2-APB, but not inhibition of the RyR calcium channels, reversed BHPI inhibition of protein synthesis (Figure 4.3E). EnR stress leads to proteolytic cleavage of ATF6α to active 50 kDa ATF6α (p50-ATF6α) (Figure 4.2) [35]. Demonstrating BHPI and E_2 activate the ATF6α arm of UPR, E_2 and BHPI increased p50-ATF6α levels in PEO-4 cells (Figure 4.3F and Figure 4.4C). Active p50-ATF6α increases production of BiP/GRP78/HSPA5 and other EnR chaperones [35]. BHPI and E_2 increased production of BiP mRNA in PEO-4 ovarian cancer cells (Figure 4.3G and Figure 4.4D). However, since BHPI inhibited protein synthesis (Figure 4.3D and E), BiP protein levels were reduced in BHPI-treated PEO-4 cells (Figure 4.3H).

Collectively, our findings in ovarian cancer cells indicate that E_2-ERα induces weak and transient anticipatory activation of the UPR and that BHPI distorts this UPR pathway resulting in strong and sustained UPR activation. These data provide a potential mechanism for inactivating MDR1 in ovarian cancer cells.

BHPI depletes intracellular ATP inactivating MDR1-mediated efflux

We hypothesize: (i) In response to the BHPI-mediated loss of EnR calcium, SERCA pumps will carry out ATP-dependent transport of Ca^{2+} from the cytosol back into the lumen of the EnR. (ii) Since BHPI elicits sustained increases in cytosolic Ca^{2+} (Figure 4.1C), indicating the IP_3R calcium channels remain open, calcium pumped from the cytosol into the lumen of the EnR leaks back out through the open IP_3R channels, creating a futile cycle that depletes ATP (Figure 4.5A). To test our hypothesis we investigated the effect of BHPI on ATP levels in ovarian cancer cells. BHPI treatment rapidly reduced intracellular ATP levels in $ER\alpha^+$ PEO-4 and OVCAR-3 ovarian cancer cells (Figure 4.5B, C). Supporting the role of the EnR SERCA pumps in ATP depletion, the SERCA pump inhibitor, thapsigargin (THG) blocked the decline in ATP levels seen after BHPI treatment (Figure 4.5B, C).

$ER\alpha^+$, multidrug resistant, OVCAR-3 ovarian cancer cells were derived from a patient whose cancer recurred after surgery and multiple rounds of chemotherapy [36]. OVCAR-3 cells have been propagated without cloning and therefore retain much of the diversity of a patient derived xenograft [36, 37]. $ER\alpha^+$ MCF-7 breast cancer cells are normally MDR1 negative and sensitive to the chemotherapy agent doxorubicin. MCF-7 doxorubicin ($MCF\text{-}7_{dox}$) resistant breast cancer cells were generated by selection in

increasing doxorubicin concentrations [38, 39]. Confirming that upregulation of MDR1 is a common mechanism in cancer cells resistant to cytotoxic chemotherapy, both the MCF-7_{dox} and OVCAR-3 cells overexpress MDR1 (Figure 4.5D). Notably, while 50 nM BHPI blocked MCF-7 proliferation, 500 nM BHPI was required to block proliferation of the MCF-7_{dox} breast cancer cells (Figure 4.6A, B). This is consistent with the possibility that BHPI may be an MDR1 substrate.

The fluorescent MDR1 substrate Rhodamine 123 (Rho-123) is widely used to quantitate MDR1-mediated efflux from cells into the medium [14, 40]. OVCAR-3 and MCF-7_{dox} cells that overexpress MDR1, and control MDR1 negative PEO-4 cells were preloaded with Rho-123 and Rho-123 efflux into the medium was quantitated. Rho-123 efflux from the MDR1 negative PEO-4 cells was negligible (Figure 4.7). OVCAR-3 and MCF-7_{dox} cells exhibited robust time-dependent efflux of Rho-123 (Figure 4.7). We tested whether BHPI-treatment, which reduces intracellular ATP levels, inhibits MDR1-mediated Rho-123 efflux. In OVCAR-3 and MCF-7_{Dox} cells BHPI nearly abolished Rho-123 efflux (Figure 4.5E, F). Consistent with the proposed futile cycle leading to ATP depletion causing inhibition of MDR1-mediated efflux (Figure 4.5A), inhibiting the rise in intracellular Ca^{2+} by either inhibiting PLCγ with U73122, or by locking the EnR IP_3R calcium channels closed with 2-APB (Figure 4.1C), reversed BHPI inhibition of MDR1-mediated efflux (Figure 4.5E, F). We next explored whether other actions of BHPI might complement ATP depletion and contribute to the near abolition of MDR1-mediated efflux.

In OVCAR-3 cells, BHPI elicited strong and sustained activation of the PERK arm of the UPR inhibiting protein synthesis cells by ~60% (Figure 4.8A). This reduced production of protein led to an ~2 fold decline in MDR1 levels (Figure 4.8B). Therefore,

the reduced level of MDR1 and the decline in the level of its substrate ATP, work together to enable BHPI to nearly abolish MDR1-mediated efflux. We therefore tested whether BHPI could restore sensitivity of OVCAR-3 and MCF-7_{dox} cells to therapeutically relevant concentrations of chemotherapy drugs.

BHPI resensitizes resistant cancer cells to paclitaxel and doxorubicin

OVCAR-3 cells were highly resistant to paclitaxel, and were not killed, even at 10,000 nM paclitaxel (Figure 4.9A). While BHPI alone blocked OVCAR-3 cell growth, it was not cytotoxic. BHPI restored the cytotoxicity of paclitaxel at 10 nM paclitaxel, reducing the number of OVCAR-3 cells by ~70% in two days (Figure 4.9A). This represents an >1,000 fold increase in sensitivity to paclitaxel. Furthermore, OVCAR-3 cells were also resistant to 1,000 nM doxorubicin; BHPI also restored sensitivity to doxorubicin (Figure 4.9B). MCF-7_{dox} breast cancer cells were resistant to 250 nM doxorubicin. BHPI restores sensitivity of the MCF-7_{dox} cells, to the lowest dose of doxorubicin tested (15 nM) (Figure 4.9C). Importantly, since the therapeutic range of concentrations is ~15-20 nM for paclitaxel and 100-150 nM for doxorubicin [37, 41, 42], BHPI restored sensitivity of multidrug resistant ovarian and breast cancer cells to therapeutically relevant concentrations of paclitaxel and doxorubicin.

We propose that BHPI restores drug sensitivity because it strongly activates the ERα-PLCγ-IP_3R pathway leading to ATP depletion and a moderate reduction in MDR1 expression. A testable alternative is that the BHPI-mediated >1,000 fold increase in sensitivity of OVACR-3 cells to killing by paclitaxel is simply due to combinatorial actions of two toxic drugs, BHPI and paclitaxel. OVCAR-3 cells are also resistant to cisplatin,

which is not a substrate of MDR1 and is therefore not pumped out by MDR1 [43]. BHPI treatment did not restore sensitivity of OVCAR-3 cells to killing by cisplatin (Figure 4.10A). Thus, BHPI's ability to abolish multidrug resistance is due to its ability to interfere with MDR1, and not to the additive effects of BHPI in combination with a chemotherapeutic. Consistent with BHPI acting through ERα, BHPI did not inhibit proliferation or restore paclitaxel sensitivity in ERα negative MDR1 overexpressing NIH/ADRes ovarian cancer cells (Figure 4.10B). In addition, the inactive structural relative of BHPI, C8, did not restore paclitaxel or doxorubicin sensitivity in OVCAR-3 cells (Figure 4.10C).

We next sought to confirm that the ability of BHPI to resensitize OVCAR-3 cells to paclitaxel was mediated by the PLCγ pathway. Although useful in short-term studies, the long-term use of PLCγ and IP_3R inhibitors U73122 and 2-APB may result in secondary effects. Since simultaneous knockdown of the three IP_3R channels is somewhat toxic [18], it cannot be combined with the two other drugs. We therefore evaluated the effect of siRNA knockdown of PLCγ on paclitaxel sensitivity in BHPI-treated OVCAR-3 cells. siRNA knockdown of PLCγ, but not a control siRNA, abolished BHPI-mediated restoration of paclitaxel sensitivity (Figure 4.9D, E). Thus, BHPI's novel mechanism of action leads to inactivation of MDR1 in multiple cell models, resulting in restoration of sensitivity to therapeutically relevant concentrations of paclitaxel and doxorubicin.

BHPI restores paclitaxel sensitivity and eliminates tumors in a multidrug resistant ovarian tumor model

To assess *in vivo* effectiveness of BHPI in restoring drug sensitivity, we used OVCAR-3 cells, which are resistant to therapeutically relevant concentrations of all

common anticancer drugs [36]. We used an orthotopic model in which OVCAR-3 cells were grafted into the bursa of one ovary, the other ovary serving as a control. At the end of the 10 week study, ovarian tumors were evident in each of the vehicle-treated mice, with an average weight of ~200 mg (Figure 4.11A, B). Surprisingly, in the paclitaxel-treated group there were large secondary tumors in adjacent tissue (Figure 4.11A). Increased metastasis of paclitaxel-treated OVCAR-3 tumors has not been previously described because this is perhaps the first use of OVCAR-3 cells in an orthotopic ovarian model [44]. BHPI alone significantly reduced tumor size and weight (Figure 4.11A, B). Notably, there were no visible OVCAR-3 ovarian tumors in the combined BHPI and paclitaxel treatment group and no secondary tumors were detected (Figure 4.11A, B). In the BHPI plus paclitaxel group, the ovary injected with OVCAR-3 cancer cells and the control ovary appeared identical.

Although tumors were not visible in the BHPI plus paclitaxel group, to more sensitively assess whether tumor cells were still present, we quantified the circulating level of serum CA125 tumor antigen. In ovarian cancer, the circulating level of CA125 is a widely used biomarker for therapeutic progress and tumor recurrence [45-47]. Although the basal level of CA125 in normal human serum is ~35 U/ml (Figure 4.11C, dashed line), the human CA125 antibody does not cross-react with control mouse serum. Thus, the level of serum CA125 is a sensitive marker for the survival of human OVCAR-3 cancer cells in the mice. Serum samples were taken in weeks 7-10 of the study and assayed after completion of the study. CA125 levels in the control vehicle-treated group and in the paclitaxel-treated group increased dramatically in weeks 7-10. Confirming that the OVCAR-3 tumors are highly paclitaxel-resistant, CA125 levels were similar in the control

vehicle-treated and paclitaxel-treated mice (Figure 4.11C). BHPI strongly reduced circulating CA125 levels compared to vehicle or paclitaxel alone, but CA125 levels rise slightly from weeks 7-10 (Figure 4.11C, green line). Strikingly, in the BHPI plus paclitaxel treated mice, CA125 levels declined from a low starting level of ~30 U/ml at week 7 to concentrations below the detection limits for all five mice at week 10 (Figure 4.11C, purple line). Since the detection limit of the assay is $\pm$ 5 U/ml and the vehicle-treated group had circulating CA125 levels of ~700 U/ml, tumor burden was reduced by 200 fold or more in mice to undetectable levels after combined BHPI and paclitaxel treatment. Measurement of mouse body weights throughout the study suggested that BHPI alone and BHPI plus paclitaxel were well tolerated and no visible toxic effects of BHPI were seen in the mice (Figure 4.12).

DISCUSSION

Although 30-70% of ovarian cancers are ERα^+ at diagnosis, endocrine therapy is largely ineffective [1-3]. The failure of endocrine therapy raises the possibility that the presence or absence of ERα has little effect on ovarian tumors and there is no selection pressure to maintain ERα in recurrent multidrug resistant tumors. However, recent studies show that estrogens, acting through ERα, enhance ovarian tumor growth and increase risk of lymphovascular space invasion [48, 49]. Moreover, ERα expression correlates with poor clinical outcome in ovarian cancer [50]. The association of ERα with late-stage therapy-resistant tumors strongly suggests that ERα is maintained in many of these tumors, making them targetable with our small molecular biomodulator.

Therapeutic options are limited for patients with recurrent multidrug resistant ovarian cancer. Overexpression of MDR1 is a major resistance mechanism [8, 13, 14]. Selective non-toxic inhibitors of MDR1 have proven difficult to identify. For MDR1 inhibitors, toxicity due to inhibition of ABC transporter family members in normal cells has been a serious concern [8]. BHPI is effective because it uses a therapeutic strategy different from classic MDR1 inhibitors and most other cytotoxic chemotherapeutic drugs [8, 14]. It works by hyperactivating the UPR, a pathway that is already partially activated as a protective mechanism in tumor cells. We recently reported that elevated expression of a UPR gene signature consisting of UPR sensors and downstream targets of UPR activation is tightly correlated with therapy resistance, tumor recurrence and a poor prognosis in ERα^+ breast cancer [32]. In contrast, the UPR is nearly off in normal healthy cells and its components are not overexpressed [32]. Consistent with this, BHPI was well tolerated in the xenograft study. While BHPI and estrogen share a common ERα-dependent pathway for UPR activation (Figure 4.2), the weak estrogen-ERα activation of the UPR induces protective chaperones and is important for subsequent estrogen-ERα activation of gene expression and induction of cell proliferation [32]. Notably, BHPI binding to ERα is not competitive with estrogen binding, indicating that they bind ERα at different sites [18]. Moreover, BHPI induces conformational changes in ERα not seen with estrogen [18]. Thus, unlike estrogen, BHPI hyperactivates the UPR, leading to persistent inhibition of protein synthesis in ERα positive cancer cells [18].

Strong and sustained activation of the UPR by BHPI creates a futile cycle leading to depletion of intracellular ATP and inactivation of MDR1-mediated efflux (Figure 4.5A). Supporting the proposed pathway is our observation that BHPI is only effective in ERα^+

cells. Furthermore, inhibitor and knockdown studies demonstrate the critical roles of PLCγ, IP_3R calcium channels and SERCA pumps. BHPI-ERα hyperactivation of the UPR results in rapid depletion of ATP leading to activation of AMPK [18]. Activated AMPK reportedly inhibits MDR1 gene expression [51, 52]. Since together the potential AMPK-mediated reduction in MDR1 gene expression and the UPR mediated inhibition of protein synthesis only reduce MDR1 protein levels ~2 fold, they are likely to be complementary, rather than central, to the dramatic and rapid reduction in MDR1 mediated efflux and to the restoration of drug sensitivity.

Despite MDR1's acute sensitivity to reduction in ATP levels therapeutic reduction of ATP levels has been an elusive target. The glyceraldehyde-3-phosphate dehydrogenase inhibitor, 3-bromopyruvate inhibits glycolysis, leading to loss of ATP and MDR1 inactivation [53]. However, lack of specificity, and toxicity in normal cells, have hindered therapeutic application of 3-bromopyruvate.

Ovarian cancers originate in the fallopian tubes or ovaries [5]. We used an orthotopic mouse xenograft model in which OVCAR-3 cells were grafted into the bursa of one ovary. Because these internal tumors cannot be directly measured until the study ends, serum levels of CA125 over the last 4 weeks of the study provide a surrogate marker for tumor progression. Serum CA125 levels in the paclitaxel and vehicle-treated mice increased rapidly in weeks 7-10. Tumor weight and CA125 levels indicated that the overall tumor burden was similar in the paclitaxel and vehicle-treated mice. Although the primary ovarian tumors were small in the paclitaxel-treated mice, these tumor-harboring mice were prone to developing large secondary (extra-ovarian) growths. Interestingly, increased metastasis following therapy has also been reported in prostate cancer

xenografts treated with abiraterone [54] and breast cancer xenografts treated with sunitinib or bevacizumab [55]. CA125 levels and tumor weight were reduced 60-80% in the BHPI treated mice. The slight increase in CA125 levels in week 7-10 suggests BHPI strongly inhibited, but did not completely block, tumor progression. In contrast, in the BHPI plus paclitaxel treatment group, the already extremely low levels of CA125 at week 7 declined progressively to undetectable levels at week 10. This suggests ongoing tumor regression in this treatment group during the last 4 weeks of the study. Although there was substantial individual variation in tumor size and weight, and in CA125 levels, in the combined treatment group, both tumors and plasma CA125 were undetectable in all 5 mice. Absence of visible tumors, or complete loss of circulating tumor markers, has not been reported in other xenograft studies using highly drug-resistant OVCAR-3 ovarian cells [53, 56, 57].

De novo and acquired multidrug resistance is a core problem in cancer chemotherapy. In ovarian cancer, the primary driver of multidrug resistance is overexpression of MDR1. BHPI alone has emerged as a promising and well-tolerated therapeutic candidate for multidrug resistant ovarian cancer. Central to BHPI's therapeutic potential is its novel mechanism of action based on strong and sustained hyperactivation of the anticipatory UPR pathway, resulting in ATP depletion and MDR1 inactivation. This enables BHPI to resensitize multidrug resistant tumors to chemotherapeutic intervention and reduce ovarian tumor burden to undetectable levels. Thus, BHPI is a unique candidate for further mechanistic exploration and therapeutic development.

MATERIALS AND METHODS

Cell culture and reagents

Cell culture medium and conditions were as previously described [18, 32]. Dr. S. Kaufmann provided PEO-4 ovarian cells. Dr. A. Parissenti provided MCF-7 and doxorubicin resistant MCF-7 ($MCF\text{-}7_{dox}$) breast cancer cells. OVCAR-3 cells were obtained from the ATCC. E_2, U73122, Rhodamine-123 (Rho-123) dye and 2-amino propyl-benzoate (2-APB) were from Sigma Aldrich (St Louis, MO, USA). Ryanodine (Ry) was from Santa Cruz Biotechnology (Danvers, MA, USA). BHPI was synthesized on gram scale via a short sequence. Detailed experimental protocols are available in supplementary materials.

Western blot

Western blotting was carried out as previously described [18, 32, 58]. The following antibodies were used: Phospho-eIF2α (Ser51) (#3398; Cell Signaling Technology), eIF2α (#5324; Cell Signaling Technologies, MA), Phospho-PERK (#3179; Cell Signaling Technology, MA), PERK (#5683; Cell Signaling Technology, MA), ATF6α (Imgenex, CA), PLCγ (#5690; Cell Signaling Technology, MA), BiP (#3177; Cell Signaling Technology, MA), MDR1/ABCB1 (#12683; Cell Signaling Technology, MA) and β-Actin (Sigma, MO). The protein and antibody complexes were detected using horseradish peroxidase-conjugated secondary antibodies and chemiluminescent immunodetection with an ECL Detection Kit (GE Healthcare, NJ), and were visualized using a PhosphorImager.

Cell proliferation assays

Cells were plated in growth media with 10% CD-FBS for three days. Subsequently, cells were resuspended in growth media with 10% CD-calf serum and plated in 96 well plates. The medium was replaced with treatment media the following day, and plates were incubated at 37^{o}C in 5% CO_2 for 2-4 days. During experiments, the medium was replaced every two days. Cell number was determined using MTS and CellTiter 96 Aqueous One Solution Reagent (Promega). For each cell line, cell number was calculated from a standard curve of the number of plated cells at A_{490}.

Assaying MDR1 efflux activity

Cells were plated in 6-well plates and allowed to reach 80% confluence. Subsequently, cells were loaded with 10 μM of Rho-123 (1% methanol, HBSS) for 10 minutes at 37 ^{o}C. Then, cells were washed three times with cold PBS to remove residual Rho-123 and efflux started by addition of pre-warmed HBSS buffer. At the end of the measured time points, cells were lysed with 2% (v/v) triton-x100 in HBSS with proteinase inhibitor cocktail. Total protein was determined and Rho-123 concentration was normalized to total protein.

Mouse xenografts

All experiments were approved by the Institutional Animal Care Committee (IACUC) of the University of Illinois at Urbana-Champaign. The immunodeficient NSG mice (Jackson Laboratory) were obtained from in-house breeding. 1 million OVCAR-3 cells were orthotopically grafted into the bursa of one ovary. Subsequently, the mice were randomly divided into four treatment groups. Starting one week after injecting the tumor cells each group received vehicle plus vehicle, paclitaxel plus vehicle, vehicle plus BHPI, or

paclitaxel plus BHPI. The paclitaxel was dissolved in Polysorbate-80 and ethanol (1:1, vol/vol) and further diluted with saline to reach final concentration. Stock BHPI was dissolved in DMSO and further diluted with 10% Tween-20 with 88% PBS to working concentration. Doses were 10 mg/kg of paclitaxel IP injected every other day, and 50mg/kg of BHPI injected IP daily.

Measuring levels of serum CA125

Plasma CA125 concentrations were determined by ELISA according to the manufacturer's protocol (#KA0205; Abnova, CA). The final serum CA125 concentrations were calculated based on a standard curve.

qRT-PCR, IP_3 quantitation, PLCγ siRNA knockdown, calcium imaging, and protein synthesis measurements

Carried out as we recently described [18, 32, 59].

Statistical analysis

R was used for the statistical analysis. For terminal tumor weights, one-way ANOVA followed by the Kruskal-Wallis *post hoc* test was used ($P < 0.05$). For CA125 serum analysis, two-way ANOVA followed by Bonferroni's *post hoc* t-test was used ($P < 0.05$). Other analyses were conducted either with two-tailed Student t tests or with one-way ANOVA followed by Tukey *post hoc* tests ($P < 0.05$). Data are reported as mean ± SEM.

FIGURES

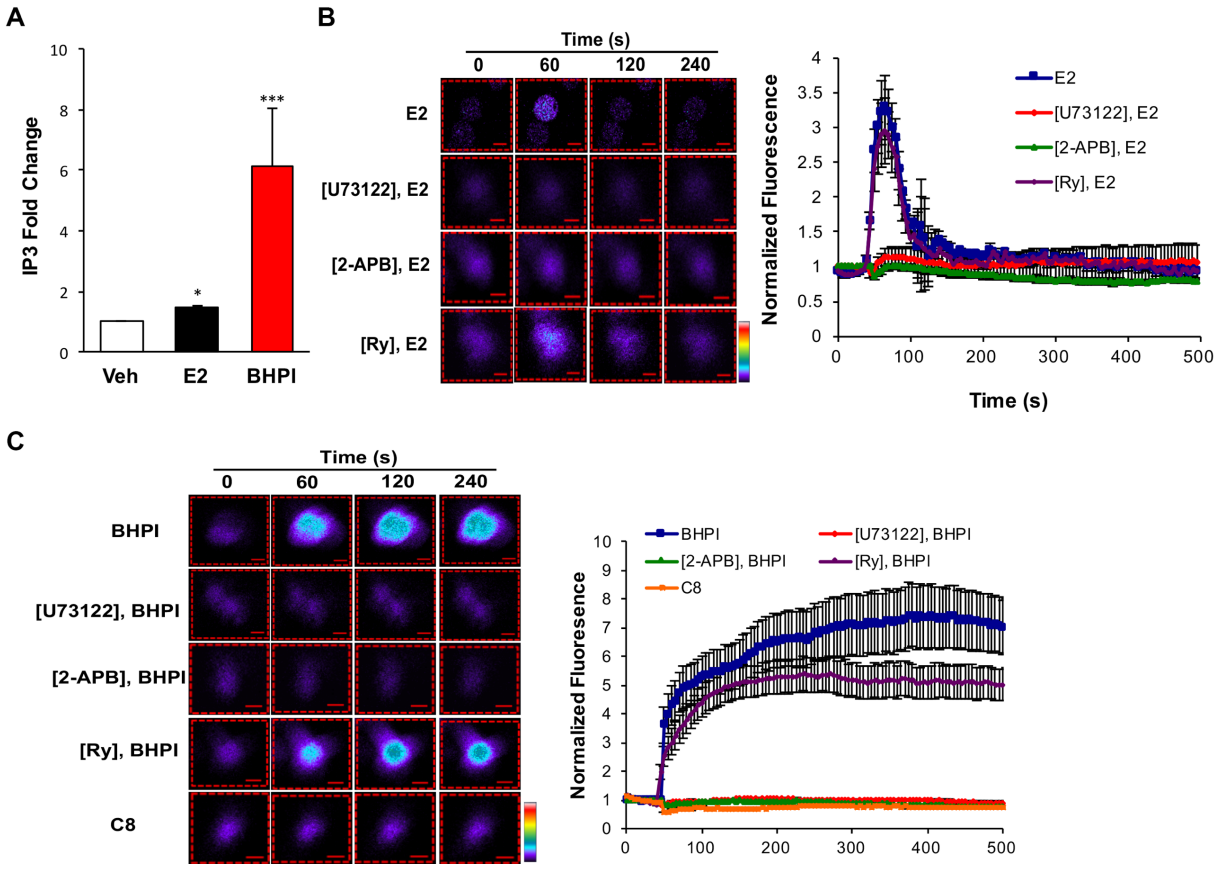

Figure 4.1. BHPI and estrogen stimulate release of calcium from the endoplasmic reticulum into the cytosol. **(A)** Quantitation of intracellular IP_3 levels after 10 min treatment with DMSO, 17β-estradiol (E_2), or BHPI in PEO-4 ovarian cells (n = 3). **(B, C)** Estrogen and BHPI increase cytosol calcium levels. Visualization of cytosolic Ca^{2+} using Fluo-4 AM; estrogen or BHPI was added to PEO-4 cells at 50 s. Color scale from basal Ca^{2+} to highest Ca^{2+}: purple, blue, green, yellow, red, white. Quantitation of cytosolic Ca^{2+} levels after pre-treating PEO-4 cells with U73122, 2-APB, or Ry followed by treatment with estrogen or BHPI (n = 12-20). Concentrations: U73122, 1 μM; 2-APB, 100 μM; Ry, C8, 10 μM; E_2, 200 nM; BHPI, 10 μM. *P < 0.05, ***P < 0.001.

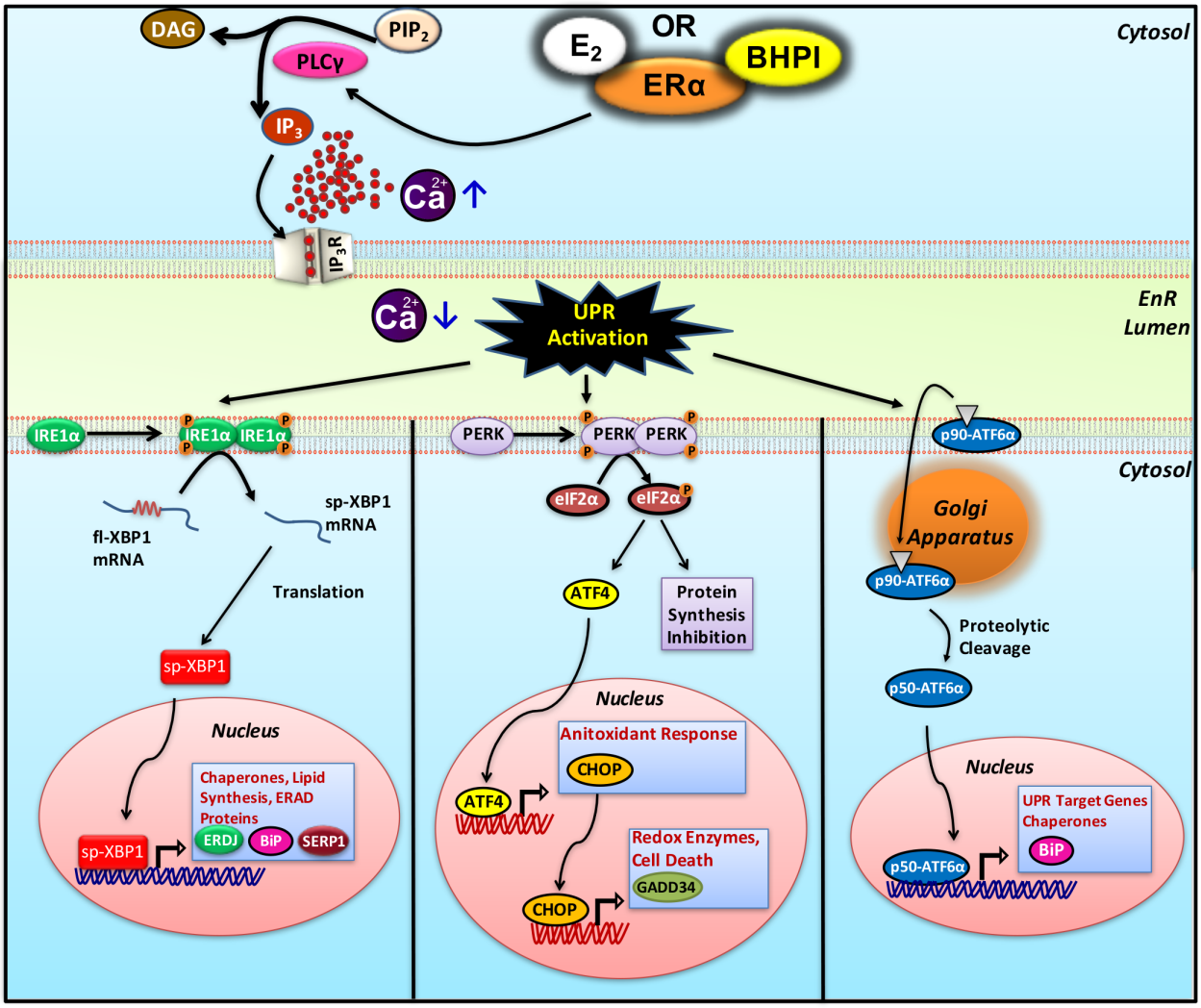

Figure 4.2. Estrogen or BHPI mediated Ca^{2+} dependent UPR activation.

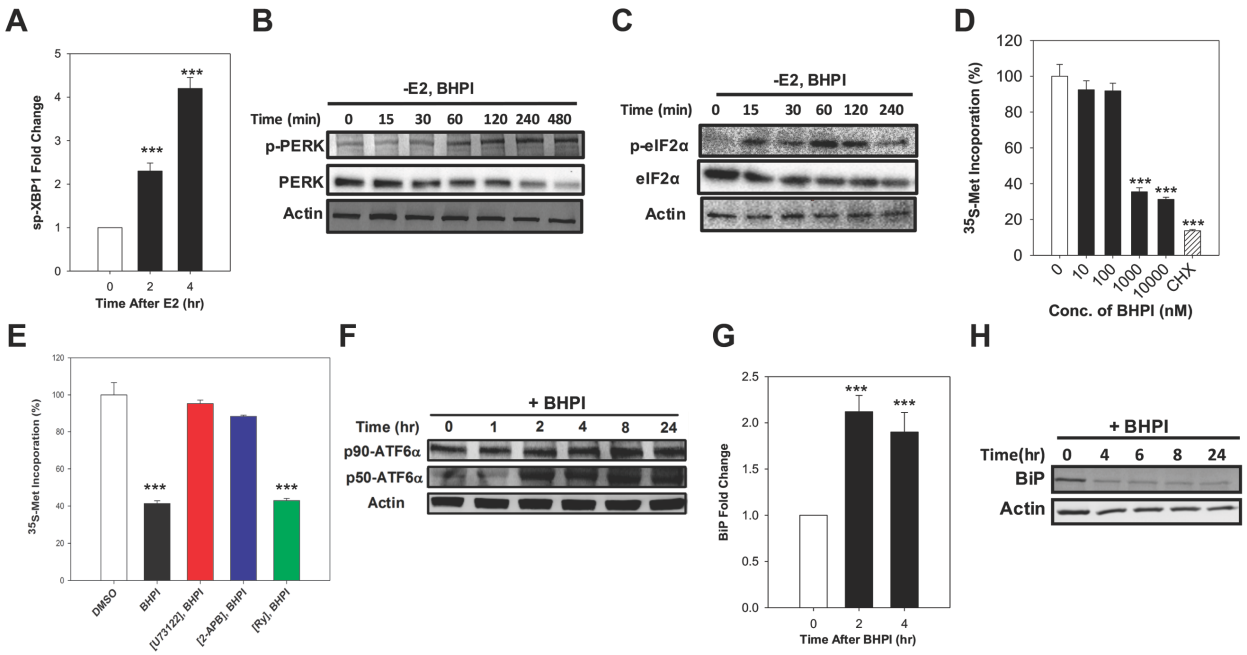

Figure 4.3. In PEO-4 ovarian cells, BHPI activates the three branches of the UPR and inhibits protein synthesis. (A) qRT-PCR analysis showing the increased level of spliced XBP1 (sp-XBP1) mRNA (n = 3). **(B, C)** Western blot analysis showing time dependent phosphorylation of PERK and eIF2α. **(D)** Protein synthesis after treating the cells with increasing concentrations of BHPI (n = 4). CHX, cycloheximide. Protein synthesis from DMSO treated control cells was set to 100%. **(E)** The level of protein synthesis after pretreating the cells with either the inhibitors U73122, 2-APB, or Ry followed by BHPI treatment (n = 4). **(F)** Western blot analysis shows full-length (p90-ATF6α) and cleaved p50-ATF6α in BHPI treated cells. Effect of BHPI on the level of BiP mRNA level **(G)** and protein **(H)**. Concentrations: U73122, 1 μM; 2-APB, 100 μM; BHPI, 500 nM **(E)** or 1 μM (other panels). ***P < 0.001.

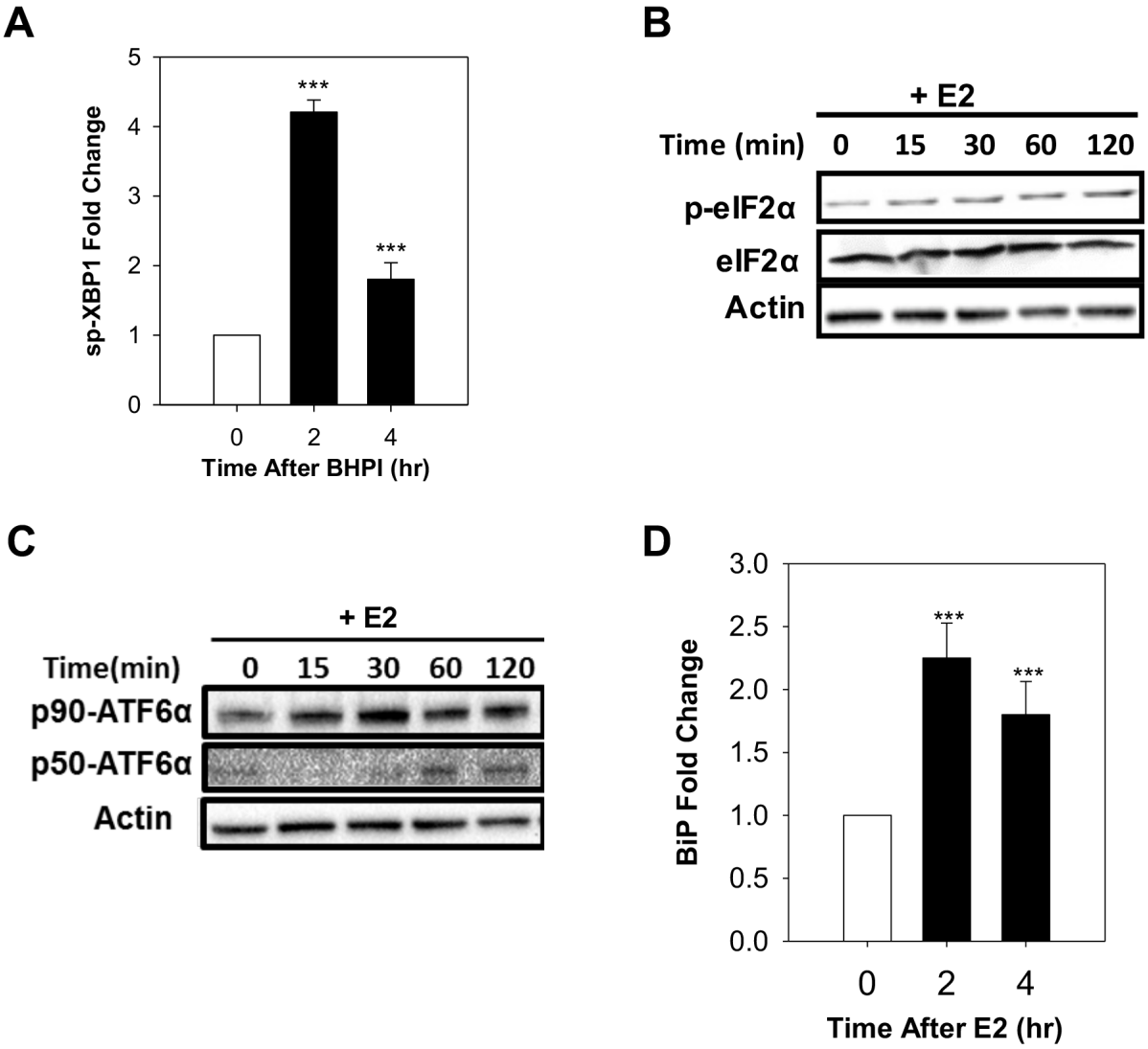

Figure 4.4. Estrogen weakly activates the three arms of the UPR in PEO-4 cells. (A) qRT-PCR analysis shows increasing sp-XBP1 mRNA after treatment with the 17β-estradiol (E_2). **(B)** Western blot showing phosphorylated eIF2α and total eIF2α proteins. **(C)** Effect of estrogen on the level of full-length (p90-ATF6α) and cleaved p50-ATF6α. **(D)** qRT-PCT quantitation of BiP mRNA at indicated time points (n = 3). The concentration of E_2 is 10 nM. ***P < 0.001.

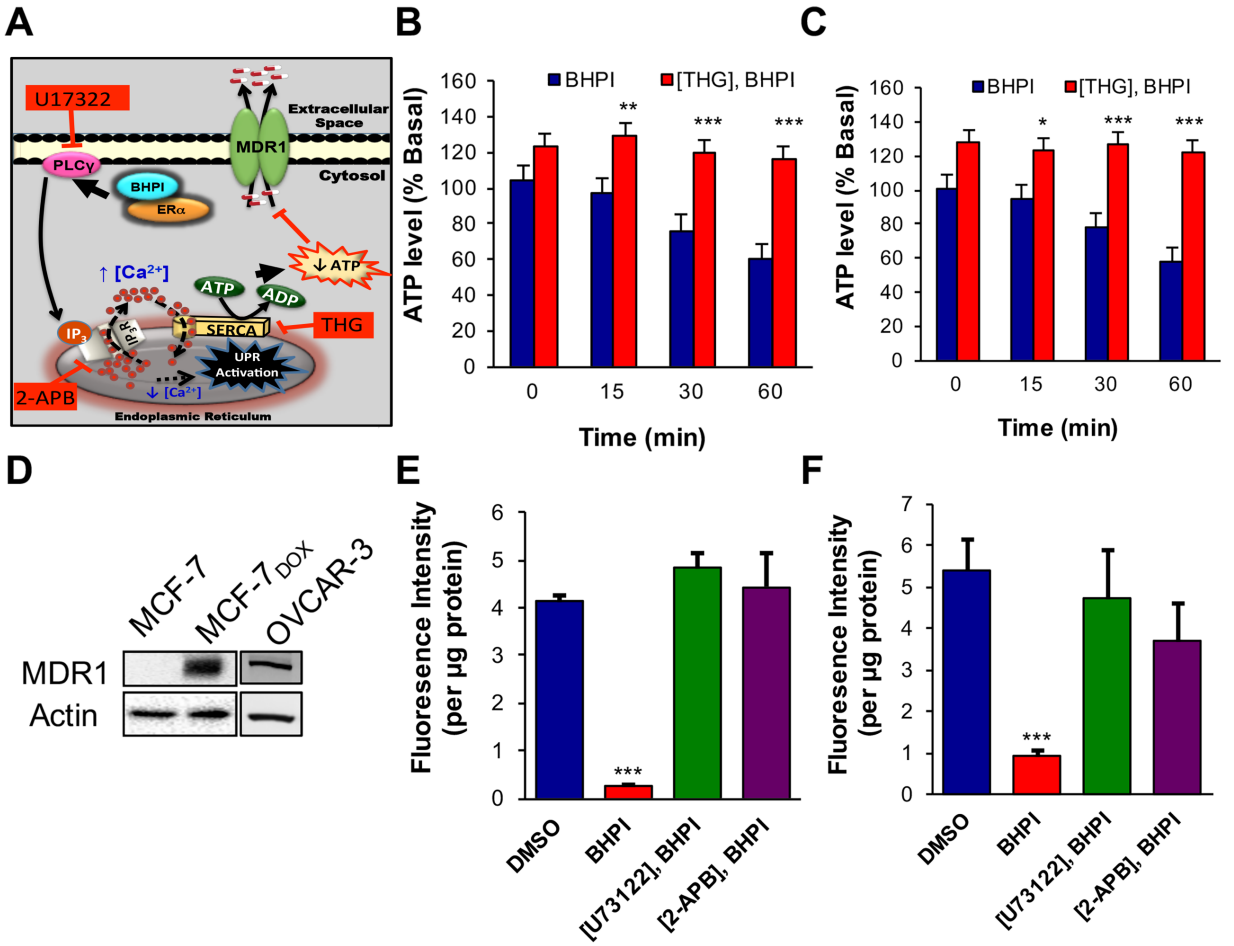

Figure 4.5. In MDR1 overexpressing cells, BHPI depletes intracellular ATP and inhibits MDR1 efflux activity. (A) Proposed model of the pathway by which BHPI inactivates MDR1. **(B, C)** Intracellular ATP quantitation showing effect of BHPI on cellular ATP level after pretreating cells with either DMSO or thapsigargin (THG) (n = 6). **(D)** Western blot analysis showing MDR1 protein level from the indicated cell lines. **(E, F)** Rhodamine-123 (Rho-123) quantitation showing the effect of BHPI on Rho-123 concentration in the media after pretreating cells with either DMSO, U73122, or 2-APB (n = 6). Concentrations: U73122, 1 µM; 2-APB, 100 µM; BHPI, 1 µM **(B, C)** or 500 nM **(E, F)**. Data is the mean ± SEM. ***P < 0.001.

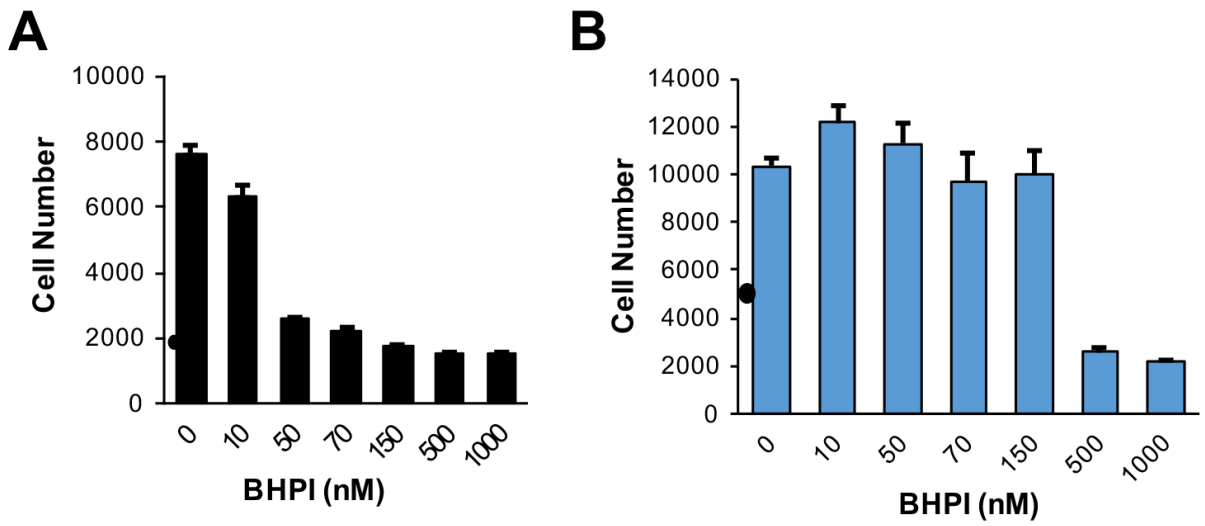

Figure 4.6. BHPI blocks proliferation of MCF-7 and doxorubicin resistant MCF-7 (MCF-7$_{dox}$) breast cancer cells. (A, B) MTS assays showing the effect of BHPI on cell proliferation. "•" on each graph denotes the number of cells at the start of the experiment. The cells were grown in medium containing 10 nM E_2 and the indicated concentrations of BHPI (n = 6). Data is the mean ± SEM.

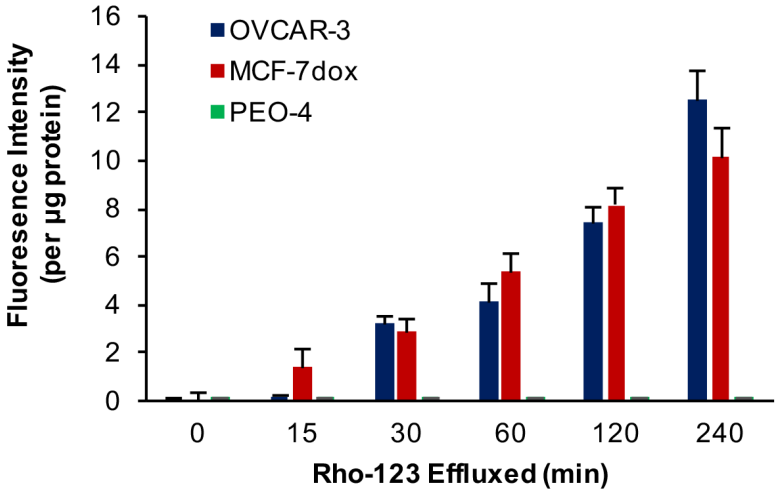

Figure 4.7. MDR1 overexpressing cells exhibit higher MDR1 efflux activity than MDR1 negative cells. For each cell line, the Rho-123 fluorescence activity in the medium is quantitated at the indicated times (n = 6). Data is the mean ± SEM.

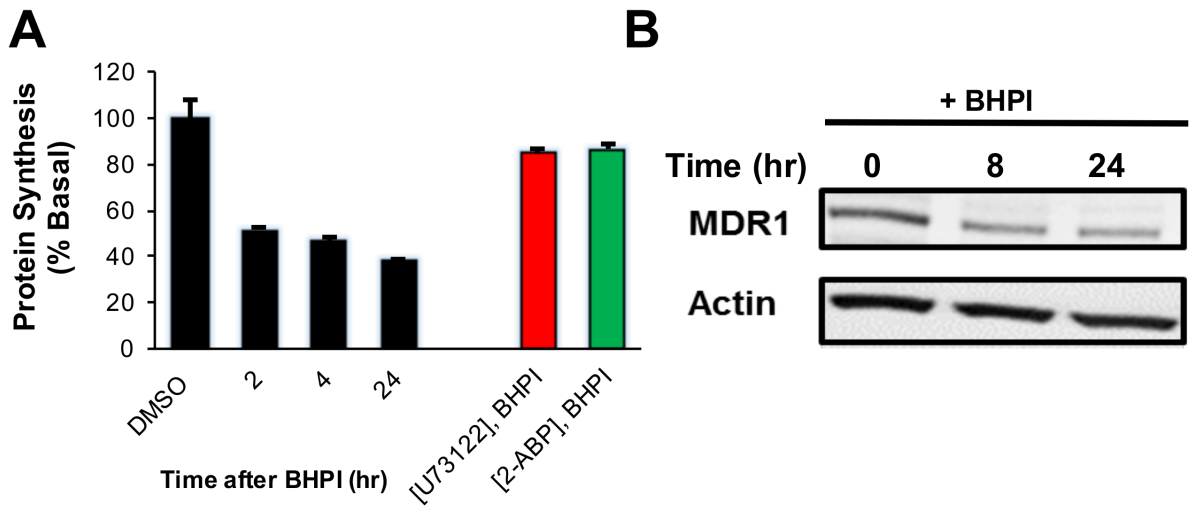

Figure 4.8. BHPI inhibits protein synthesis and reduces the level of MDR1 protein in OVCAR-3 cells. (A) Protein synthesis was measured using the incorporation of ^{35}S methionine into protein at the indicated times after pretreating cells for 20 min. with either DMSO, U73122, or 2-APB (n = 4). **(B)** Western blot indicating the MDR1 protein level at indicated time points after BHPI treatment. Concentrations: U73122, 1 μM; 2-APB, 100 μM; BHPI, 500 nM **(A)** or 1 μM **(B)**. Data is the mean ± SEM.

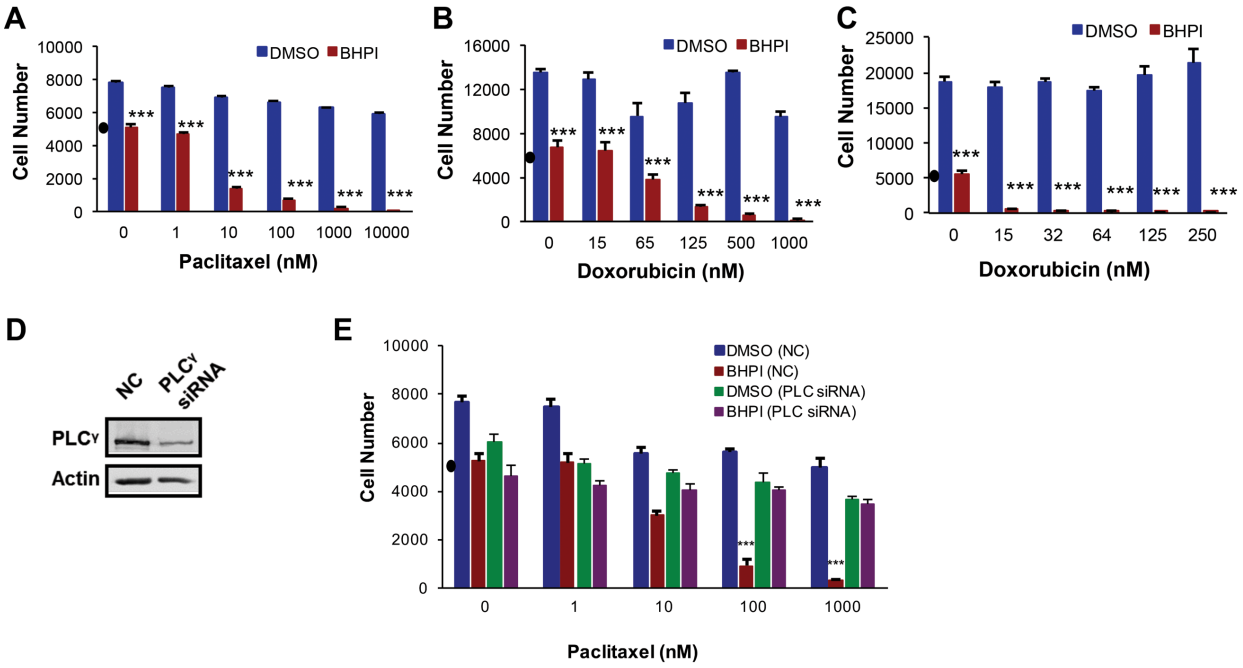

Figure 4.9. BHPI restores drug sensitivity in MDR1 overexpressing cells. MTS assays showing the effect of BHPI (1 μM) plus either DMSO or the indicated concentrations of paclitaxel **(A)** or doxorubicin **(B)** in OVCAR-3 ovarian cells (n = 6) or doxorubicin in MCF-7_{dox} breast cells **(C)** (n = 6). **(D)** Western blot analysis showing the PLCγ protein level after transfecting the cells with either non-coding SmartPool siRNA or 100 nM SmartPool PLCγ siRNA. **(E)** PLCγ knockdown abolishes the ability of BHPI to reverse multidrug resistance. OVCAR-3 cells were transfected with either non-coding control or PLCγ siRNA and the effect on cell number in cells treated with vehicle of BHPI was determined (n = 6). Cell number in a-e is from standard curves of absorbance versus cell number for each cell line. "•" on each graph denotes the number of cells at the start of the experiments. Data is the mean ± SEM. ***P < 0.001.

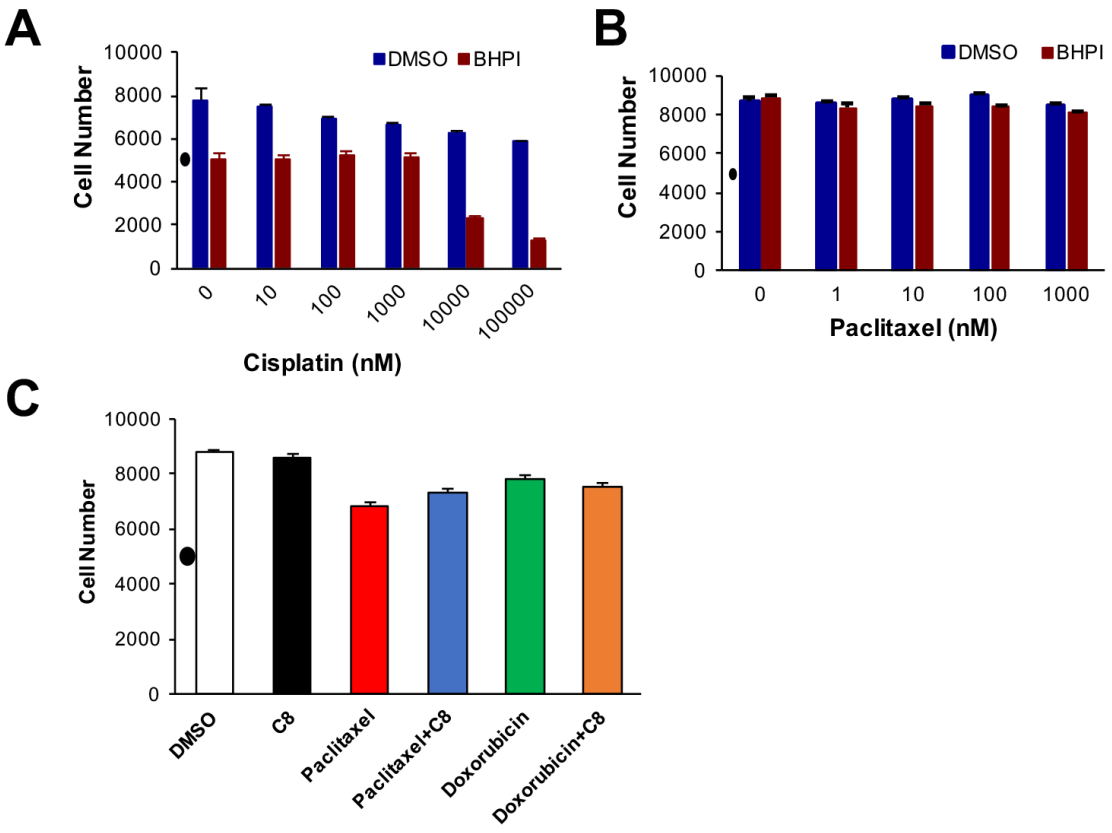

Figure 4.10. BHPI does not restore cisplatin sensitivity in OVCAR-3 cells, does not restore paclitaxel sensitivity in MDR1 overexpressing ERα negative cells, and exhibits structure specificity. MTS assays showing the effect of BHPI on cisplatin sensitivity in ERα positive OVCAR-3 cells **(A)** and on paclitaxel sensitivity in ERα negative NIH/ADRes cells **(B)** (n = 6). **(C)** The effect of an inactive close structural relative of BHPI compound 8 (C8) on OVCAR-3 cell proliferation was evaluated with either DMSO vehicle and together with paclitaxel or doxorubicin in (n = 6). "•" on each graph denotes the number of cells at the start of the experiment. The concentrations of BHPI, C8, paclitaxel and doxorubicin were 10 μM, 10 μM, 10 μM and 1 μM, respectively. Data is the mean ± SEM.

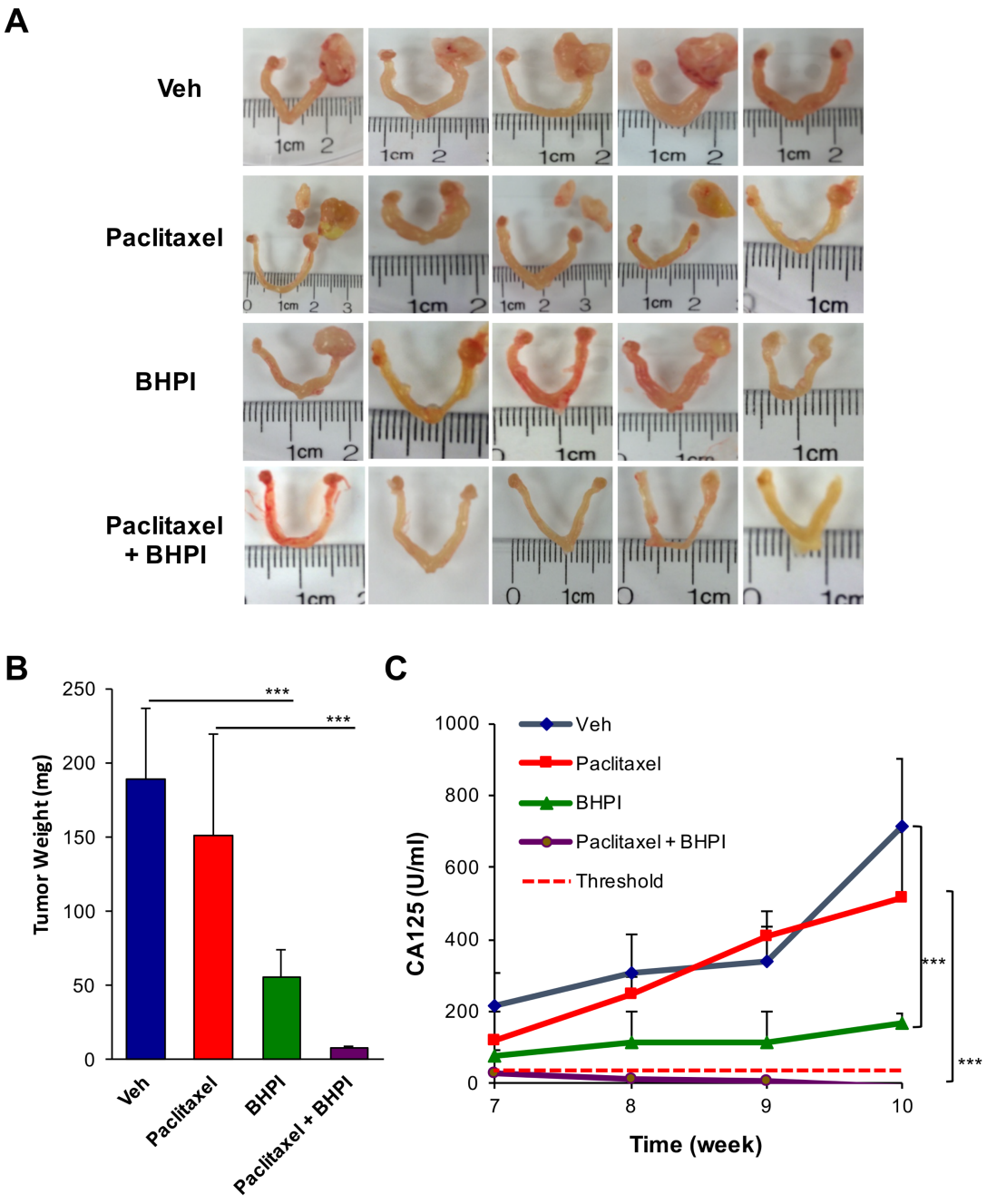

Figure 4.11. BHPI plus paclitaxel eliminates orthotopic multidrug resistant OVCAR-3 tumors. (A) Tumor images showing the size of OVCAR-3 tumors in vehicle (Veh), paclitaxel, BHPI or paclitaxel plus BHPI treatment groups (n = 5). **(B)** Average tumor weight from each treatment group (n = 5). For the paclitaxel group the secondary growths were included in tumor weight. **(C)** Circulating serum CA125 biomarker quantitation showing the progression of tumors in each treatment group (n = 5). Threshold in humans (dashed line) denotes 35 U/ml of circulating CA125. Data is the mean ± SEM. ***P < 0.001.

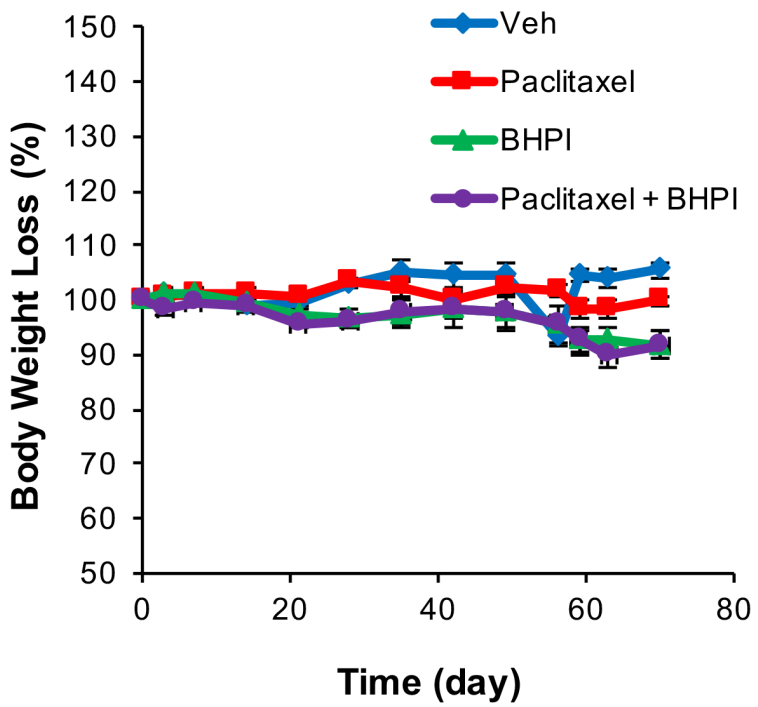

Figure 4.12. BHPI and paclitaxel are well tolerated in mice. The body weight of mice was measured at the indicated time points. Data is the mean ± SEM (n =5).

REFERENCES

1. Kumar, A., et al., *Chemotherapy is of Value in Second Line and Beyond, Relapsed High-grade, Serous Epithelial Ovarian Cancer: An Analysis of Outcomes Obtained With Oral Etoposide.* Am J Clin Oncol, 2016.
2. Romero, I. and R.C. Bast, Jr., *Minireview: human ovarian cancer: biology, current management, and paths to personalizing therapy.* Endocrinology, 2012. **153**(4): p. 1593-602.
3. Yap, T.A., C.P. Carden, and S.B. Kaye, *Beyond chemotherapy: targeted therapies in ovarian cancer.* Nat Rev Cancer, 2009. **9**(3): p. 167-81.
4. Deroo, B.J. and K.S. Korach, *Estrogen receptors and human disease.* J Clin Invest, 2006. **116**(3): p. 561-70.
5. Sjoquist, K.M., et al., *The role of hormonal therapy in gynecological cancers-current status and future directions.* Int J Gynecol Cancer, 2011. **21**(7): p. 1328-33.
6. Spoerri, M., et al., *Endocrine control of canine mammary neoplasms: serum reproductive hormone levels and tissue expression of steroid hormone, prolactin and growth hormone receptors.* BMC Vet Res, 2015. **11**: p. 235.
7. Bast, R.C., Jr., B. Hennessy, and G.B. Mills, *The biology of ovarian cancer: new opportunities for translation.* Nat Rev Cancer, 2009. **9**(6): p. 415-28.
8. Montanari, F. and G.F. Ecker, *Prediction of drug-ABC-transporter interaction--Recent advances and future challenges.* Adv Drug Deliv Rev, 2015. **86**: p. 17-26.
9. Lawlor, D., et al., *PARP Inhibitors as P-glyoprotein Substrates.* J Pharm Sci, 2014. **103**(6): p. 1913-20.

10. Santos, S.A. and A. Paulo, *Small molecule inhibitors of multidrug resistance gene (MDR1) expression: preclinical evaluation and mechanisms of action.* Curr Cancer Drug Targets, 2013. **13**(8): p. 814-28.
11. Szakacs, G., et al., *Targeting multidrug resistance in cancer.* Nat Rev Drug Discov, 2006. **5**(3): p. 219-34.
12. Kenicer, J., et al., *Molecular characterisation of isogenic taxane resistant cell lines identify novel drivers of drug resistance.* BMC Cancer, 2014. **14**: p. 762.
13. Patch, A.M., et al., *Whole-genome characterization of chemoresistant ovarian cancer.* Nature, 2015. **521**(7553): p. 489-94.
14. Silva, R., et al., *Modulation of P-glycoprotein efflux pump: induction and activation as a therapeutic strategy.* Pharmacol Ther, 2015. **149**: p. 1-123.
15. Horio, M., et al., *Transepithelial transport of drugs by the multidrug transporter in cultured Madin-Darby canine kidney cell epithelia.* J Biol Chem, 1989. **264**(25): p. 14880-4.
16. Inaba, M., et al., *Active efflux of daunorubicin and adriamycin in sensitive and resistant sublines of P388 leukemia.* Cancer Res, 1979. **39**(6 Pt 1): p. 2200-3.
17. Sarkadi, B., et al., *Expression of the human multidrug resistance cDNA in insect cells generates a high activity drug-stimulated membrane ATPase.* J Biol Chem, 1992. **267**(7): p. 4854-8.
18. Andruska, N.D., et al., *Estrogen receptor alpha inhibitor activates the unfolded protein response, blocks protein synthesis, and induces tumor regression.* Proc Natl Acad Sci U S A, 2015. **112**(15): p. 4737-42.

19. Wang, M. and R.J. Kaufman, *The impact of the endoplasmic reticulum protein-folding environment on cancer development.* Nat Rev Cancer, 2014. **14**(9): p. 581-97.

20. Walter, P. and D. Ron, *The unfolded protein response: from stress pathway to homeostatic regulation.* Science, 2011. **334**(6059): p. 1081-6.

21. Bravo, R., et al., *Endoplasmic reticulum and the unfolded protein response: dynamics and metabolic integration.* Int Rev Cell Mol Biol, 2013. **301**: p. 215-90.

22. Shapiro, D.J., et al., *Anticipatory UPR Activation: A Protective Pathway and Target in Cancer.* Trends Endocrinol Metab, 2016.

23. Zheng, X., et al., *Interplay between steroid hormone activation of the unfolded protein response and nuclear receptor action.* Steroids, 2016.

24. Monteith, G.R., et al., *Calcium and cancer: targeting Ca2+ transport.* Nat Rev Cancer, 2007. **7**(7): p. 519-30.

25. Papp, B. and J.P. Brouland, *Altered Endoplasmic Reticulum Calcium Pump Expression during Breast Tumorigenesis.* Breast Cancer (Auckl), 2011. **5**: p. 163-74.

26. Abdul, M., S. Ramlal, and N. Hoosein, *Ryanodine receptor expression correlates with tumor grade in breast cancer.* Pathol Oncol Res, 2008. **14**(2): p. 157-60.

27. Lanner, J.T., et al., *Ryanodine receptors: structure, expression, molecular details, and function in calcium release.* Cold Spring Harb Perspect Biol, 2010. **2**(11): p. a003996.

28. Maxwell, J.T., S. Natesan, and G.A. Mignery, *Modulation of inositol 1,4,5-trisphosphate receptor type 2 channel activity by Ca2+/calmodulin-dependent*

protein kinase II (CaMKII)-mediated phosphorylation. J Biol Chem, 2012. **287**(47): p. 39419-28.

29. Alonso, M.T., I.M. Manjarres, and J. Garcia-Sancho, *Privileged coupling between Ca(2+) entry through plasma membrane store-operated Ca(2+) channels and the endoplasmic reticulum Ca(2+) pump.* Mol Cell Endocrinol, 2012. **353**(1-2): p. 37-44.
30. Arbabian, A., et al., *Endoplasmic reticulum calcium pumps and cancer.* Biofactors, 2011. **37**(3): p. 139-49.
31. Bublitz, M., et al., *Ion pathways in the sarcoplasmic reticulum Ca2+-ATPase.* J Biol Chem, 2013. **288**(15): p. 10759-65.
32. Andruska, N., et al., *Anticipatory estrogen activation of the unfolded protein response is linked to cell proliferation and poor survival in estrogen receptor alpha-positive breast cancer.* Oncogene, 2015. **34**(29): p. 3760-9.
33. Chen, Y. and F. Brandizzi, *IRE1: ER stress sensor and cell fate executor.* Trends Cell Biol, 2013. **23**(11): p. 547-55.
34. Gardner, B.M., et al., *Endoplasmic reticulum stress sensing in the unfolded protein response.* Cold Spring Harb Perspect Biol, 2013. **5**(3): p. a013169.
35. Korennykh, A. and P. Walter, *Structural basis of the unfolded protein response.* Annu Rev Cell Dev Biol, 2012. **28**: p. 251-77.
36. Hamilton, T.C., et al., *Characterization of a human ovarian carcinoma cell line (NIH:OVCAR-3) with androgen and estrogen receptors.* Cancer Res, 1983. **43**(11): p. 5379-89.

37. Kim, H.J., et al., *Synergistic Effect of COX-2 Inhibitor on Paclitaxel-Induced Apoptosis in the Human Ovarian Cancer Cell Line OVCAR-3.* Cancer Res Treat, 2014. **46**(1): p. 81-92.

38. Guo, B., et al., *Cross-resistance studies of isogenic drug-resistant breast tumor cell lines support recent clinical evidence suggesting that sensitivity to paclitaxel may be strongly compromised by prior doxorubicin exposure.* Breast Cancer Res Treat, 2004. **85**(1): p. 31-51.

39. Reed, K., et al., *The temporal relationship between ABCB1 promoter hypomethylation, ABCB1 expression and acquisition of drug resistance.* Pharmacogenomics J, 2010. **10**(6): p. 489-504.

40. Forster, S., et al., *Characterization of rhodamine-123 as a tracer dye for use in in vitro drug transport assays.* PLoS One, 2012. **7**(3): p. e33253.

41. Yoshizawa, Y., et al., *A novel approach to overcome multidrug resistance: utilization of P-gp mediated efflux of paclitaxel to attack neighboring vascular endothelial cells in tumors.* Eur J Pharm Sci, 2014. **62**: p. 274-80.

42. Olszewski, W., et al., *Topoisomerase 2alpha status in invasive breast carcinoma - comparison of its clinical value according to immunohistochemical and fluorescence in situ hybridization methods of evaluation.* Pol J Pathol, 2014. **65**(4): p. 283-90.

43. Galluzzi, L., et al., *Systems biology of cisplatin resistance: past, present and future.* Cell Death Dis, 2014. **5**: p. e1257.

44. Mitra, A.K., et al., *In vivo tumor growth of high-grade serous ovarian cancer cell lines.* Gynecol Oncol, 2015. **138**(2): p. 372-7.

45. Burbridge, M.F., et al., *Biological and pharmacological characterisation of three models of human ovarian carcinoma established in nude mice: use of the CA125 tumour marker to predict antitumour activity.* Int J Oncol, 1999. **15**(6): p. 1155-62.

46. Goodell, C.A., et al., *Characterization of the tumor marker muc16 (ca125) expressed by murine ovarian tumor cell lines and identification of a panel of cross-reactive monoclonal antibodies.* J Ovarian Res, 2009. **2**(1): p. 8.

47. Zhang, J., et al., *Establishment of a new representative model of human ovarian cancer in mice.* J Ovarian Res, 2013. **6**(1): p. 9.

48. Spillman, M.A., et al., *Tissue-specific pathways for estrogen regulation of ovarian cancer growth and metastasis.* Cancer Res, 2010. **70**(21): p. 8927-36.

49. Matsuo, K., et al., *Estrogen receptor expression and increased risk of lymphovascular space invasion in high-grade serous ovarian carcinoma.* Gynecol Oncol, 2014. **133**(3): p. 473-9.

50. van Kruchten, M., et al., *Hormone receptors as a marker of poor survival in epithelial ovarian cancer.* Gynecol Oncol, 2015. **138**(3): p. 634-9.

51. Kim, H.G., et al., *Metformin inhibits P-glycoprotein expression via the NF-kappaB pathway and CRE transcriptional activity through AMPK activation.* Br J Pharmacol, 2011. **162**(5): p. 1096-108.

52. Wang, Z., et al., *Resveratrol induces AMPK-dependent MDR1 inhibition in colorectal cancer HCT116/L-OHP cells by preventing activation of NF-kappaB signaling and suppressing cAMP-responsive element transcriptional activity.* Tumour Biol, 2015. **36**(12): p. 9499-510.

53. Xu, R.H., et al., *Inhibition of glycolysis in cancer cells: a novel strategy to overcome drug resistance associated with mitochondrial respiratory defect and hypoxia.* Cancer Res, 2005. **65**(2): p. 613-21.

54. Vignani, F., et al., *Skeletal metastases and impact of anticancer and bone-targeted agents in patients with castration-resistant prostate cancer.* Cancer Treat Rev, 2016. **44**: p. 61-73.

55. Conley, S.J., et al., *Antiangiogenic agents increase breast cancer stem cells via the generation of tumor hypoxia.* Proc Natl Acad Sci U S A, 2012. **109**(8): p. 2784-9.

56. Kenmogne, L.C., et al., *The Aminosteroid Derivative RM-133 Shows In Vitro and In Vivo Antitumor Activity in Human Ovarian and Pancreatic Cancers.* PLoS One, 2015. **10**(12): p. e0144890.

57. Pourgholami, M.H., et al., *Minocycline inhibits growth of epithelial ovarian cancer.* Gynecol Oncol, 2012. **125**(2): p. 433-40.

58. Cheng, J., C. Zhang, and D.J. Shapiro, *A functional serine 118 phosphorylation site in estrogen receptor-alpha is required for down-regulation of gene expression by 17beta-estradiol and 4-hydroxytamoxifen.* Endocrinology, 2007. **148**(10): p. 4634-41.

59. Yu, L., et al., *Anticipatory activation of the unfolded protein response by epidermal growth factor is required for immediate early gene expression and cell proliferation.* Mol Cell Endocrinol, 2015.

CHAPTER 5

INTERPLAY BETWEEN STEROID HORMONE ACTIVATION OF THE UNFOLDED PROTEIN RESPONSE AND NUCLEAR RECEPTOR ACTION [4]

ABSTRACT

To identify new pathways of estrogen action and novel estrogen receptor α (ERα) biomodulators, we performed high throughput screening and used follow on assays and bioinformatics to identify small molecule ERα inhibitors with a novel mode of action. These studies led to identification of rapid extranuclear activation of the endoplasmic reticulum stress sensor, the unfolded protein response (UPR), as a new pathway of estrogen-ERα action. Moreover, increasing evidence indicates that the mechanism underlying anticipatory activation of the UPR is shared among steroid and peptide hormones and is conserved from insects to humans. It is likely that this newly unveiled extranuclear pathway is used by diverse mitogenic hormones to prepare cells for the increased protein folding load that will occur during subsequent cell proliferation. Demonstrating biological relevance, elevated expression of a UPR gene signature in ERα positive breast cancer is a powerful new prognostic marker tightly correlated with subsequent resistance to tamoxifen, tumor recurrence and poor survival. In addition, overexpression of epidermal growth factor receptor and HER2/neu is positively correlated with increased UPR activation in breast cancer. This review describes recent research

[4] This chapter appeared in its entirety in the *Steroids.* **Xiaobin Zheng**, Neal Andruska, Liqun Yu, Chengjian Mao, Ji Eun Kim, Mara Livezey, William G Helferich, David J Shapiro. (2016) Interplay between steroid hormone activation of the unfolded protein response and nuclear receptor action. Steroid. DOI: 10.1016/j.steroids.2016.03.014.

that demonstrates the importance of anticipatory UPR activation in therapy resistant tumors and discusses a promising small molecule biomodulator that inhibits tumor growth by tuning this UPR signaling pathway.

KEYWORDS

Steroid Receptor; Breast cancer; Unfolded protein response; Cell death; Hormone action; Cancer.

ABBREVIATIONS

AR, androgen receptor;

CAMKIII/eEF2K, eukaryotic elongation factor 2 kinase;

Ec, ecdysone;

EcR, ecdysone receptor;

EGF, epidermal growth factor;

EGFR, epidermal growth factor receptor;

eIF2α, eukaryotic initiation factor 2 α;

EnR, endoplasmic reticulum;

ERα, estrogen receptor α;

IP_3, inositol triphosphate;

IP_3R, inositol triphosphate receptor;

PERK, protein kinase RNA-like endoplasmic reticulum kinase;

PLCγ, phospholipase C gamma;

SERCA, sarco/endoplasmic reticulum Ca^{2+}-ATPase;

UPR, unfolded protein response;

VEGF, vascular endothelial growth factor;

INTRODUCTION

The endoplasmic reticulum (EnR) plays a key role in synthesis, folding and transport of nascent peptides. Protein maturation in the EnR is a critical step in normal cell function and in cell survival. Modest changes in the cellular environment, such as changes in the intracellular Ca^{2+} level in the lumen of the EnR, nutrient availability, redox state, or in the rate of protein synthesis, can cause accumulation of misfolded or unfolded proteins. The resulting EnR stress [1, 2] leads to activation of the EnR stress response pathway, the unfolded protein response (UPR). The UPR consists of three main branches that together balance the synthesis of new proteins with the availability of chaperones and other proteins to help fold and transport proteins within cells. EnR stress activates autophosphorylation of the transmembrane kinase PERK (protein kinase RNA-like endoplasmic reticulum kinase) [2, 3]. Activated p-PERK phosphorylates eukaryotic initiation factor 2α (eIF2α), resulting in transient inhibition of most protein synthesis and increased translation of $p58^{IPK}$ and GADD34. If the stress is moderate, the $p58^{IPK}$ binds PERK, inhibiting PERK activation, and the GADD34 dephosphorylates eIF2α. This ultimately reverses PERK activation and protein synthesis is restored [4, 5]. The other arms of the UPR initiate with activation of the transcription factor ATF6α, leading to increased protein folding capacity and activation of the splicing factor IRE1α, which alternatively splices the transcription factor XBP1, leading to production of active spliced

XBP1 (sp-XBP1), increased protein folding capacity and altered mRNA decay and translation (Figure 5.1) [1-3].

Diverse mitogenic hormones, acting via their respective receptors, stimulate cell proliferation and tumor growth [6-11]. Enhanced cell proliferation requires increased protein production, potentially leading to insufficient protein folding capacity and EnR stress. Although UPR activation has been described in multiple cancers [2, 12-15], until recently, it has not been a major research focus in hormone-dependent cancers. This review focuses on the pathophysiological importance of anticipatory UPR activation in hormone signaling as an early component of the cellular proliferation program and discusses the preclinical promises of targeting the UPR.

STEROID/PEPTIDE HORMONE ACTIVATION OF THE UPR

Steroid and peptide hormones execute their biological functions through direct interaction with hormone-specific receptors [8, 9]. These include binding of mitogenic steroid hormones, 17β-estradiol (E_2; estrogen), dihydrotestosterone (DHT; androgen) and ecdysone (Ec) to their respective nuclear receptors (ERα, AR and EcR) and of the peptide hormones epidermal growth factor (EGF) and vascular endothelial growth factor (VEGF) to their receptors (EGFR and VEGFR). Steroid hormones exert their molecular functions by regulating gene expression in the nucleus and cross-talking with diverse extranuclear signal transduction pathways. In the classical genomic action of steroid hormones, here illustrated using estrogen, estrogens bind to ERα; this results in receptor dimerization. Estrogen-ERα binds directly to genomic response elements and interacts with DNA indirectly through tethering to other proteins. This results in activation of a genomic

program that alters the expression of thousands of genes and plays an important role in promoting the proliferation of ERα positive cancer cells [16-18].

While the genomic actions of steroid hormones are initiated rapidly, they play out over many hours. A disparate set of rapid extranuclear actions of steroid receptors, often initiated at or near the plasma membrane, influence diverse cell functions and also play a pivotal role in modulating the receptors genomic program [19-21]. While much attention focused on rapid effects of steroid hormones on established signal transduction pathways, rapid effects of estrogen and other steroid hormones on activation of the UPR were largely unexplored. We recently showed that, within 1 minute, estrogens, acting via ERα, activate phospholipase C gamma (PLCγ), producing inositol triphosphate (IP_3). The IP_3 binds to and opens the EnR inositol triphosphate receptor (IP_3R) calcium channels allowing rapid efflux of calcium from the lumen of the EnR into the cytosol (Figure 5.1). This rapid calcium efflux activates the UPR, inducing chaperones (Figure 5.1). Notably, inhibition or knockdown of pathway components strongly inhibits estrogen stimulated cell proliferation and nearly abolishes subsequent estrogen-ERα induction and repression of gene expression (Figure 5.1) [22]. Moreover, analysis of data from approximately 1,000 ERα positive breast cancers shows that elevated expression of a UPR gene signature at diagnosis is a powerful new prognostic marker tightly correlated with subsequent resistance to tamoxifen, tumor recurrence and poor survival [22].

The well-studied oncogenic mitogen EGF, acting through EGF receptors, rapidly activates the ERK and AKT signaling pathways and alters gene expression. EGF-EGFR activation of these pathways promotes tumor growth and invasion, and is antiapoptotic [23-25]. Although EGF is a peptide hormone and EGFR is a plasma membrane receptor,

EGF-EGFR and E_2-ERα share the same general pathway for rapid anticipatory activation of the UPR (Figure 5.1; see Section 2 above) [26]. Activation of the anticipatory UPR pathway is a newly described action of EGF, and it facilitates EGF stimulated cell cycle progression in different ways [26]. We find that EGF-EGFR activation of the anticipatory UPR pathway is required for EGF induced immediate early gene expression. Notably, while blocking UPR activation abolishes EGF regulated immediate early gene expression, it has no effect on EGF activation of the ERK and AKT pathways. This indicates that at early times, the anticipatory UPR pathway and the ERK pathway are independent regulators, which converge at the level of gene expression [26]. EGF induced chaperone production also contribute to cell proliferation; knocking down the chaperone producing arms of the UPR inhibits EGF stimulated cell proliferation [26].

Tumor growth and metastasis depends on new growth in the vascular network [27]. In endothelial cells, vascular endothelial growth factor (VEGF), acting through VEGF receptors, promotes cell viability and angiogenesis, the formation of new blood vessels [27-29]. Recently, anticipatory activation of the UPR has been identified as a new mode of action in VEGF signaling. In a notable difference between the estrogen and VEGF pathways, the activation mechanism is reported to be independent of the PLCγ-IP_3-calcium pathway [30]. In the absence of EnR stresses, VEGF primes cells by activating the ATF6α and PERK arms of the UPR and anticipates the needs for subsequent VEGF-induced vascularization [30].

Prostate cancer is a leading cause of cancer in men. Androgens, such as testosterone and dihydrotestosterone (DHT), exert their biological functions through the androgen receptor and play a pivotal role in proliferation of prostate cancer [31, 32]. At

early time points, DHT did not rapidly induce sp-XBP1 and BiP mRNA (Figure 5.2). As a control, in the AR-positive LNCaP and LAPC4 human prostate cancer cell lines, prostate-specific antigen (PSA), which is a classic DHT inducible gene, is rapidly and robustly induced (8 h; Figure 5.2). Thus, rapid UPR activation is not part of DHT signaling pathway. However, activation of the UPR was observed at later times (e.g. 24 to 48 h) [33]. Together, these data suggest DHT may activate the UPR through a reactive UPR mechanism, in which UPR activation is stimulated by accumulation of misfolded and unfolded proteins as the cells proliferate, or through a nuclear gene expression program that induces UPR-related mRNAs. Although the exact molecular mechanism underlying DHT activation of the UPR requires further exploration, pharmacological inhibition of IRE1α significantly reduces prostate tumor growth [33]. This supports the biological significance of activation of the UPR pathway in prostate cancer progression.

The transformation of insects from larvae to adults is commonly known as metamorphosis. Neuronal remodeling is a crucial process for development of both vertebrates and invertebrates but is particularly critical for metamorphosis. During this process, axons and dendrites undergo a precisely controlled program of pruning via cell death followed by regrowth [34]. This remodeling of axons and dendrite events ultimately depends on the molecular function of Ec-EcR [34]. As a part of rapid extranuclear action of Ec-EcR, Ec regulates the cytosolic calcium level through a PLCγ-IP_3-calcium dependent pathway, resulting in phosphorylation and activation of protein kinase C that modulates transcriptional activity of ultraspircle in the lepidopteran insect *Helicoverpa armigera* [35]. Depletion of PLCγ leads to metamorphosis defects and blocks induction of Ec regulated genes [35].

Although the mechanisms underlying anticipatory UPR activation vary among different hormone-mediated signaling pathways, an important consequence of anticipatory UPR activation is the induction of molecular chaperones that primes cells to mitigate damage due to future cell stress that may occur during proliferation, or under various physiological conditions. Activation of the UPR before the cellular stress and before the accumulation of unfolded protein is the key feature that distinguishes the anticipatory UPR pathway from the well-studied reactive UPR pathway.

THE UPR ACTS AS A DOUBLE-EDGED SWORD TO CONTROL CELL FATE

Anticipatory UPR activation is protective; deletion or inhibition of UPR components is an emerging therapeutic strategy that reduces tumor growth and increases susceptibility of cancer cells to therapeutic agents [33, 36, 37]. Recently, we described a novel strategy to target cancer cells, not by inhibiting the UPR, but by toxic hyperactivation of the UPR. Through high throughput screening follow on assays and bioinformatics, we identified a clinically promising small molecule ERα biomodulator, BHPI [38, 39]. BHPI binds non-competitively to ERα and distorts and exaggerates the normal estrogen-ERα pathway for anticipatory activation of the UPR [39]. Comparing the cytotoxic actions of BHPI to the protective anticipatory activation of the UPR by estrogen, BHPI induces hyperactivation of PLCγ, which leads to greatly increased production of IP_3 and a massive efflux of calcium stored in the lumen of EnR into the cytosol. Because of this massive release of calcium into the cytosol, the magnitude and duration of UPR activation by BHPI is much larger than what is seen with estrogens [22, 39]. This leads to strong activation of the PERK arm of the UPR, resulting in extensive eIF2α phosphorylation and near

quantitative inhibition of protein synthesis [39]. Cytosolic calcium levels are tightly regulated because high levels of calcium in the cytosol are toxic [40-43]. To maintain cellular calcium homeostasis, the cell activates sarco/endoplasmic reticulum Ca^{2+}-ATPase (SERCA) pumps, which catalyze ATP-dependent transfer of calcium from the cytosol into the lumen of the EnR [44-46]. Since the IP_3R calcium channels are still open, the calcium pumped into the EnR leaks back out to cytosol creating a futile cycle that rapidly depletes cellular ATP. This ATP depletion results in increased AMP, which activates the metabolic sensor AMPK [39]. Together, high levels of cytosolic calcium and AMPK activation activate the $Ca^{2+/}$calmodulin-dependent kinase, eukaryotic elongation factor 2 kinase (CAMKIII/eEF2K). This results in phosphorylation and inactivation of eukaryotic elongation factor 2 (eEF2), inhibiting protein synthesis at a second site [39, 47, 48]. Anticipatory UPR activation by estrogen is weak and transient because the induced expression of UPR molecular chaperones helps resolve UPR stress and ultimately reverses UPR activation [1, 4, 12]. In contrast, since BHPI blocks global protein synthesis including synthesis of UPR-induced molecular chaperones such as $p58^{IPK}$, GADD34, and BiP, BHPI activation of UPR is unresolvable.

BHPI is exceptionally effective as a new preclinical anticancer drug. It works in ERα positive cancer cells that do not require estrogens or ERα for growth and also in cells that are therapy-resistant [39]. Importantly, at nanomolar concentrations, BHPI does not only stop cancer cell growth, but also kills many breast and endometrial cancer cell lines. In the mouse xenograft model of breast cancer in which BHPI treatment was initiated when tumors reached about 45 mm^2, control and BHPI treated tumors were both continuously exposed to estrogen. BHPI, at the reasonable dose of 15 mg/kg daily for 10

days, rapidly stopped tumor growth and induced substantial regression of 48 out of 52 tumors [39]. Moreover, BHPI was well tolerated by the mice [39].

An intriguing question to ask is, since BHPI hyperactivates the UPR converting it from protective to toxic, why is BHPI not toxic to normal ERα positive cells? The UPR is nearly off in most normal cells. We hypothesize that since UPR expression is already elevated as part of the mechanism that protects cancer cells [39], it is actually easier for BHPI hyperactivation of the UPR to push the already activated UPR from cytoprotective to cytotoxic in a cancer cell than it is in a normal cell that starts with a much lower level of UPR activation.

In summary, BHPI is the first example of an ERα biomodulator that targets the UPR pathway and converts it from cytoprotective to cytotoxic.

CONCLUSION

Steroid and peptide hormones play key roles in normal cell physiology and in pathology. The ability to tolerate various cellular stresses is crucial for cell survival, especially in the tumor microenvironment. Anticipatory UPR activation is an emerging rapid extranuclear signaling pathway that is activated by different mitogenic hormones to resolve future cellular stresses. These rapid responses and early events can also lead to downstream genomic effects and are important in cross-talk, leading to reciprocal regulation of the nuclear and extranuclear pathways. Identification of the players that communicate molecular messages, especially elevated intracellular calcium and increased chaperone levels from the UPR pathway to the nucleus is essential to understanding how the UPR pathway influences the gene regulation network. Moreover,

disruption or strong enhancement of the UPR offers a new approach to cancer therapy and to overcoming resistance to current therapies.

ACKNOWLEDGEMENTS

Supported by NIH RO1 DK 071909 and DOD BCRP W81XWH-13 (to D.S.), Carter (to X.Z.), Westcott and Carter (to N.A.) and NSF (to M.L.) predoctoral fellowships.

FIGURES

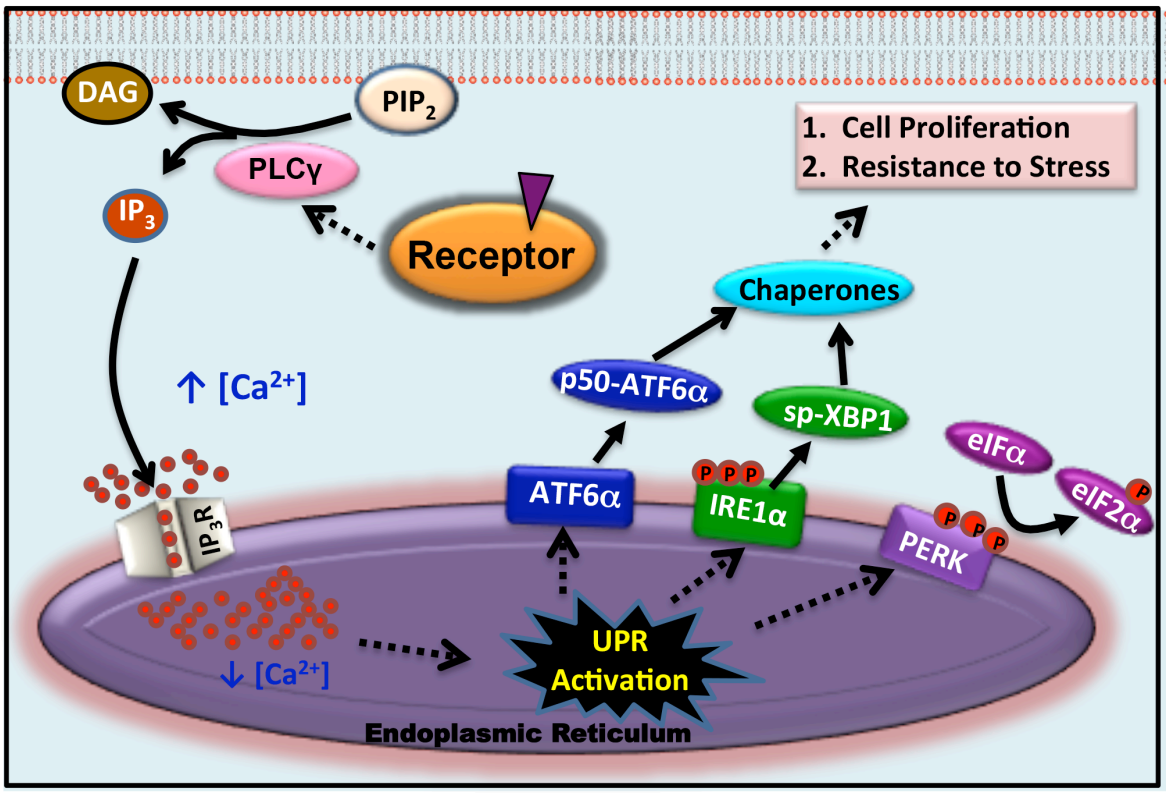

Figure 5.1. Model for activation of the UPR by steroid or peptide hormones.

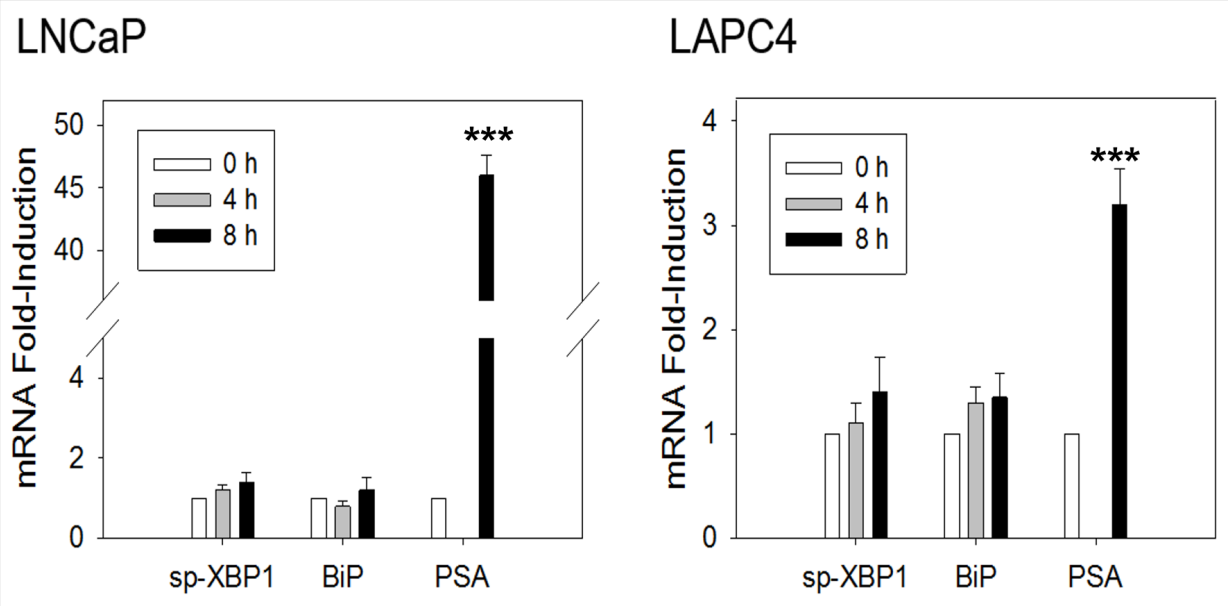

Figure 5.2. DHT does not induce rapid activation of the IRE1α and ATF6α arms of the UPR in prostate cancer cells. qRT-PCR time course comparing the effect of DHT on DHT-AR induction of spliced-XBP1 (sp-XBP1), BiP and prostate-specific antigen (PSA) in AR positive LNCaP and LAPC4 cells. The qRT-PCR procedures have been described previously [22, 39]. Briefly, the cells were plated in RPMI growth medium with 10% charcoal stripped fetal bovine serum for three days prior to treating the cells with 10 nM DHT at the indicated times. (n=3; 0 h set to 1). Data are mean ± s.e.m. ***P < 0.001.

REFERENCES

1. Ron, D. and P. Walter, *Signal integration in the endoplasmic reticulum unfolded protein response.* Nat Rev Mol Cell Biol, 2007. **8**(7): p. 519-29.
2. Wang, M. and R.J. Kaufman, *The impact of the endoplasmic reticulum protein-folding environment on cancer development.* Nat Rev Cancer, 2014. **14**(9): p. 581-97.
3. Korennykh, A. and P. Walter, *Structural basis of the unfolded protein response.* Annu Rev Cell Dev Biol, 2012. **28**: p. 251-77.
4. Novoa, I., et al., *Feedback inhibition of the unfolded protein response by GADD34-mediated dephosphorylation of eIF2alpha.* J Cell Biol, 2001. **153**(5): p. 1011-22.
5. Yan, W., et al., *Control of PERK eIF2alpha kinase activity by the endoplasmic reticulum stress-induced molecular chaperone P58IPK.* Proc Natl Acad Sci U S A, 2002. **99**(25): p. 15920-5.
6. Deroo, B.J. and K.S. Korach, *Estrogen receptors and human disease.* J Clin Invest, 2006. **116**(3): p. 561-70.
7. Evans, R.M., *The steroid and thyroid hormone receptor superfamily.* Science, 1988. **240**(4854): p. 889-95.
8. Huang, P., V. Chandra, and F. Rastinejad, *Structural overview of the nuclear receptor superfamily: insights into physiology and therapeutics.* Annu Rev Physiol, 2010. **72**: p. 247-72.
9. Katzenellenbogen, B.S., *Dynamics of steroid hormone receptor action.* Annu Rev Physiol, 1980. **42**: p. 17-35.

10. Musgrove, E.A. and R.L. Sutherland, *Biological determinants of endocrine resistance in breast cancer.* Nat Rev Cancer, 2009. **9**(9): p. 631-43.
11. Tyson, J.J., et al., *Dynamic modelling of oestrogen signalling and cell fate in breast cancer cells.* Nat Rev Cancer, 2011. **11**(7): p. 523-32.
12. Bravo, R., et al., *Endoplasmic reticulum and the unfolded protein response: dynamics and metabolic integration.* Int Rev Cell Mol Biol, 2013. **301**: p. 215-90.
13. Gao, Y., et al., *PERK is required in the adult pancreas and is essential for maintenance of glucose homeostasis.* Mol Cell Biol, 2012. **32**(24): p. 5129-39.
14. Hotamisligil, G.S., *Endoplasmic reticulum stress and the inflammatory basis of metabolic disease.* Cell, 2010. **140**(6): p. 900-17.
15. Malhi, H. and R.J. Kaufman, *Endoplasmic reticulum stress in liver disease.* J Hepatol, 2011. **54**(4): p. 795-809.
16. Carroll, J.S., et al., *Chromosome-wide mapping of estrogen receptor binding reveals long-range regulation requiring the forkhead protein FoxA1.* Cell, 2005. **122**(1): p. 33-43.
17. Hah, N., et al., *A rapid, extensive, and transient transcriptional response to estrogen signaling in breast cancer cells.* Cell, 2011. **145**(4): p. 622-34.
18. York, B. and B.W. O'Malley, *Steroid receptor coactivator (SRC) family: masters of systems biology.* J Biol Chem, 2010. **285**(50): p. 38743-50.
19. Hammes, S.R. and P.J. Davis, *Overlapping nongenomic and genomic actions of thyroid hormone and steroids.* Best Pract Res Clin Endocrinol Metab, 2015. **29**(4): p. 581-93.

20. Levin, E.R., *Plasma membrane estrogen receptors.* Trends Endocrinol Metab, 2009. **20**(10): p. 477-82.

21. Song, R.X. and R.J. Santen, *Membrane initiated estrogen signaling in breast cancer.* Biol Reprod, 2006. **75**(1): p. 9-16.

22. Andruska, N., et al., *Anticipatory estrogen activation of the unfolded protein response is linked to cell proliferation and poor survival in estrogen receptor alpha-positive breast cancer.* Oncogene, 2015. **34**(29): p. 3760-9.

23. Masuda, H., et al., *Role of epidermal growth factor receptor in breast cancer.* Breast Cancer Res Treat, 2012. **136**(2): p. 331-45.

24. Sainsbury, J.R., et al., *Epidermal-growth-factor receptor status as predictor of early recurrence of and death from breast cancer.* Lancet, 1987. **1**(8547): p. 1398-402.

25. Salomon, D.S., et al., *Epidermal growth factor-related peptides and their receptors in human malignancies.* Crit Rev Oncol Hematol, 1995. **19**(3): p. 183-232.

26. Yu, L., et al., *Anticipatory activation of the unfolded protein response by epidermal growth factor is required for immediate early gene expression and cell proliferation.* Mol Cell Endocrinol, 2015.

27. Folkman, J., *Tumor angiogenesis: therapeutic implications.* N Engl J Med, 1971. **285**(21): p. 1182-6.

28. Kieran, M.W., R. Kalluri, and Y.J. Cho, *The VEGF pathway in cancer and disease: responses, resistance, and the path forward.* Cold Spring Harb Perspect Med, 2012. **2**(12): p. a006593.

29. Nishida, N., et al., *Angiogenesis in cancer.* Vasc Health Risk Manag, 2006. **2**(3): p. 213-9.

30. Karali, E., et al., *VEGF Signals through ATF6 and PERK to promote endothelial cell survival and angiogenesis in the absence of ER stress.* Mol Cell, 2014. **54**(4): p. 559-72.

31. Perner, S., et al., *Adaptive responses of androgen receptor signaling in castration-resistant prostate cancer.* Oncotarget, 2015. **6**(34): p. 35542-55.

32. Watson, P.A., V.K. Arora, and C.L. Sawyers, *Emerging mechanisms of resistance to androgen receptor inhibitors in prostate cancer.* Nat Rev Cancer, 2015. **15**(12): p. 701-11.

33. Sheng, X., et al., *Divergent androgen regulation of unfolded protein response pathways drives prostate cancer.* EMBO Mol Med, 2015. **7**(6): p. 788-801.

34. Boulanger, A. and J.M. Dura, *Nuclear receptors and Drosophila neuronal remodeling.* Biochim Biophys Acta, 2015. **1849**(2): p. 187-95.

35. Liu, W., et al., *Phospholipase Cgamma1 connects the cell membrane pathway to the nuclear receptor pathway in insect steroid hormone signaling.* J Biol Chem, 2014. **289**(19): p. 13026-41.

36. Das, I., et al., *Preventing proteostasis diseases by selective inhibition of a phosphatase regulatory subunit.* Science, 2015. **348**(6231): p. 239-42.

37. Harding, H.P., A.F. Zyryanova, and D. Ron, *Uncoupling proteostasis and development in vitro with a small molecule inhibitor of the pancreatic endoplasmic reticulum kinase, PERK.* J Biol Chem, 2012. **287**(53): p. 44338-44.

38. Andruska, N., et al., *Evaluation of a luciferase-based reporter assay as a screen for inhibitors of estrogen-ERalpha-induced proliferation of breast cancer cells.* J Biomol Screen, 2012. **17**(7): p. 921-32.

39. Andruska, N.D., et al., *Estrogen receptor alpha inhibitor activates the unfolded protein response, blocks protein synthesis, and induces tumor regression.* Proc Natl Acad Sci U S A, 2015. **112**(15): p. 4737-42.

40. Monteith, G.R., et al., *Calcium and cancer: targeting Ca2+ transport.* Nat Rev Cancer, 2007. **7**(7): p. 519-30.

41. Orrenius, S., B. Zhivotovsky, and P. Nicotera, *Regulation of cell death: the calcium-apoptosis link.* Nat Rev Mol Cell Biol, 2003. **4**(7): p. 552-65.

42. Papp, B. and J.P. Brouland, *Altered Endoplasmic Reticulum Calcium Pump Expression during Breast Tumorigenesis.* Breast Cancer (Auckl), 2011. **5**: p. 163-74.

43. Roderick, H.L. and S.J. Cook, *Ca2+ signalling checkpoints in cancer: remodelling Ca2+ for cancer cell proliferation and survival.* Nat Rev Cancer, 2008. **8**(5): p. 361-75.

44. Alonso, M.T., I.M. Manjarres, and J. Garcia-Sancho, *Privileged coupling between Ca(2+) entry through plasma membrane store-operated Ca(2+) channels and the endoplasmic reticulum Ca(2+) pump.* Mol Cell Endocrinol, 2012. **353**(1-2): p. 37-44.

45. Arbabian, A., et al., *Endoplasmic reticulum calcium pumps and cancer.* Biofactors, 2011. **37**(3): p. 139-49.

46. Bublitz, M., et al., *Ion pathways in the sarcoplasmic reticulum Ca2+-ATPase.* J Biol Chem, 2013. **288**(15): p. 10759-65.

47. Leprivier, G., et al., *The eEF2 kinase confers resistance to nutrient deprivation by blocking translation* elongation. Cell, 2013. **153**(5): p. 1064-79.

48. Proud, C.G., *Signalling to translation: how signal transduction pathways control the protein synthetic machinery.* Biochem J, 2007. **403**(2): p. 217-34.

CHAPTER 6

DISCUSSION AND FUTURE PERSPECTIVES

Endocrine therapy using aromatase inhibitors to inhibit estrogen production, or tamoxifen and other antiestrogens that compete with estrogens for binding to ERα, is a mainstay in treatment of ERα-positive breast cancers [1, 2]. Selection and outgrowth of breast cancers resistant to endocrine therapy is common, and the most lethal, therapy resistant metastatic tumors continue to express ERα [1]. Many epithelial ovarian tumors are ERα-positive, but all are resistant to endocrine therapy and ultimately develop resistance to standard chemotherapy [3, 4]. Therapeutic options for these resistant ovarian tumors are limited, and clinical outcomes are poor [5-7]. Most importantly, although resistance mechanisms are diverse, the presence of ERα in gynecologic cancers suggests additional modes of ERα action that contribute to therapy resistance and are potentially targetable with small molecules.

We describe a new pathway that represents the initial cell response to estrogens and is required for subsequent actions of E_2-ERα. In less than 1 minute, E_2 elicits ERα-dependent activation of phospholipase C γ (PLCγ), producing inositol triphosphate (IP_3) and diacrylglycerol (DAG). On the one hand, IP_3 binds to and opens EnR IP_3R calcium channels, resulting in a rapid efflux of calcium from the lumen of the EnR into the cell body. Loss of EnR calcium activates the EnR stress sensors, the unfolded protein response (UPR) and increases intracellular calcium. Moreover, we demonstrated that E_2-ERα activation of the UPR is mild and protects against estrogen-mediated proliferative stress. On the other hand, DAG, a lipid secondary messenger transiently generated upon PLC activation, is a classic activator of Protein Kinase C superfamily that plays an

important role in tumor development and progression, including in late stages of the disease and metastasis [8]. However, the pathophysiological roles of DAG remain elusive. Notably, ErbB2-dependent activation of PKC promotes cell invasion in breast cancer cells [9]. MCF-7 breast cancer cells that overexpress PKC show enhanced motility; this was attributed to decreased expression of E-cadherin and β-catenin and to high expression of matrix metalloprotease (MMP)-2/MMP-9 [10, 11].

Estrogen or Epidermal Growth Factor (EGF) rapidly activates the PERK arm of the UPR, resulting in transient phosphorylation of eIF2α and inhibition of global protein synthesis (Figure 2.4 A-C and Figure 3 in [12]). At early times after mild UPR activation, p-PERK induces expression of diverse protective microRNAs. These include miR-211 microRNA expression that increases histone methylation at the CHOP promoter region to repress CHOP expression, which is a pro-apoptotic transcription factor [13]. Altered glucose metabolism as a result of increased glycolysis and glucose uptake is a hallmark of cancer. miR-122 is one of most abundant microRNA in the liver and can also be regulated through the UPR [14, 15]. Most importantly, studies show that breast cancer cells can secret vesicles that contain a high level of miR-122 that suppresses glucose uptake by non-tumor cells in the pre-metastatic niche to increase nutrient availability. High expressions of miR-122 in the circulation have been associated with metastatic breast cancer patients [16].

Abundant nutrient supplies coupled with limited physical activity are responsible for the rising incidence of obesity-related diseases and cancers, including type 2 diabetes, metabolic syndrome, and nonalcoholic fatty liver disease [17-20]. Although multiple mechanisms have been put forth to explain these phenomena, excess nutrients can

trigger EnR stress and UPR activation in premalignant and transformed cells in the tumor microenvironment, which contribute to cancer development and tumor cell metabolism [17]. Hypercholesterolemia is a risk factor for ERα-positive breast cancer and is also associated with endocrine therapy resistance [21, 22]. 27-hydroxycholesterol, a primary metabolite of cholesterol, can stimulate ERα-dependent tumor growth and increase liver X receptor-mediated breast cancer metastatic potential [21, 22]. Taken together, it will be of great interest to determine the pathophysiological importance of estrogen-mediated PLC downstream targets and roles of anticipatory UPR signaling in tumor progression, development, metabolism, and invasion.

The preclinical anticancer drug BHPI causes lethal hyperactivation of the UPR, blocking proliferation of diverse therapy-resistant and ERα-positive breast cancer cells. BHPI was the most effective biomodulator to emerge from an unbiased high throughput screen for small molecules that inhibit the expression of an E_2-ERα regulated luciferase reporter. Surprisingly, BHPI elicited rapid, near quantitative inhibition of protein synthesis, a seemingly unlikely action for a small molecule inhibitor of E_2-ERα regulated gene expression. The PERK arm of the UPR was identified as the pathway responsible for rapid BHPI inhibition of protein synthesis. This led to the finding that BHPI works by hyperactivating the little-studied anticipatory UPR pathway. Although identified in precursors to immunoglobulin secreting B cells, this pathway had not been studied in the context of hormone action. Compared with E_2, BHPI more strongly activates PLCγ, producing much higher IP_3 levels, calcium release from the EnR, and UPR activation. BHPI potently inhibits protein synthesis by inducing rapid and robust phosphorylation of PERK and eIF2α. Supporting the role of the PERK arm of the UPR in inhibiting protein

synthesis, knockdown and inhibition of ERα, PLCγ, the IP_3Rs, and PERK blocked rapid BHPI inhibition of protein synthesis. The substantial level of IP_3 produced by strong BHPI activation of PLCγ binds to and opens the EnR IP_3Rs, resulting in the rapid efflux of calcium stored in the lumen of the EnR into the cytosol. To restore EnR calcium, the cell activates SERCA pumps, which catalyze the ATP-dependent transfer of calcium from the cytosol into the lumen of the EnR. Since the IP_3R calcium channels are still open, the calcium pumped into the EnR leaks back out creating a futile cycle that rapidly depletes cell ATP. Depleting intracellular ATP activates the metabolic sensor, AMP kinase (AMPK). Supporting this model, thapsigargin, which inhibits the SERCA pumps, blocks the BHPI-mediated decline in ATP levels and AMPK activation. Together, AMPK activation and elevated intracellular calcium activate the eukaryotic elongation factor 2 kinase (CAMKIII/eEF2K). Activated eEF2K phosphorylates eEF2, inhibiting protein synthesis at a second site. This prevents synthesis of BiP and other chaperones and $p58^{IPK}$ and GADD34 (growth arrest and DNA damage-inducible protein 34) that normally reverse PERK activation. Working together, several actions of BHPI, including long-term inhibition of protein synthesis, sustained UPR activation, ATP depletion and AMPK activation likely contribute to BHPI's ability to block proliferation and often kill ERα-positive cancer cells. At nanomolar concentrations, BHPI blocked growth and killed diverse ERα-positive breast, ovarian, and endometrial cancer cells that are resistant to endocrine therapies. In a mouse xenograft model of breast cancer, BHPI stopped tumor growth and induced rapid and substantial regression of large tumors.

Mild UPR activation enhances protein folding capacity to meet the need for increased protein synthesis and cell proliferation [23]. Cancer cells adopt the protective

features of the UPR pathway to exhibit constitutive activation of IRE1α or increased expression of BiP, which is anti-apoptotic [24-27]. In contrast, sustained hyperactivation of UPR is lethal. Long-term PERK activation can induce CHOP, which binds to and induce transcription of the promoters of p53 an upregulated modulator of apoptosis, lipocalin 2, tribbles homologue 3, and death receptor 5 that is responsible for EnR stress-induced apoptosis via caspase 8 in cancer cells [28-32]. In addition, CHOP can transcriptionally activate of the AKT inhibitor TRIB3 [30], which inhibits mTOR pathway to block proliferation and activate autophagy, a stress-adaptive self-eating process [33]. While activation of autophagy has been documented in some cancer cells to be protective, similar to UPR activation, activation of autophagy can also lead to cell death [33]. Similar to PERK, if IREα signaling is not attenuated, sustained IRE1α activation can trigger apoptosis [24]. Hyperactivated IRE1α cleaves many mRNA in addition to its well-known substrate, XBP1, a process called regulated IRE1-dependent decay (RIDD) [34]. RIDD reduces the expression of some microRNAs that repress caspase 2 expression [35]. Whether caspase 2 plays a role in UPR-induced apoptosis is unknown [35]. In addition, activated IRE1α binds to TNF receptor-associated factor 2, which recruits apoptosis signal-regulating kinase 1 and JUN N-terminal kinase (JNK), resulting in JNK-mediated apoptosis [36]. Sustained UPR activation by pharmacological UPR inhibitors (Tunicamycin, Thapsigargin) can cause these UPR-induced apoptosis cascades [37]. However, BHPI is a new class of UPR biomodulator that works by hyperactivating the UPR, resulting in persistent inhibition of global protein synthesis. While the exact mechanism underlying BHPI induced cell death is under investigation, we anticipate that BHPI integrates multiple UPR-induced cell death pathways to kill ERα-positive tumors.

BHPI indirectly inactivates MDR1 activity and restores sensitivity to chemotherapy in resistant ovarian cancer by selectively depleting intracellular ATP. *De novo* and acquired multidrug resistance is a core problem in cancer chemotherapy [5]. In ovarian cancer, the primary driver of multidrug resistance is overexpression of energy dependent MDR1 pumps [38]. BHPI has emerged as a uniquely promising and well-tolerated therapeutic candidate for multidrug resistant ovarian cancer. Central to BHPI's therapeutic potential is its novel mechanism of action based on robust and sustained hyperactivation of the anticipatory UPR pathway, resulting in ATP depletion and MDR1 inactivation. This enables BHPI to resensitize multidrug resistant tumors to chemotherapeutic intervention and reduce ovarian tumor burden to undetectable levels. Interestingly, in an orthotopic xenograft study, using paclitaxel resistant MDR1 overexpressing ovarian cancer cells, the control paclitaxel-treated group exhibited large metastases. This is a previously unexplored phenotype and may represent a new resistance mechanism induced by chemotherapy agents in multidrug resistant cells. BHPI is a novel candidate for further development for combination therapy for the treatment of multidrug resistant ovarian cancer.

Although tumors often exhibit multiple regulatory alterations, anticancer leads usually focus on inhibiting a protein target or pathway. We employ an alternative approach and use BHPI to hyperactivate the up-regulated tumor-protective UPR pathway, converting it from protective to lethal. Targeting therapy-resistant cancer cells through proteins overexpressed as part of a therapy resistance mechanism is a novel therapeutic idea, with the potential for significant impact on the treatment of aggressive and therapy-resistant ERα-positive breast and ovarian tumors.

REFERENCES

1. Musgrove, E.A. and R.L. Sutherland, *Biological determinants of endocrine resistance in breast cancer.* Nat Rev Cancer, 2009. **9**(9): p. 631-43.
2. Tyson, J.J., et al., *Dynamic modelling of oestrogen signalling and cell fate in breast cancer cells.* Nat Rev Cancer, 2011. **11**(7): p. 523-32.
3. Bast, R.C., Jr., B. Hennessy, and G.B. Mills, *The biology of ovarian cancer: new opportunities for translation.* Nat Rev Cancer, 2009. **9**(6): p. 415-28.
4. Deroo, B.J. and K.S. Korach, *Estrogen receptors and human disease.* J Clin Invest, 2006. **116**(3): p. 561-70.
5. Kumar, A., et al., *Chemotherapy is of Value in Second Line and Beyond, Relapsed High-grade, Serous Epithelial Ovarian Cancer: An Analysis of Outcomes Obtained With Oral Etoposide.* Am J Clin Oncol, 2016.
6. Yap, T.A., C.P. Carden, and S.B. Kaye, *Beyond chemotherapy: targeted therapies in ovarian cancer.* Nat Rev Cancer, 2009. **9**(3): p. 167-81.
7. Romero, I. and R.C. Bast, Jr., *Minireview: human ovarian cancer: biology, current management, and paths to personalizing therapy.* Endocrinology, 2012. **153**(4): p. 1593-602.
8. Garg, R., et al., *Protein kinase C and cancer: what we know and what we do not.* Oncogene, 2014. **33**(45): p. 5225-37.
9. Tan, M., et al., *Upregulation and activation of PKC alpha by ErbB2 through Src promotes breast cancer cell invasion that can be blocked by combined treatment with PKC alpha and Src inhibitors.* Oncogene, 2006. **25**(23): p. 3286-95.

10. Kim, S., et al., *Berberine suppresses the TPA-induced MMP-1 and MMP-9 expressions through the inhibition of PKC-alpha in breast cancer cells.* J Surg Res, 2012. **176**(1): p. e21-9.

11. Lahn, M., et al., *Protein kinase C alpha expression in breast and ovarian cancer.* Oncology, 2004. **67**(1): p. 1-10.

12. Yu, L., et al., *Anticipatory activation of the unfolded protein response by epidermal growth factor is required for immediate early gene expression and cell proliferation.* Mol Cell Endocrinol, 2015.

13. Chitnis, N.S., et al., *miR-211 is a prosurvival microRNA that regulates chop expression in a PERK-dependent manner.* Mol Cell, 2012. **48**(3): p. 353-64.

14. Yang, F., et al., *Modulation of the unfolded protein response is the core of microRNA-122-involved sensitivity to chemotherapy in hepatocellular carcinoma.* Neoplasia, 2011. **13**(7): p. 590-600.

15. Bandiera, S., et al., *miR-122--a key factor and therapeutic target in liver disease.* J Hepatol, 2015. **62**(2): p. 448-57.

16. Fong, M.Y., et al., *Breast-cancer-secreted miR-122 reprograms glucose metabolism in premetastatic niche to promote metastasis.* Nat Cell Biol, 2015. **17**(2): p. 183-94.

17. Wang, M. and R.J. Kaufman, *The impact of the endoplasmic reticulum protein-folding environment on cancer development.* Nat Rev Cancer, 2014. **14**(9): p. 581-97.

18. Hotamisligil, G.S., *Endoplasmic reticulum stress and the inflammatory basis of metabolic disease.* Cell, 2010. **140**(6): p. 900-17.

19. Papa, F.R., *Endoplasmic reticulum stress, pancreatic beta-cell degeneration, and diabetes.* Cold Spring Harb Perspect Med, 2012. **2**(9): p. a007666.

20. McDonnell, D.P., et al., *Obesity, cholesterol metabolism, and breast cancer pathogenesis.* Cancer Res, 2014. **74**(18): p. 4976-82.

21. Nelson, E.R., C.Y. Chang, and D.P. McDonnell, *Cholesterol and breast cancer pathophysiology.* Trends Endocrinol Metab, 2014. **25**(12): p. 649-55.

22. Nelson, E.R., et al., *27-Hydroxycholesterol links hypercholesterolemia and breast cancer pathophysiology.* Science, 2013. **342**(6162): p. 1094-8.

23. Shapiro, D.J., et al., *Anticipatory UPR Activation: A Protective Pathway and Target in Cancer.* Trends Endocrinol Metab, 2016.

24. Chen, Y. and F. Brandizzi, *IRE1: ER stress sensor and cell fate executor.* Trends Cell Biol, 2013. **23**(11): p. 547-55.

25. Taylor, R.C. and A. Dillin, *XBP-1 Is a Cell-Nonautonomous Regulator of Stress Resistance and Longevity.* Cell, 2013. **153**(7): p. 1435-47.

26. Preissler, S., et al., *Physiological modulation of BiP activity by trans-protomer engagement of the interdomain linker.* Elife, 2015. **4**: p. e08961.

27. Behnke, J., M.J. Feige, and L.M. Hendershot, *BiP and its nucleotide exchange factors Grp170 and Sil1: mechanisms of action and biological functions.* J Mol Biol, 2015. **427**(7): p. 1589-608.

28. Galehdar, Z., et al., *Neuronal apoptosis induced by endoplasmic reticulum stress is regulated by ATF4-CHOP-mediated induction of the Bcl-2 homology 3-only member PUMA.* J Neurosci, 2010. **30**(50): p. 16938-48.

29. Hsin, I.L., et al., *Lipocalin 2, a new GADD153 target gene, as an apoptosis inducer of endoplasmic reticulum stress in lung cancer cells.* Toxicol Appl Pharmacol, 2012. **263**(3): p. 330-7.

30. Ohoka, N., et al., *TRB3, a novel ER stress-inducible gene, is induced via ATF4-CHOP pathway and is involved in cell death.* EMBO J, 2005. **24**(6): p. 1243-55.

31. Zou, W., et al., *Coupling of endoplasmic reticulum stress to CDDO-Me-induced up-regulation of death receptor 5 via a CHOP-dependent mechanism involving JNK activation.* Cancer Res, 2008. **68**(18): p. 7484-92.

32. Yamaguchi, H. and H.G. Wang, *CHOP is involved in endoplasmic reticulum stress-induced apoptosis by enhancing DR5 expression in human carcinoma cells.* J Biol Chem, 2004. **279**(44): p. 45495-502.

33. Marino, G., et al., *Self-consumption: the interplay of autophagy and apoptosis.* Nat Rev Mol Cell Biol, 2014. **15**(2): p. 81-94.

34. Ghosh, R., et al., *Allosteric inhibition of the IRE1alpha RNase preserves cell viability and function during endoplasmic reticulum stress.* Cell, 2014. **158**(3): p. 534-48.

35. Upton, J.P., et al., *IRE1alpha cleaves select microRNAs during ER stress to derepress translation of proapoptotic Caspase-2.* Science, 2012. **338**(6108): p. 818-22.

36. Urano, F., et al., *Coupling of stress in the ER to activation of JNK protein kinases by transmembrane protein kinase IRE1.* Science, 2000. **287**(5453): p. 664-6.

37. Sano, R. and J.C. Reed, *ER stress-induced cell death mechanisms.* Biochim Biophys Acta, 2013. **1833**(12): p. 3460-70.

38. Silva, R., et al., *Modulation of P-glycoprotein efflux pump: induction and activation as a therapeutic strategy.* Pharmacol Ther, 2015. **149**: p. 1-123.